Von Herzen, R. P., Robinson, P. T., et al., 1991
Proceedings of the Ocean Drilling Program, Scientific Results, Vol. 118

3. MINERALOGY AND TEXTURES OF IRON-TITANIUM OXIDE GABBROS AND ASSOCIATED OLIVINE GABBROS FROM HOLE 735B[1]

Kazuhito Ozawa,[2] Peter S. Meyer,[3] and Sherman H. Bloomer[4]

ABSTRACT

Abundant iron-titanium (Fe-Ti) oxide gabbro, olivine gabbro, and troctolite were drilled at Hole 735B adjacent to the Atlantis II Fracture Zone of the Southwest Indian Ridge during Leg 118. The Fe-Ti oxide gabbro occurs as intrusive bodies into olivine gabbro with very sharp intrusive contacts. The size of the intrusive bodies varies from a millimeter to a few tens of meters. Mineralogical parameters, such as anorthite content of plagioclase and Mg/(Mg+Fe) ratios of mafic minerals exhibit bimodal distributions corresponding to olivine and Fe-Ti oxide gabbros, respectively. When the two major gabbro types are looked at separately, several downhole mineralogical cycles are recognized. The Fe-Ti oxide gabbros exhibit two such cycles with plagioclase becoming more sodic and mafic minerals becoming more iron-rich downward in the drill core. The olivine gabbros and troctolites, however, exhibit two cycles showing an upward increase in sodium in plagioclase and iron in mafic minerals. The mineralogical variations of these gabbros and the intrusive contact relationships probably resulted from downward intrusion of evolved magma into underlying solid or almost solidified olivine gabbros and troctolite. The dense evolved melt at the top of the cumulus pile probably formed from the crystallization of olivine gabbro cumulates followed by extreme fractional crystallization of residual melt in an isolated, ephemeral magma chamber. The interlayered occurrence of evolved and primitive gabbros from Hole 735B represents a typical section of lower ocean crust formed at a very slow spreading ridge.

INTRODUCTION

Basalts erupt on the seafloor after undergoing varying degrees of crystallization in magma chambers beneath mid-ocean ridges. The crystallization products of mid-ocean ridge basalts (MORB) form gabbros that make up oceanic layer 3. To date, most oceanic gabbros have been dredged from fracture zones and rift valley walls (Hodges and Papike, 1976; Miyashiro and Shido, 1980; Tiezzi and Scott, 1980; Hébert et al., 1983; Walker and DeLong, 1984; Batiza and Vanko, 1985; Elthon, 1987; Meyer et al., 1989). The fragmental nature of dredged samples, however, limits their usefulness for petrologic modeling of magmatic accretion at mid-ocean ridges. Drilling at Site 735 on Leg 118, however, succeeded in recovering an almost complete 500-m section of gabbroic rocks that originally formed at the axis of the Southwest Indian Ridge. The core from Hole 735B provides the first view of lower oceanic-crust stratigraphy and offers an opportunity to study the remnants of a mid-ocean ridge magmatic system. These gabbroic rocks exhibit remarkable chemical variations and may represent accumulated crystals at various stages in the evolution of a mid-ocean ridge magma chamber.

This study reports petrographic and mineralogical characteristics of Fe-Ti oxide gabbros that may be related to a localized occurrence of evolved magma beneath a slow-spreading ridge. The Fe-Ti oxide gabbros are present throughout the whole sequence of the drilled section as intrusive bodies into olivine gabbros and rarely into troctolite. This mixed occurrence of evolved and primitive gabbros with a clear mineralogical gap may be representative of lower oceanic crust at slow spreading ridges particularly in the proximity of transform faults.

Olivine-Bearing Gabbro, Olivine Gabbro, and Troctolite

The petrography of olivine-bearing gabbro, olivine gabbro, and troctolite has been summarized by Bloomer et al. (this volume). Olivine-bearing and olivine gabbros are the most abundant rock types recovered from Hole 735B. They are the main rock types in lithologic Units II, V, and VI, and contain trace amounts of interstitial orthopyroxene and opaque minerals, which are commonly sulfide or ilmenite. Modal proportions of olivine, plagioclase, and clinopyroxene vary considerably, which reflects modal layering or irregular distribution of crystals in coarse-grained rocks. The troctolites from Hole 735B exhibit either medium-grained poikilitic or fine-grained equigranular textures. They contain trace amounts of spinel (up to 1%) and sulfide, but no primary Fe-Ti oxides have been observed. Troctolites or troctolitic gabbros are common in Unit VI and their frequency tends to increase toward the bottom of the hole. Some olivine gabbros contain clinopyroxene that is vermicularly intergrown with orthopyroxene + pale brown amphibole. Such olivine gabbros tend to be more primitive than those without clinopyroxene free of the vermicular intergrowth (Fig. 1).

Iron-Titanium Oxide Gabbro

Iron-titanium (Fe-Ti) oxide gabbros generally contain greater than 2% (rarely less than 1%) Fe-Ti oxides (ilmenite and magnetite). In addition to Fe-Ti oxides, these gabbros contain clinopyroxene with Mg#s ($100 \times Mg/(Mg+Fe)$) <75, plagioclase with An contents <50, ±olivine (Mg#s <65), ±orthopyroxene, and ±inverted pigeonite. Accessory primary phases include common brown hornblende and rare apatite and zircon.

Most of these Fe-Ti oxide gabbros have been metamorphosed and contain green hornblende, actinolite, epidote, albite, chlorite, and sphene as metamorphic minerals. They

[1] Von Herzen, R. P., Robinson, P. T., et al., 1991. *Proc. ODP, Sci. Results*, 118: College Station, TX U.S.A. (Ocean Drilling Program).
[2] Geological Institute, Faculty of Science, University of Tokyo, Tokyo, 113, Japan.
[3] Woods Hole Oceanographic Institution, Woods Hole, MA 02543, U.S.A.
[4] Department of Geology, 675 Commonwealth Ave., Boston University, Boston, MA 02215, U.S.A.

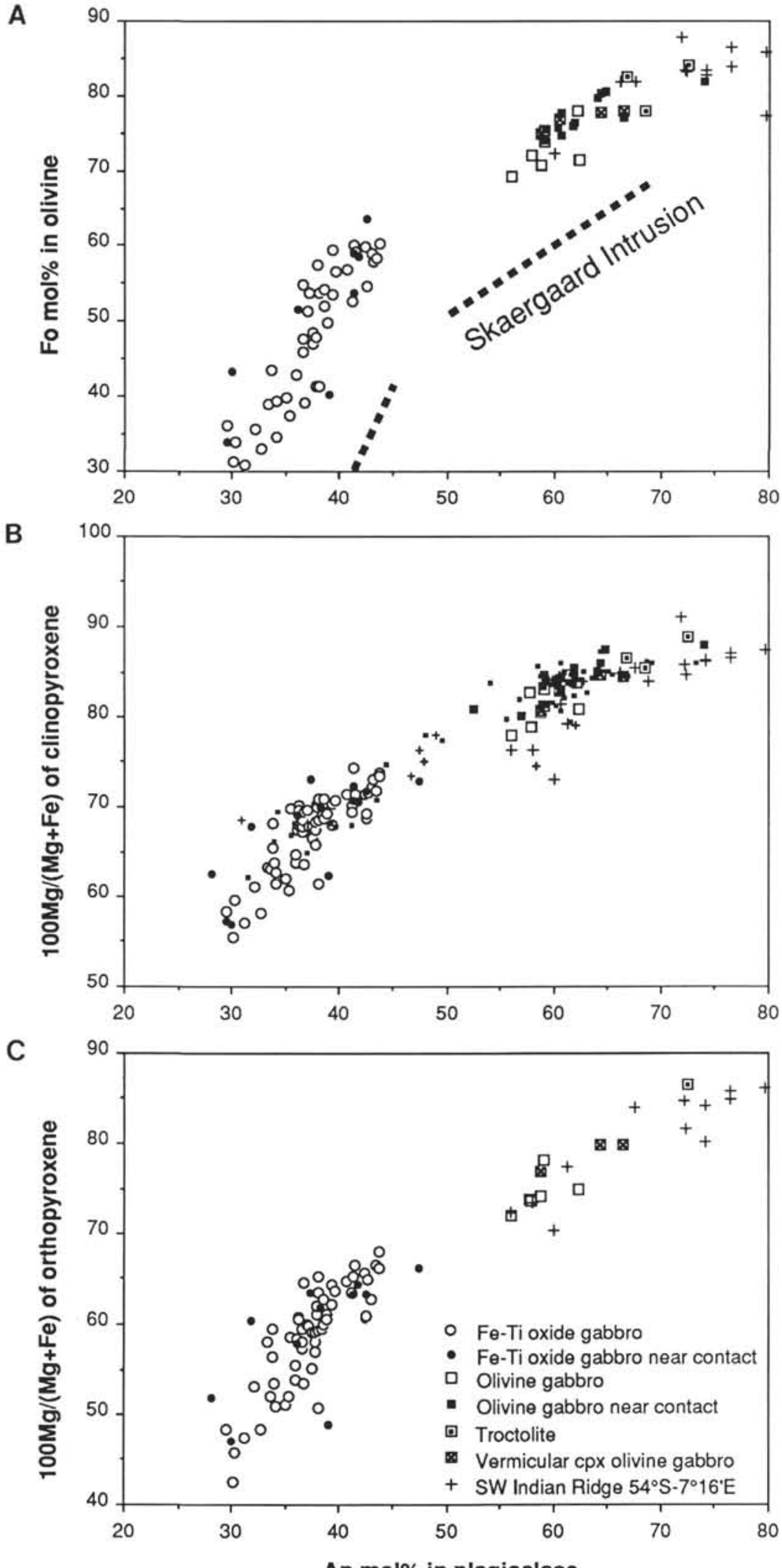

Figure 1. Average An content in plagioclase vs. average Mg/(Mg+Fe) ratios of mafic minerals (**A**, Olivine. **B**, Clinopyroxene. **C**, Orthopyroxene) in gabbros from Hole 735B. Solid small symbols imply the gabbros in contact with each other in thin sections. Those data for olivine gabbro were obtained from cores 1–3 cm away from the contact. Small solid squares and small pluses are the data obtained by P. S. Meyer at MIT (Bloomer et al., this volume) and those for deformed and metamorphosed samples in Unit 1, respectively. Data for Southwest Indian Ridge are taken from Meyer et al. (1989) and those for Skaergaard Intrusion are from Wager and Brown (1967).

Table 1. Petrographic table of the studied Fe-Ti oxide gabbros from Hole 735B.

Core, section, interval (cm)	Depth (mbsf)	Opaque (%)	Olivine (%)	Opx+pig (%)	Ca-poor px	Metamorphism	Deformation	Foliation/layer	Grain size	Rock type
118-735B-										
12R-1, 45–47	39.92	<2	0?	10–5	Opx+pig?	Extensive	Porphy	Def?	5.0	Gabbronorite
14R-1, 93–97	51.98	<2	tr./alt.	<1	Opx	Minor	Mylonitic		7.0	Inst ol gabbro?
19R-5, 47–50	83.02	tr.	0	10–15	Opx	Mod	Porphy		4.0	Gabbronorite
19R-5, 55–60	83.12	<1	0	5	Opx	Weak	Porphy		6.0	Gabbronorite
20R-1, 111–114	85.89	<1	70–80	2	Opx+pig	Weak-mod	Porphy		4.0	Pl wehrlite
21R-1-2, 82–89 FETI	90.47	5–10	2	1	Opx (pig?)	Extensive	Weak porphy	? sz-mod lay	7.0	Inst ol gabbro
21R-2, 27–32	91.06	5	0	2	Opx+pig	Weak-mod	Weak local pph	+	18.0	Pig gabbro
23R-3, 33–37	102.61	20	0?	3–5	Opx+pig	Weak-mod	Weak		9.0	Pig gabbro
23R-3, 34–37	102.61	5–7	0	5–10	Opx+pig	Weak	Weak		15.0	Pig gabbro
24R-2, 95–97	107.94	8–10	0	2–5	Opx	Mod-ext	Weak-mod		4.0	Gabbronorite
24R-2, 120–126	108.20	10–20	0	10–20	Pig	Mod	Weak		7.0	Pig gabbro
28R-1, 109–114	127.47	<5	0	2–3	Pig+opx	Weak-mod	Mod-porphy		4.0	Pig gabbro
28R-3, 72–77	129.54	5–10	0?	3–5	Pig	Weak-mod	Mod		30.0	Pig gabbro
34R-4, 8–12	163.23	20	2.5	1	Opx+pig	Weak	Weak		15.0	Inst ol gb +r
36R-4, 5–9	174.80	<1	5–10	1–2	Opx	Weak-mod	Mod-porphy	+ siz lay	2.0	Diss ox ol gb
37R-3-2, 71–76 FETI	180.13	1	1–3	<1	Opx+pig ?	Minor	Weak	+	0.5	Diss ox ol gb
37R-3, 76–79	180.18	1–3	5	1.5	Opx+pig	Mod	Weak	+ siz lay	1.0	Ol pig gabbro
37R-3, 80–82	180.23	2–3	2–3	1–3	Pig	Weak-mod	Weak	+	2.5	Ol pig gabbro
38R-3, 85–88	184.25	5	1–2 ? alt.	10	Pig	Weak-mod	Mod		20.0	Ol pig gabbro
38R-4, 24–28	184.88	2–3	2–3	5–10	Pig+opx	Weak	Weak	++ mod lay	4.0	Ol pig gabbro
40R-5, 0–4	195.45	3–5	5	10	Opx	Minor	Minor-no	Weak	7.0	Ol gabbronort
40R-5, 4–8	195.49	2	10	2–3	Opx	Minor	Minor-no	+ siz-mod lay	1.0	Diss ox ol gb
43R-3, 95–102	209.45	1–10/locz	5	1–5	Opx	Minor	Very Minor	+ siz-mod lay	4.0	Ol gabbronort
43R-4, 64–66	210.23	1–2/locz	3	1	Opx	No	No	++ mod lay	3.0	Diss ox ol gb
44R-2, 16–24	212.37	10	0	10	Opx+pig	Weak	Weak	+?	10.0	Pig gabbro
45R-1, 5–12	216.07	1–5/locz	1–5	10–20	Opx+pig(locz)	Mod	Very minor	+ siz-mod lay	3.0	Ol pig gabbro
46R-1, 48–58 FETI	221.47	1	5	<1	Opx	Minor	No	++	3.5	Diss ox ol gb?
46R-3, 121–128	224.68	4/locz	5	<1	Opx	Weak	No	+ siz-mod lay	0.8	Diss ox ol gb
46R-4, 109–113	225.83	10	0	1	Opx (pig?)	Weak	Weak		20.0	Pig gabbro
47R-2, 117–127	228.52	10	1	<1	Opx	Weak	Very minor		15.0	Inst ol gabbro
47R-3, 56–61	229.26	15	1–2	1	Opx+pig	Weak	Weak	Weak	5.0	Inst ol gb +r
47R-3-2, 143–149 FETI	230.10	10–20	5	<1	Opx	Weak	Minor	+	5.0	Inst ol gabbro
48R-2, 56–65	232.80	5	1–2	2	Pig	Weak-mod	Weak	+	4.0	Inst ol gabbro
48R-2, 109–113	233.28	3–5	4	<1?	?	Minor	No	+ siz-mod lay	0.3	Ol feti microgb
48R-3, 112–116	234.53	5–10	2–3	1–2	Opx+pig	Weak-mod	Weak	+	4.0	Inst ol gabbro
48R-4, 82–84	235.51	5	2–1	1–2	Opx	Weak	Weak	+	2.5	Inst ol gabbro
49R-1, 42–46	236.34	15	2	<1	Opx+pig?	Minor	No	+	2.5	Inst ol gabbro
49R-2, 94–100	237.21	10	2–3	1–2	Opx+pig	Weak	Weak	++	5.0	Inst ol gb +r
50R-2, 43–47	239.34	10–20	2–3	1–2	Opx+pig	Weak	No	+	4.0	Inst ol gabbro
50R-3, 62–67	240.82	10–15	1	1–2	Opx+pig	Weak	Weak	+ mod-siz lay?	4.0	Inst ol gabbro
51R-1, 94–99	244.03	5–10	1	2	Opx+pig?	Weak-mod	Weak	+ mod lay	5.0	Inst ol gabbro
51R-1, 99–103	244.09	5–15	1–2	2–3	Opx+pig	Weak	Weak	+ mod-siz lay	4.5	Inst ol gabbro
52R-1, 91–100	248.93	5	2	1	Opx	Weak-mod	Minor	+	4.0	Inst ol gb +r
52R-3, 121–123	251.60	2	2–3	<1	Opx	Mod	Weak-porphy	++	2.0	Inst ol gabbro
52R-4, 88–94	252.67	10	1/alt.	<1	Opx	Weak-mod	Weak-porphy	++	4.0	Inst ol gabbro
53R-1, 47–54	253.45	8	2	<<1	Opx(pig?)	Weak	Weak porphy	+	1.0	Inst ol gabbro
53R-1, 123–127	254.12	5–10	1–2	<1	Opx+pig?	Mod	Weak-mod	+ siz-mod lay	4.0	Inst ol gabbro
53R-2, 31–39	254.55	5–10	1	<<1	Opx	Mod	Weak-mod	+ siz mod lay	3.0	Inst ol gabbro
54R-1, 131–136	259.25	6	10	<1	Opx	Weak	Porphy		4.0	Ol feti gabbro
54R-3, 20–24	260.84	5–10	20	1	Opx	Mod	Weak-mod pph	Def ?	8.0	Ol feti gabbro
54R-3, 125–127	261.81	10	15–20	1	Opx	Weak	Porphy	Def ?	3.0	Ol feti gabbro
54R-5, 117–119	264.39	7	2–3	1	Opx	Weak	Mod-porphy	Def ?	7.5	Inst ol gabbro
55R-2, 101–105	267.50	13	1–2	1	Opx+pig	Weak	Mod-porphy		7.0	Inst ol gabbro
55R-2, 110–120	267.62	10–15	4–7	<1	Opx	Mod	Mod	Weak	9.0	Ol feti gabbro
55R-3, 83–86	268.81	5	5	<1	Opx	Weak-mod	Porphy-myl		1.0	Ol feti gabbro
56R-2, 11–14	271.52	5–10	3	<<1	Opx	No	Mylonitic		2.0	Ol feti gabbro
73R-4-2, 82–87 FETI	370.23	5–10	0	2–3	Opx	Minor	Weak-mod pph	Def ?	2.0	Gabbronorite
73R-5-2, 72–78 FETI	371.58	5–10	0	1–2	Opx	Minor	No		3.0	Gabbronorite
74R-6, 27–35	382.13	5	0	10	Opx	Minor	No		0.4	Poik gabbnort
76R-1-2, 63–70 FETI	394.69	5–10	<1	15–20	Opx	Minor	No		10.0	Gabbronorite
76R-1, 70–73 FETI	394.74	1	0	2	Opx	Minor	No		8.0	Gabbronorite
76R-1, 99–110 FETI	395.08	5	0	5–10	Opx	Minor	No		8.0	Gabbronorite
76R-3-2, 35–41 FETI	397.06	5	3–5	5–10	Opx	Minor	No	++ mod lay	0.8	Ol gabbronort
76R-4, 12–19	398.20	3	<1	20	Opx+pig	Minor	No	++ siz-mod lay	1.0	Gabbronorite
77R-2, 5–8	404.96	<1	5–10	?	?	Weak	Weak-mod	Def ?	0.8	Diss ox ol gb
77R-2, 101–107	405.89	1	10–20	4–8	Opx	Minor	Weak-mod pph	Weak	7.5	Ol gabbronort
79R-7-2, 2–9 FETI	422.82	5	5–10	5	Opx	Minor	Porphy-myl		3.0	Ol gabbronort
80R-3, 67–71	427.35	5–10	5–10	1	Opx+pig?	Weak	Porphy		6.0	Ol feti gabbro
80R-6, 130–135	431.98	5	10–20	2	Opx+pig	Weak	Porphy		9.0	Ol feti gabbro
80R-7, 10–18	432.23	<5	3–5	<1	Opx	Mod	Weak	Siz lay def?	0.8	Ol feti microgb
80R-7, 23–25	432.32	5	7	<1	Opx	Weak-mod	Weak	+	0.5	Ol feti microgb
82R-3-2, 0–5 FETI	445.72	10	0?	10	Opx	Mod	Weak-mod	+ mod lay	3.0	Gabbronorite
86R-4, 123–130	486.60	5–10	5–10	<1	Opx	Mod	Porphy		6.5	Ol feti gabbro
86R-6, 143–145	489.57	5	2	3	Opx	Weak-mod	Porphy		3.0	Inst ol gabbro

Note: Abbreviations are: loclz, localized; alt., altered; tr., trace; cpx, clinopyroxene; opx, orthopyroxene; pig, inverted pigeonite; mod, moderate; ext, extensive; porphy or pph, porphyroclastic; myl, mylonitic; def, deformation; siz, size; mod, modal; lay, layering; ol, olivine; opq, opaque mineral; +, strong magmatic lamination; ++, very strong magmatic lamination; inst ol gabbro, interstitial olivine-bearing oxide gabbro; pl, plagioclase; inst ol gb +r, interstitial olvine-bearing oxide gabbro with corona structure; diss ox ol gb, disseminated Fe-Ti oxide olivine gabbro; ol feti microgb, olivine Fe-Ti oxide microgabbro; ol feti gabbro, olivine Fe-Ti oxide gabbro; poik gabbnort, poikilitic gabbronorite. Fe-Ti oxide gabbro in contact with olivine gabbro is indicated by "FETI" in the interval column. Grain size is representative one for clinopyroxene.

commonly exhibit porphyroclastic or mylonitic textures with remarkable foliation and lineation, indicating that these gabbros were subjected to strong subsolidus deformation. Some specimens also exhibit a magmatic lamination which likely resulted from hypersolidus deformation of the cumulate pile (Dick et al., this volume). Magmatic lamination is always cut by deformation foliation, which can be clearly seen by the redistribution patterns of Fe-Ti oxides (Robinson, Von Herzen, et al., 1989). Magmatic lamination can be discriminated from deformation foliation by the absence of highly deformed plagioclase and olivine exhibiting strong wavy extinction, kink bands, or recrystallization. Magmatic lamination at levels shallower than 170 mbsf is weak or absent, or possibly overprinted by deformation (Table 1; Fig. 7 in Robinson, Von Herzen, et al., 1989).

In spite of these secondary processes, primary magmatic structures, textures, and mineralogical characteristics are well preserved. Because this study focuses on igneous processes, only magmatic features are presented in the following petrographic descriptions. Some gabbros exhibit magmatic modal and/or size layering. They also commonly exhibit magmatic lamination defined by an elongate aggregate of Fe-Ti oxides or preferred orientations of elongate plagioclase and clinopyroxene crystals. Fe-Ti oxide gabbros commonly occur as centimeter to meter scale veins and layers within the olivine gabbro. The boundaries between the Fe-Ti oxide gabbros and olivine gabbro are very sharp and are generally marked by the abrupt appearance of Fe-Ti oxides. This mixed occurrence of evolved and primitive gabbros over a 500-m depth range is the most distinctive feature of the gabbros from Hole 735B. Some zones having thicknesses of more than a few meters also occur: these are located in the gabbronorite in the top 28 m of Unit I and in the 50-m-thick massive Fe-Ti oxide gabbro zone Unit IV. In the upper two thirds of Unit V, Fe-Ti oxide gabbro is almost absent (Fig. 2). In Unit IV, two zones of olivine gabbros having thicknesses of 50 cm and 1 m are present near the top of the massive Fe-Ti oxide gabbro. The proportion of Fe-Ti oxide gabbro increases downward from Units I to IV and from Units V to VI (Robinson, Von Herzen, et al., 1989). These two zones in the core are also marked by a downward increase in the abundance of Fe-Ti oxides and by downward trends to more evolved mineral compositions, e.g., lower An contents in plagioclase and lower Mg#s in olivines and clinopyroxenes (Fig. 2 and 3).

Fe-Ti oxide gabbros can be divided into eight types according to modal proportions of primary phases and textural relationships (Table 1). These are gabbronorite, olivine gabbronorite, disseminated Fe-Ti oxide olivine gabbro, olivine pigeonite gabbro, pigeonite gabbro, interstitial olivine-bearing Fe-Ti oxide gabbro, olivine Fe-Ti oxide gabbro, olivine Fe-Ti oxide microgabbro.

GEOLOGICAL SETTING OF HOLE 735B

Hole 735B is located on a shallow platform in about 700 m of water on the east rim of the Atlantis II Fracture Zone, which is a 210-km left lateral offset formed during ridge extension of the Southwest Indian Ridge at about 58 Ma (Robinson, Von Herzen, et al., 1989). The platform is 9 km long in a north-south direction and 4 km wide, and is one of a series of uplifted blocks aligned to form a linear ridge parallel to the Atlantis II Fracture Zone. This platform has a flat, probably wave-cut, surface and locally is covered with a thin layer of sediments. The crustal age of Site 735 is inferred to be about 12 Ma on the basis of magnetic anomaly patterns on the eastern transform wall. The surface feature is characterized by development of a steeply dipping foliation and a regular pattern of faults and joints, (Robinson, Von Herzen, et al., 1989). The section drilled in Hole 735B was originally divided into six lithologic units on the basis of primary igneous modal mineralogy, mineral and bulk chemical compositions, and degree and style of deformation (Robinson, Von Herzen, et al., 1989). Dick et al. (this volume) redescribed the entire core at the Ocean Drilling Repository, dividing it into six units, three of which were further subdivided into two to four subunits. In this paper, this lithostratigraphic division is employed in the description and discussion.

PETROGRAPHY

Gabbros from Hole 735B can be divided into primitive gabbros (olivine-bearing gabbro, olivine gabbro, and troctolite) and evolved gabbros (gabbronorite, pigeonite gabbro, olivine iron-titanium (Fe-Ti) oxide gabbro). Olivine gabbros mostly without Fe-Ti oxide are the main constituent of the hole. These two groups can be discriminated by the presence or absence of Fe-Ti oxides and by the compositions of plagioclase, clinopyroxene, and olivine which exhibit bimodal populations in An mol% ($100 \times Ca/(Ca+Na+K)$) of plagioclase and Mg# ($100 \times Mg/(Mg+Fe)$) of mafic minerals (Fig. 4). As described later, the contacts between olivine gabbro and Fe-Ti oxide gabbro generally are sharp (mineralogical gradients are confined to zones less than 1 cm) resulting in few gabbros with intermediate compositions.

Cinopyroxenes in Fe-Ti oxide gabbros are generally subhedral to euhedral and have (001) exsolution lamellae and irregular orthopyroxene patches (Fig. 22 of Robinson, Von Herzen, et al., 1989), whereas those in olivine gabbro are generally anhedral and have no (001) exsolution lamellae.

Gabbronorite

Gabbronorite consists mainly of orthopyroxene, clinopyroxene, plagioclase, and Fe-Ti oxides (Pl. 1, Fig. 1). Modal abundances of Fe-Ti oxide are generally less than a few percent. The oxides exhibit scattered local concentration that defines a thin layer, which is parallel to the lamination. Trace amounts of olivine are rarely present. Reddish-brown amphibole is present as a minor phase at the rim of or partially replacing clinopyroxene. Zircon is present as an isolated euhedral grain in some gabbronorites. Orthopyroxene is subhedral to anhedral and exhibits various types of intergrowth with clinopyroxene. The most common type of intergrowth (0.1–1 mm in size) is characterized by a host orthopyroxene and optically continuous clinopyroxene having a poikilitic appearance (e.g., Sample 118-735B-76R-4, 12–19 cm). The margins of euhedral orthopyroxene rarely exhibit fine intergrowths (10–60 μm in size) with optically continuous clinopyroxene (Sample 118-735B-19R-5, 47–50 cm).

A rare poikilitic gabbronorite occurs as an intrusion into olivine gabbro (118-735B-74R-6 [Piece 1 through Piece 4C]). It consists of euhedral clinopyroxene, euhedral plagioclase, and 5- to 10-mm oikocrysts of orthopyroxene containing abundant slightly corroded plagioclase and opaque minerals as chadacrysts and very rare clinopyroxene chadacrysts. Euhedral apatite is also present. Euhedral to subhedral magnetite and ilmenite are homogeneously distributed, being independent of orthopyroxene oikocrysts. Such euhedral Fe-Ti oxides are rare among the rest of the Fe-Ti oxide gabbros from Hole 735B, whose Fe-Ti oxides are generally anhedral and fill the interstitial spaces between the silicate minerals.

A gabbronorite sample (Sample 118-735B-76R-1, 63–70 cm), which is in contact with olivine gabbro, contains an anhedral grain of olivine surrounded by an intergrowth of orthopyroxene and Fe-Ti oxide (Pl. 1, Fig. 4). This corona structure is located 1 cm from the contact. The occurrence of the corona structure at the contact suggest a reaction of olivine in the olivine gabbro with the evolved melt that crystallized gabbronorite. A similar orthopyroxene-magnetite

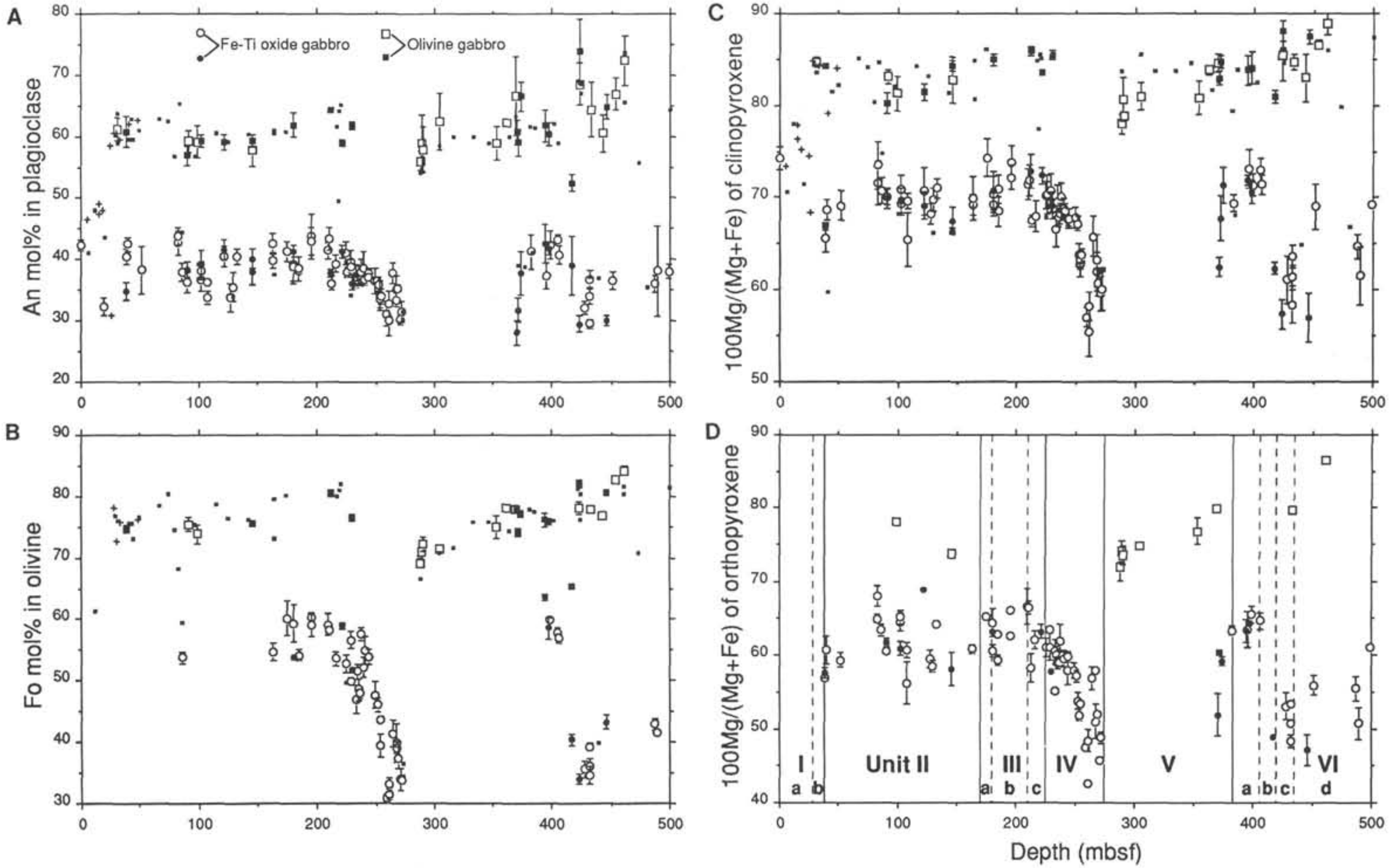

Figure 2. Downhole mineralogical variations (average An content in plagioclase (**A**) and average Mg/(Mg+Fe) ratios for the main mafic minerals (**B–D**)) for gabbros from Hole 735B. Solid symbols indicate data near the contact between olivine gabbro and iron-titanium oxide gabbro. The data for olivine gabbros and troctolites in contact with iron-titanium oxide gabbro are analyses of cores 1–3 cm away from the contact. Bars indicate standard deviations. The unit boundaries (Dick et al., this volume) are shown in (**D**). Small solid squares in (**A**), (**B**), and (**C**) are the data obtained by P. S. Meyer at MIT (Bloomer et al., this volume). Pluses in Unit I are for fairly deformed and metamorphosed samples, original rock types of which are difficult to identify.

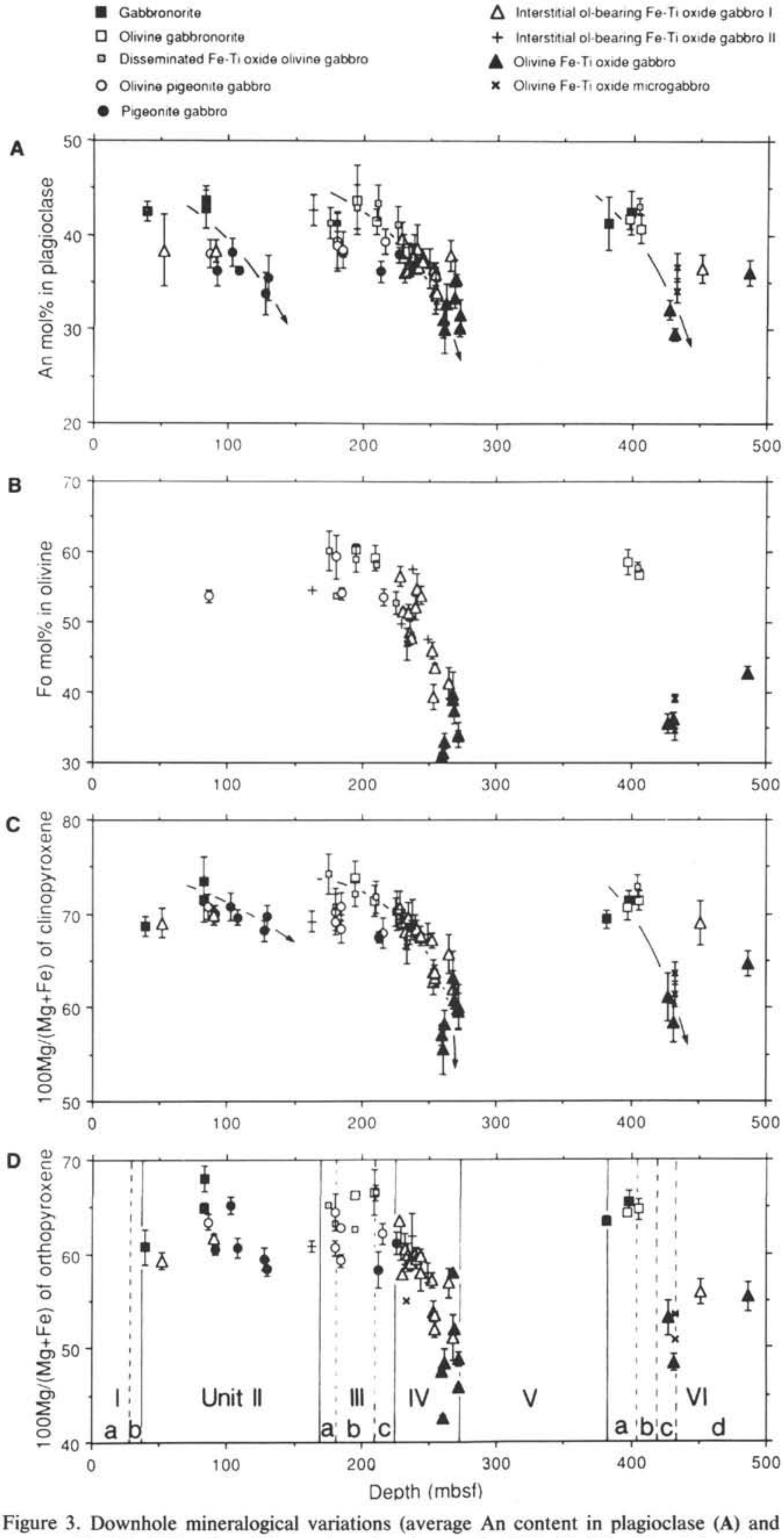

Figure 3. Downhole mineralogical variations (average An content in plagioclase (**A**) and average Mg/(Mg+Fe) ratios of the main mafic minerals (**B–D**)) for Fe-Ti oxide gabbros from Hole 735B. Interstitial olivine-bearing Fe-Ti oxide gabbro II contains, but I does not have a corona structure. The corona structure consists of calcium-poor pyroxenes (inverted pigeonite or orthopyroxene) surrounded by clinopyroxene, which is further surrounded by olivine. Intergrowth of olivine and clinopyroxene rarely surrounds calcium-poor pyroxenes. Bars indicate standard deviations. The unit boundaries (Dick et al., this volume) are shown in (**D**). Three main cycles are depicted with arrows in (**A**) and (**C**).

intergrowth around primary cumulus olivine has been noted in several layered intrusions and has been interpreted as a reaction between cumulus olivine and pore liquid (e.g., Ambler and Ashley, 1977).

Olivine Gabbronorite

Olivine gabbronorite consists of olivine, orthopyroxene, clinopyroxene, plagioclase, and Fe-Ti oxides (Pl. 1, Fig. 2). Minor amounts of brown hornblende are included in clinopyroxene, which is commonly associated with the opaque minerals. Hornblende also occurs at the contact between clinopyroxene and interstitial Fe-Ti oxides. The modal abundance of Fe-Ti oxides is generally less than a few percent. Texturally, Fe-Ti oxides are anhedral, except for those that are included in pyroxenes and are locally concentrated, defining a remarkable modal layering. Olivine is commonly present as isolated grains or aggregates. Orthopyroxene is anhedral to subhedral, and the subhedral grains are elongate and show preferred orientation. Anhedral orthopyroxene is poikilitic and encloses plagioclase, olivine, and opaque minerals. Olivine gabbronorite commonly exhibits lamination and/or size and modal layering. In some layered specimens (e.g., Sample 118-735B-43R-3, 95–102 cm), olivine is present as an interstitial phase rimming opaque minerals in the olivine-poor and opaque-rich upper portion. In another layered specimen (Sample 118-735B-45R-1, 5–12 cm), a lower olivine gabbronorite layer is in contact with an opaque-rich pigeonite gabbro layer without olivine. The layer boundary is nearly horizontal and is marked by a sudden increase in opaque phases. Weak lamination, defined by elongate clinopyroxene, plagioclase, and Fe-Ti oxides, is nearly vertical and thus oblique to the layer boundary. The modal abundance of orthopyroxene decreases downward suddenly in one layered specimen (Sample 118-735B-40R-5, 0–8 cm) and creates the appearance of disseminated Fe-Ti oxide olivine gabbro, which will be described later. In this specimen, the Fe-Ti oxide is rich in the olivine gabbronorite layer, but is poor in the disseminated oxide olivine gabbro layer.

Disseminated Fe-Ti Oxide Gabbro

This gabbro consists of olivine, clinopyroxene, Fe-Ti oxides, ±orthopyroxene, and brown hornblende as an accessory primary phase (Pl. 1, Fig. 3). Disseminated Fe-Ti oxide olivine gabbro has a modal abundance similar to olivine gabbro, but shows more evolved mineralogical characteristics and always contains minor amounts of Fe-Ti oxides. Its modal abundance also is similar to an olivine Fe-Ti oxide gabbro, except for the difference in the opaque abundance and mineral chemistries. The modal abundance of Fe-Ti oxides is mostly less than 1%. Orthopyroxene is present (less than 1%) as anhedral grains, often in contact with olivine or clinopyroxene. Olivine is present as isolated grains or in aggregates. Disseminated Fe-Ti oxide olivine gabbro commonly shows layering and a marked lamination. Olivine shows local concentrations in layers parallel to other types of modal or size layering. Magmatic lamination is often bowed and commonly oblique to the layer boundaries. One disseminated Fe-Ti oxide olivine gabbro (Sample 118-735B-40R-5, 0–8 cm) is in contact with upper olivine gabbronorite. The disseminated Fe-Ti oxide olivine gabbro contains slightly more sodic plagioclase and Fe-rich mafic minerals than the olivine gabbronorite.

Olivine Pigeonite Gabbro

Olivine pigeonite gabbro consists mainly of olivine, inverted pigeonite, clinopyroxene, plagioclase, Fe-Ti oxides, and ±orthopyroxene. Modal abundance of the Fe-Ti oxides is variable and ranges from 1% to 5%, which is distinctly higher than that of gabbronorite, olivine gabbronorite, and disseminated Fe-Ti oxide olivine gabbro. The modal abundance of olivine is commonly less than 5%, but some gabbros exhibit marked concentration of olivine, up to 70%, giving rise to wehrlitic lithology. Olivine and Fe-Ti oxides show local concentrations forming thin, olivine and/or opaque-rich layers. Olivine is present either as isolated aggregates or as interstitial grains generally associated with opaque minerals.In rare cases, olivine occurs in intergrowths with clinopyroxene in close proximity to inverted pigeonite. Inverted pigeonite is present as subhedral isolated grains (Pl. 1, Fig. 5) or in cores of clinopyroxenes sharing its crystallographic c axis; thus (001) clinopyroxene exsolution lamellae in inverted pigeonite have the same extinction position as its host (Pl. 1, Fig. 6). The contacts between host clinopyroxene and inverted pigeonite are fairly irregular. This mode of occurrence of inverted pigeonite, which is more common in pigeonite gabbro and olivine-bearing Fe-Ti oxide gabbro, suggests that the pigeonite became unstable at some stage of crystallization and started to corrode, and then clinopyroxene grew over it. Such corroded inverted pigeonite in clinopyroxene is also observed in olivine Fe-Ti oxide gabbro, but is quite rare. Modal abundance of inverted pigeonite ranges from 1% to 7%. In one specimen of olivine pigeonite gabbro (Sample 118-735B-45R-1, 5–12 cm), olivine and pigeonite appear to be incompatible and are present in different layers. The pigeonite-bearing layer is rich in opaque minerals in contrast to the olivine-rich layer. In a remarkably laminated specimen (Sample 118-735B-38R-4, 24–28 cm), containing a 5-mm-thick olivine and an opaque-rich layer (steeply inclining at 60°), inverted pigeonite occurs within 1 cm above the olivine-rich bands. Below this, orthopyroxene appears instead of inverted pigeonite, both of which are further sandwiched by disseminated Fe-Ti oxide olivine gabbro.

Pigeonite Gabbro

Pigeonite gabbro consists mainly of inverted pigeonite, clinopyroxene, ±orthopyroxene, plagioclase, and Fe-Ti oxides (Figs. 19A 19B in Robinson, Von Herzen, et al., 1989). Olivine is absent and trace amounts of brown amphibole occur at the rim of, or included in, clinopyroxene. Euhedral apatite is rarely present. Modal abundance of Fe-Ti oxides ranges from 3% to 20%, which is distinctly greater than that of the gabbros described above. They are anhedral filling interstitial spaces between pyroxenes and plagioclase. The contacts between the Fe-Ti oxides and pyroxenes are bowed and are characterized by the common occurrence of cusps of Fe-Ti oxides projecting into clinopyroxene. Inverted pigeonite occurs either as anhedral single grains enclosed by clinopyroxene or as isolated euhedral-to-subhedral grains commonly associated with the Fe-Ti oxides. The modal abundance of inverted pigeonite is commonly less than a few percent, but rarely reaches 15% (e.g., Sample 118-735B-24R-2, 120–126 cm). Pigeonite gabbros are generally coarser (with grains up to 30 mm) than the other types of gabbros (Table 1). Intergrowth of Fe-Ti oxides and calcium-poor pyroxene is rarely present. The intergrowth may be a product of a reaction between olivine and liquid (see discussion above under gabbronorite).

Interstitial Olivine-Bearing Fe-Ti Oxide Gabbro

This type of gabbro is characterized by the occurrence of small amounts of intercumulus olivine, commonly associated with Fe-Ti oxides (Pl. 2, Figs. 1 to 4). It consists of clinopyroxene, plagioclase, Fe-Ti oxides, olivine, ±inverted pigeonite, and ±orthopyroxene. The modal abundance of Fe-Ti oxides varies from a few percent to 15%. They are fairly anhedral, and fill the interstitial spaces between plagioclase and clinopyroxene. The modal abundance of olivine is less than a few percent. Olivine occurs as an interstitial phase between Fe-Ti oxides and clinopyroxene (Pl. 2, Fig. 1) or sometimes as a filmy mantle around oxides adjacent to plagioclase (50–500μm; Pl. 2, Fig. 2). A similar occurrence of olivine has been reported from the Skaergaard Intrusion (Wager and Brown, 1967). Olivine is, furthermore, often present as a fine intergrowth with clinopyroxene, which sometimes surrounds inverted pigeonite (Pl. 2, Fig. 4). Olivine is rarely present as a monomineralic aggregate. Clinopyroxene is subhedral and commonly rounded with cusps of Fe-Ti oxides projecting into clinopyroxene. Inverted pigeonite and orthopyroxene are present in the cores of clinopyroxenes. They have fairly irregular corroded shapes (Pl. 2, Fig. 3). Some interstitial olivine-bearing Fe-Ti oxide gabbros have a corona structure exhibiting a reaction relation between calcium-poor pyroxene and silicate melt. Calcium-poor pyroxene (inverted pigeonite or orthopyroxene) is surrounded by clinopyroxene-olivine intergrowth, which is further surrounded by olivine (Pl. 2, Fig. 4; Fig. 23 in Robinson, Von Herzen, et al., 1989). This type of corona structure is wholly or partly enclosed by Fe-Ti oxides. The intergrowth (without a core of calcium-poor pyroxene) is common for more than one-half of the interstitial olivine-bearing gabbros. Interstitial olivine-bearing Fe-Ti oxide gabbros often show modal and size layering or banding; plagioclase-poor, clinopyroxene- and opaque-rich bands are common. These gabbros are also characterized by well-developed igneous lamination which in most cases is parallel to the layering.

Olivine Fe-Ti Oxide Gabbro

Olivine Fe-Ti oxide gabbro is characterized by the presence of abundant, large, euhedral to subhedral olivine (Pl. 2, Fig. 5), suggesting that this olivine was a cumulus phase. Olivine Fe-Ti oxide gabbro consists of olivine clinopyroxene Fe-Ti oxides plagioclase, ±orthopyroxene, and +inverted pigeonite and can be easily discriminated from olivine gabbro and disseminated Fe-Ti oxide olivine gabbro by its evolved chemical nature and by the occurrence of much more abundant Fe-Ti oxides. Brown hornblende and apatite are common minor phases and zircon is present in some olivine Fe-Ti oxide gabbros. In rare cases, the modal abundance of apatite reaches 2%–4%, and it is present as an aggregate with Fe-Ti oxides. The modal abundance of olivine ranges from a few percent to 10%. Olivine also occurs as an interstitial phase that is commonly associated with Fe-Ti oxides. The modal abundance of Fe-Ti oxides ranges from a few percent to 20%. These oxides are anhedral, filling interstitial spaces between the silicate minerals. Inverted pigeonite is rarely present, but if present, is always in the core of clinopyroxene as an anhedral corroded grain. Orthopyroxene also is present, rimming euhedral olivine crystals. Layering is not developed in olivine Fe-Ti oxide gabbro, and the magmatic lamination is weak.

Olivine Fe-Ti Oxide Microgabbro

Olivine Fe-Ti oxide microgabbro consists mainly of olivine, clinopyroxene, plagioclase, and Fe-Ti oxides (Pl. 2, Fig. 6). Minor amounts of brown hornblende are also present. Calcium-poor pyroxenes are absent with the exception of irregular orthopyroxene patches in the clinopyroxene. Olivine is anhedral and commonly associated with Fe-Ti oxides. The microgabbro often exhibits layering and weak lamination. In medium-grained layers in contact with fine-grained layers, the olivine is clearly interstitial to clinopyroxene and plagioclase, indicating that the olivine Fe-Ti oxide microgabbro is a fine-grained interstitial olivine-bearing Fe-Ti oxide gabbro.

Downhole Petrographic Variation

Even though these Fe-Ti oxide gabbros occur mixed with olivine gabbros at various scales, they exhibit a regular pattern of downhole petrographic and mineral chemical variations. As the depth increases from Unit I to IV, the Fe-Ti oxide gabbros tend to become more evolved. Three major cycles can be identified (Fig. 3; Table 1). From Units I to IV, the types of gabbro change as follows: gabbronorite, olivine-bearing Fe-Ti oxide gabbro, olivine pigeonite gabbro, pigeonite gabbro (the first cycle), disseminated Fe-Ti oxide olivine gabbro, olivine gabbronorite, olivine pigeonite gabbro, pigeonite gabbro, olivine-bearing Fe-Ti oxide gabbro, and olivine Fe-Ti oxide gabbro (the second cycle) (Fig. 3, Table 1). Olivine Fe-Ti oxide gabbro, the most evolved Fe-Ti oxide gabbro, is in particular restricted to a 50-m thick zone of massive Fe-Ti oxide gabbro at the base of Unit IV. Below Unit V, the variation is more erratic but still shows the same downward tendency (the third cycle); gabbronorite, olivine gabbronorite, and disseminated Fe-Ti oxide olivine gabbro are present in the shallower levels (<400 mbsf), and olivine-bearing Fe-Ti oxide gabbro and olivine Fe-Ti oxide gabbro are present in the deeper levels (>400 mbsf, Fig. 3; Table 1).

Modal abundances of Fe-Ti oxides also show systematic downhole variations that follow the petrographic cycles mentioned above. Abundances increase from Unit I to the bottom of Unit II where pigeonite gabbro occurs. In Unit IIIB, where gabbronorite and disseminated Fe-Ti oxide olivine gabbro occur, the abundances abruptly decrease and then increase again until reaching a maximum in the middle of Unit IV, where pigeonite gabbro and olivine-bearing oxide gabbro occur. Near the bottom of Unit IV, the abundances of Fe-Ti oxides tend to decrease. Below Unit V, the abundances show a steady increase downward. Modal abundances of olivine increase from Unit I to Unit IV, where the proportion of olivine reaches 20%, with the exception of local concentrations (e.g., Sample 118-735B-20R-1, 111–114 cm). For Units V and VI, olivine tends to increase downward.

Fe-Ti oxide gabbros commonly exhibit magmatic lamination. This magmatic lamination is developed in Units III and IV (below 180 mbsf, down to 250 mbsf). In the Unit IV, the lamination is well-developed, but is very weak or absent near the bottom, where olivine Fe-Ti oxide gabbro is present. The lamination dips at 45° in Unit III. The dip of this lamination gradually decreases from 45° at the top of Unit IV to almost horizontal near the bottom of the unit (Robinson, Von Herzen, et al., 1989). The gradual decrease in the dips of magmatic lamination, deformational foliation, and stable magnetic inclination (all by ~40°) towards the bottom of Unit IV (Robinson, Von Herzen, et al., 1989) suggest a progressive rotation possibly due to faulting along the mylonite zone at the bottom of Unit IV.

The primary grain size of Fe-Ti oxide gabbros exhibits downhole variation (Table 1). The representative grain size (the most common grain size) of clinopyroxene ranges from 0.2 to 30 mm. Grain size ranges 2 to 10 mm in Unit I and upper half of Unit II, 2 to 30 mm in the bottom half of Unit II, and 0.2 to 20 mm in Units III and IV. Thus, the maximum grain size first increases downward and then reaches a maximum at ~130 mbsf, followed by a decrease to the bottom of Unit IV. The minimum grain size tends to decrease from Unit I to Unit IV. In Units V and VI, the grain size ranges from 0.3 to 10mm.

Fe-Ti oxide gabbro commonly shows size and/or modal banding on a scale of a few millimeters (Robinson, Von Herzen, et al., 1989). This type of banding is best developed in Units III and IV, where lamination is well developed (Table 1).

MINERAL CHEMISTRY

Minerals were analyzed by an electron microprobe analyzer (JEOL JCMA 733 Mk-II) at the Geological Institute, the University of Tokyo, under the following conditions: 2–3 μm beam size, 15 kV accelerating voltage, 1.2×10^{-8} A specimen current, and ZAF correction procedure. Other conditions are the same as those applied by Nakamura and Kushiro (1970). In the area analyses, the specimen stage was automatically driven at 20–150 μm/s. The pixel size ranged from 10 to 100 μm. The beam size ranged from 5 to 50 μm.

Major and minor element abundances in cumulus minerals in gabbros can be used as indicators of magma evolution, but first the effects of postcumulus crystallization and subsolidus reequilibration must be considered. In Hole 735B gabbros, subsolidus effects are probably negligible for all elements in plagioclase and most elements (except for Ca, Mg, and Fe) in clinopyroxene, because plagioclase and clinopyroxene exhibit magmatic zoning (rarely oscillatory) for these elements. Magnesium and iron in mafic minerals are most affected by subsolidus exchange reactions as indicated by the Mg-Fe distribution coefficients. However, the good correlations of Mg#s of all the mafic minerals indicate that the Mg#s can be used as a parameter of degree of the magma evolution.

Clinopyroxene grains are typically strongly zoned toward their rims. Core compositions, therefore, are more representative of cumulus compositions and better indicators of magma evolution. So most of the clinopyroxene analyses are of cores. Olivine is always fairly homogeneous so rims and cores have not been discriminated in the following discussion. The analyses of orthopyroxenes are of subhedral cumulus grains (in gabbronorite or olivine gabbronorite), hosts of inverted pigeonites (in olivine pigeonite gabbro or pigeonite gabbro), patchy grains (in Fe-Ti oxide gabbro), and interstitial grains (in olivine gabbro and troctolite). Plagioclase in the Fe-Ti oxide gabbros generally exhibits normal zoning, so most of the analyses are of cores. Average chemical compositions of olivine, plagioclase, clinopyroxene, and orthopyroxene are listed in Tables 3 to 6. In Table 2 average An mol% of plagioclase and Mg#s of mafic minerals are listed with the number of analyses for each mineral.

Relationships Between Rock Type and Mineral Chemistry

The mineral chemistry of Fe-Ti oxides gabbros from Hole 735B shows distinct correlation with rock types (modal variation) and textural characteristics (e.g., grain size and reaction texture). The An content in plagioclase and Mg# of mafic minerals decrease with overlap in the following order: gabbronorite, olivine gabbronorite, disseminated Fe-Ti oxide olivine gabbro, olivine pigeonite gabbro, pigeonite gabbro, interstitial olivine-bearing Fe-Ti oxide gabbro, and olivine Fe-Ti oxide gabbro (Fig. 5). Olivine Fe-Ti oxide microgabbros have similar mineral chemistries to olivine-bearing Fe-Ti oxide gabbros, but their plagioclase is slightly more An-rich. Olivine-bearing Fe-Ti oxide gabbros with relatively unevolved mineralogical characteristics often exhibit corona structures (Pl. 2, Fig. 4; Fig. 5). Gabbronorites and olivine pigeonite gabbros that exhibit intergrowths of calcium-poor pyroxene and Fe-Ti oxides (rarely surrounding olivine) have mineralogical characteristics similar to the less evolved olivine-bearing Fe-Ti oxide gabbros. The co-variation trend of An content in plagioclase and Mg# of mafic minerals for the gabbros from Hole 735B is nearly parallel to that of the layered series of the Skaergaard Intrusion (Wager and Brown, 1967; Naslund, 1976; Hoover, 1978), and is characterized by a rapid decrease in Mg# of mafic minerals for relatively evolved gabbros with smaller variations in the An content of plagioclase, compared with olivine gabbro and troctolite (Fig. 4). These facts suggest that the Fe-Ti oxide gabbros were derived from the same magma which formed the host troctolites and olivine gabbros.

The variation of mineral chemistry, reaction texture, and appearance and disappearance of minerals all indicate that as crystallization proceeds, the liquidus mafic phases vary as follows: orthopyroxene + clinopyroxene ± olivine, pigeonite + clinopyroxene ± orthopyroxene ± olivine, pigeonite + clinopyroxene, olivine + clinopyroxene. These changes in cumulus phase are similar to those observed in the Skaergaard Intrusion, although in Hole 735B, orthopyroxene was an important liquidus phase before pigeonite started to crystallize. Temporary cessation of olivine crystallization is suggested by either the complete absence of olivine (e.g., in pigeonite gabbros) or by the presence of interstitial olivine in place of isolated cumulus grains (e.g., in interstitial olivine-bearing Fe-Ti oxide gabbros). This reaction relationship and the disappearance of olivine has been documented experimentally in the system MgO-FeO-SiO_2 (Bowen and Schairer, 1935). The Fo content of olivine marking the disappearance and reappearance of olivine for Hole 735B is nearly the same as for the Skaergaard Intrusion; Fo = 50–52 and Fo = 40–45, respectively. The An content in plagioclase is, however, much more sodic than that of the Skaergaard Intrusion. The common occurrence of inverted pigeonite in the cores of clinopyroxenes in interstitial olivine-bearing Fe-Ti oxide gabbro suggests restricted adcumulus growth and extensive reaction between cumulus pigeonite and interstitial evolved melt occurred. The Mg# of mafic minerals marking the first appearance of pigeonite as a liquidus phase ranges from 60 to 70, which indicates that the temperature of a magma crystallizing pigeonite or olivine pigeonite gabbros was approximately 1050°C (Davidson and Lindsley, 1989).

Downhole Mineralogical Variations in the Fe-Ti Oxide Gabbros

The primary minerals in the Fe-Ti oxide gabbros show systematic downhole chemical variations consistent with the downhole distribution of rock types (Fig. 3). The An content in plagioclase and Mg# ($100 \times Mg/(Mg+Fe)$) of mafic minerals show positive correlations and tend to decrease from Unit I to the bottom of Unit IV, with two major cycles, which are characterized by progressive downward evolution (Fig. 3). These cycles are further subdivided into a few minor cycles. The start of each cycle is marked by an abrupt increase in An content and Mg# of mafic minerals. Within a cycle, those values decrease gradually until they abruptly increase again, and the next cycle begins (Fig. 3). The cycles identified in Units I to IV are:. (1) from 75 to 125 mbsf, (2) from 175to 184 mbsf, (3) from 195to 234 mbsf, (4) from 237to 260 mbsf, and (5) from 262 to 271 mbsf. In spite of these downward repetitions of mineral chemistry, An content and Mg# of mafic minerals show a steady decrease as a whole until the bottom of Unit IV is reached and olivine Fe-Ti oxide gabbro occurs, which contains the most sodic plagioclase (An_{30}) and the most iron-rich olivine (Fo_{30}) in Hole 735B (Fig. 3). Below Unit V, An content and Mg# of mafic minerals tend to decrease downward as in the case of Units I to IV. The downhole mineralogical variations of the Fe-Ti oxide gabbros are in marked contrast to those observed for the olivine gabbros and troctolites, which are characterized by two cycles showing a gradual downward increase in the An content of plagioclase and the Mg# of mafic minerals (Fig. 2).

Table 2. Average An mol% of plagioclase and magnesium of mafic minerals in gabbros from Hole 735B.

Core, section, interval (cm)	Depth (mbsf)	Rock type	Fo (mol%)	Fo SD	No. ol	An (mol%)	An SD	No. pl	XMg cpx	XMgc SD	No. cp	XMg opx	XMgo SD	No. op
118-735B-														
8D-1, 45–48	31.29	Ol gabbro			0	61.23	1.92	8	84.70	0.60	3			0
12R-1, 45–47	39.92	Gabbronorite			0	42.51	1.09	6	68.73	1.10	14	60.79	1.92	7
14R-1, 93–97	51.98	Inst of gabbro?			0	38.36	3.88	3	69.12	1.61	6	59.41	0.91	4
19R-5, 47–50	83.02	Gabbronorite			0	42.76	2.01	5	71.60	2.34	8	64.97	0.56	8
19R-5, 55–60	83.12	Gabbronorite			0	43.76	1.48	6	73.51	2.57	3	68.04	1.38	5
20R-1, 111–114	85.89	Pl wehrlite	53.73	0.95	4	38.04	1.47	5	70.78	1.35	4	63.46	0.82	4
21R-1-1, 82–89 OLGB	90.47	Ol gabbro			0	56.95	1.57	4	80.22	1.11	4			0
21R-1-2, 82–89 FETI	90.47	Inst of gabbro			0	38.33	1.23	5	69.93	1.05	3	61.80	0.44	3
21R-2, 27–32	91.06	Pig gabbro			0	36.23	1.68	5	70.10	0.86	3	60.52	0.52	5
21R-2, 49–51	91.38	Ol gabbro	75.43	1.12	4	59.20	1.78	4	83.12	0.79	9			0
22R-3, 118–120	99.00	Ol gabbro	73.81	1.61	5	59.17	2.60	6	81.31	1.88	7	78.15		1
23R-3, 33–37	102.61	Pig gabbro			0	36.74	1.89	5	69.40	1.23	9	64.54	1.16	7
24R-2, 95–97	107.94	Gabbronorite			0	33.87	1.03	6	65.42	2.92	7	56.28	2.90	3
24R-2, 120–126	108.20	Pig gabbro			0	36.24	0.40	4	69.66	0.83	4	60.69	1.02	4
27R-1-1, 26–33 OLGB	121.80	Ol gabbro			0	59.12	1.18	6	81.44	0.88	6			0
28R-1, 109–114	127.47	Pig gabbro			0	33.80	2.28	5	68.25	1.17	4	59.51	1.19	3
28R-3, 72–77	129.54	Pig gabbro			0	35.49	2.42	6	69.75	1.27	4	58.52	0.76	6
31R-2-1, 116–119 OLGB	145.94	Ol gabbro	75.50	0.40	4	59.25	1.07	4	84.23	0.55	2			0
31R-2, 120–122	145.96	Ol gabbro			0	57.75	2.58	6	82.78	2.47	6	73.75		0
34R-4, 8–12	163.23	Inst ol gb +r	54.67	1.36	6	42.63	1.64	13	69.27	1.11	15	60.83	0.62	9
36R-4, 5–9	174.80	Diss ox ol gb	60.17	2.87	7	41.34	1.68	8	74.32	2.06	6	65.24	0.12	2
37R-3-1, 71–76 OLGB	180.13	Ol gabbro			0	61.86	1.98	3	84.96	0.64	3			0
37R-3-2, 71–76 FETI	180.13	Diss ox ol gb	53.75	0.31	2	41.37	0.97	2	70.78	2.08	4	63.23	0.17	3
37R-3, 76–79	180.18	Ol pig gabbro	59.35	3.07	4	39.29	3.15	7	70.30	1.93	5	64.43	1.90	2
37R-3, 80–82	180.23	Ol pig gabbro			0	38.90	2.35	8	69.22	1.31	13	60.63	0.83	4
38R-3, 85–88	184.25	Ol pig gabbro			0	38.18	0.51	5	68.47	1.55	5	59.30	0.70	3
38R-4, 24–28	184.88	Ol pig gabbro	54.11	0.95	6	38.51	1.96	6	70.90	1.50	6	62.78	0.17	4
40R-5, 0–4	195.45	Ol gabbronort	60.30	0.88	6	43.74	3.67	6	73.84	1.78	4	66.18	0.35	5
40R-5, 4–8	195.49	Diss ox ol gb	59.00	1.85	10	42.99	2.31	8	72.20	1.36	4	62.65		1
43R-3, 95–102	209.45	Ol gabbronort	59.16	1.82	10	41.45	1.37	9	71.46	1.69	9	66.60	2.42	5
43R-4, 64–66	210.23	Diss ox ol gb	58.26	0.50	10	43.44	1.89	12	71.84	1.67	15	66.51	0.82	3
44R-1-1, 113–120 CLGB	212.13	Ol gabbro	80.40	0.52	3	64.28	0.29	3	85.92	0.45	3			0
44R-2, 16–24	212.37	Pig gabbro			0	36.15	1.10	4	67.52	0.61	4	58.32	1.94	4
45R-1, 5–12	216.07	Ol pig gabbro	53.53	1.17	4	39.31	1.38	7	68.01	1.71	4	62.13	1.14	5
46R-1-1, 48–58 OLGB	221.47	Ol gabbro			0	58.97	0.48	2	83.53		1			0
46R-1-2, 48–58 FETI	221.47	Diss ox ol gb?	58.96	0.56	8	41.40	1.07	11	72.38	0.91	9	63.25	0.94	4
46R-3, 121–128	224.68	Diss ox ol gb	52.79	1.52	11	41.17	1.93	12	70.26	1.49	11			0
46R-4, 109–113	225.83	Pig gabbro			0	37.94	0.86	6	70.36	2.08	4	61.13	1.24	3
47R-2, 117–127	228.52	Inst of gabbro	56.65	1.43	4	39.70	1.79	6	70.76	1.78	9	63.57		1
47R-3, 50–52 OLGB	229.20	Ol gabbro	79.83	0.44	7	63.97	1.30	8	85.17	0.46	4			0
47R-3, 56–61	229.26	Inst ob gb +r	49.90	0.54	5	38.82	1.30	8	69.46	1.05	10	61.14	1.84	6
47R-3-1, 143–149 OLGB	230.10	Ol gabbro	76.57	0.52	4	61.89	0.65	3	85.47	0.53	3			0
47R-3-2, 143–149 FETI	230.10	Inst of gabbro	51.67	0.28	2	36.04	1.00	10	69.14	1.47	7	57.81		1
48R-2, 56–65	232.80	Inst of gabbro			0	36.25	0.86	8	68.09	1.74	5	60.53	1.68	5
48R-2, 109–113	233.28	Ol feti microgb	46.98	2.30	8	37.44	1.71	7	66.55	1.90	8	55.07		1
48R-3, 112–116	234.53	Inst of gabbro	51.46	1.13	4	37.04	0.29	5	69.58	1.77	7	59.97	1.25	2
48R-4, 82–84	235.51	Inst of gabbro	48.52	1.76	4	37.56	1.36	12	67.82	0.98	15	59.01	0.93	4
49R-1, 42–46	236.34	Inst of gabbro	47.89	0.74	3	37.85	1.21	8	68.31	1.10	9	59.05	0.69	3
49R-2, 94–100	237.21	Inst ol gb +r	57.57	1.02	6	37.98	2.08	7	70.00	1.61	6	61.92	2.36	3
50R-2, 43–47	239.34	Inst of gabbro	52.11	1.68	6	38.59	2.63	11	68.81	1.07	7	60.00	0.58	4
50R-3, 62–67	240.82	Inst of gabbro	54.81	2.28	4	36.64	0.79	6	68.50	0.88	6	59.54	1.12	5
51R-1, 94–99	244.03	Inst of glabbro			0	37.77	0.81	4	67.50	0.50	7	58.03	2.03	9
51R-1, 99–103	244.09	Inst of glabbro	53.85	1.32	6	37.19	0.24	7	67.75	1.03	7	59.86	0.73	3
52R-1, 91–100	248.93	Inst of gb +r	47.65	2.14	10	36.55	2.10	10	67.83	1.15	12	57.95	1.06	4
52R-3, 121–123	251.60	Inst of gabbro	46.01	1.11	12	36.54	0.63	19	67.20	0.80	21	57.21	0.81	2
52R-4, 88–94	252.67	Inst of gabbro			0	35.96	1.19	8	63.84	1.24	8	53.83	1.10	2
53R-1, 47–54	253.45	Inst of gabbro	39.40	1.85	6	34.15	2.43	8	62.80	1.37	11			0
53R-1, 123–127	254.12	Inst of gabbro	43.63	0.52	3	33.65	1.56	7	63.18	0.86	5	51.93	0.83	2
53R-2, 31–39	254.55	Inst of gabbro			0	34.02	1.26	6	63.77	0.78	5	53.43	0.41	2
54R-1, 131–136	259.25	Ol feti gabbro	30.79	0.61	13	31.15	1.94	11	57.03	1.03	5	47.53	0.45	4
54R-3, 20–24	260.84	Ol feti gabbro	31.41	0.82	6	30.12	2.67	4	55.49	2.69	6	42.61	0.23	3
54R-3, 125–127	261.81	Ol feti gabbro	33.05	1.10	12	32.80	2.07	10	58.25	1.53	12	48.44	1.44	3
54R-5, 117–119	264.39	Inst of gabbro	41.39	2.29	7	37.84	1.66	7	65.79	2.13	7	56.90	1.56	4
55R-2, 101–105	267.50	Inst of gabbro	39.89	3.12	7	35.11	2.23	9	61.94	2.08	6	51.06	2.42	3
55R-2, 110–120	267.62	Ol feti gabbro	39.04	0.92	5	33.42	1.18	6	63.20	2.89	8	57.95		1
55R-3, 83–86	268.81	Ol feti gabbro	37.41	1.78	6	35.27	0.56	8	60.77	1.45	6	51.98		1
56R-2, 11–14	271.52	Ol feti gabbro	33.94	1.77	8	30.22	0.85	12	59.59	1.90	11	45.81	0.13	2
59R-3, 70–72	288.73	Ol gabbro	69.19	0.73	9	56.05	1.64	11	77.97	1.08	7	72.03	1.88	8
59R-4, 29–35	289.65	Ol gabbro	70.88	1.25	8	58.79	4.72	10	80.62	2.36	12	74.13	1.45	4
60R-1, 18–20	290.68	Ol gabbro	72.14	1.23	5	57.89	3.68	10	78.86	0.31	4	73.64	1.27	3
62R-4, 21–24	304.30	Ol gabbro	71.43	0.51	5	62.38	4.62	4	80.99	1.44	5	74.89	0.16	2
71R-2, 82–84	353.01	Ol gabbro	75.01	1.92	7	58.84	2.73	6	80.81	1.83	7	76.84	1.85	2
72R-5, 123–125	362.15	Ol gabbro	78.04	0.18	4	62.17	0.49	4	83.81	0.53	4			0
73R-3, 73–75	369.02	Ol gabbro	77.94	0.52	8	66.55	6.48	15	84.55	1.00	27	79.86	0.61	7
73R-4-1, 82–87 OLGB	370.23	Ol gabbro	77.88	0.41	6	60.67	2.06	6	82.95	0.72	5			0

Table 2 (continued).

Core, section, interval (cm)	Depth (mbsf)	Rock type	Fo (mol%)	Fo SD	No. ol	An (mol%)	An SD	No. pl	XMg cpx	XMgc SD	No. cp	XMg opx	XMgo SD	No. op
73R-4-2, 82–87 FETI	370.23	Gabbronorite			0	28.09	2.00	5	62.47	1.09	3	51.89	2.89	4
73R-5-1, 72–78 OLGB	371.58	Ol gabbro	74.13	0.57	3	59.06	2.20	6	84.68	0.72	5			0
73R-5-2, 72–78 FETI	371.58	Gabbronorite			0	31.80	2.04	5	67.73	2.41	8	60.43	0.34	2
73R-7-1, 0–5 OLGB	373.56	Ol gabbro	77.15	0.48	6	66.54	2.43	6			0			0
74R-6, 27–35	382.13	Poik gabbnort			0	41.24	2.84	10	69.44	0.96	9	63.43	0.54	5
76R-1-1, 63–70 OLGB	394.69	Ol gabbro	76.10	1.08	3	61.77	2.59	4	83.80	1.60	4	81.26		1
76R-1-2, 63–70 FETI	394.69	Gabbronorite	63.64	0.54	3	42.53	3.16	7	71.84	0.58	5	63.34	1.56	3
76R-1, 70–73 FETI	394.74	Gabbronorite			0	47.41	4.15	9	72.97	1.70	7	66.17	1.34	9
76R-1, 99–110 FETI	395.08	Gabbronorite			0	37.35	2.19	13	73.16	2.05	15	63.49	2.39	16
76R-3-1, 35–41 OLGB	397.06	Ol gabbro	75.86	0.59	5	60.31	1.93	6	84.07	1.74	2			0
76R-3-2, 35–41 FETI	397.06	Ol gabbronort	58.55	1.81	7	41.74	0.98	6	70.63	1.32	5	64.34		1
76R-4, 12–19	398.20	Gabbronorite	59.97	0.04	2	42.43	2.26	13	71.38	1.19	11	65.55	1.12	10
77R-2, 5–8	404.96	Diss ox ol gb	57.89	0.77	7	43.15	0.81	3	73.01	1.21	4			0
77R-2, 101–107	405.89	Ol gabbronort	56.87	0.72	9	40.64	1.50	7	71.42	1.02	15	64.68	1.11	5
79R-2-1, 55–61 OLGB	416.49	Ol gabbro	65.35	0.15	4	52.47	1.33	4	80.94	0.74	4			0
79R-7-1, 2–9 OLGB	422.82	Ol gabbro	82.03	0.62	8	74.01	5.07	12	88.05	1.12	5			0
79R-7-2, 2–9 FETI	422.82	Ol gabbronort	34.01	0.77	5	29.49	1.37	6	57.34	1.64	8			0
79R-7, 99–102	423.74	Troct. microgb	78.07	0.96	9	68.56	3.44	28	85.37	2.78	5			0
80R-3, 67–71	427.35	Ol feti gabbro	35.58	1.40	6	32.14	1.05	5	61.12	2.55	5	53.13	1.82	2
80R-6, 130–135	431.98	Ol feti gabbro	36.13	1.11	7	29.53	0.70	9	58.37	2.02	6	48.41	0.84	7
80R-7, 10–18	432.23	Ol feti microgb	34.55	1.41	6	34.11	1.27	8	61.39	1.34	7	50.87		1
80R-7, 23–25	432.32	Ol feti microgb	39.17	0.64	5	36.69	1.53	6	63.67	1.24	4	53.44	0.05	2
81R-5, 1–7	433.54	Ol gabbro	77.86	0.45	10	64.40	4.53	16	84.70	0.85	26	79.80		1
81R-7, 64–66	442.33	Ol gabbro	76.83	0.73	7	60.49	3.00	6	82.99	2.61	5			0
82R-3-1, 0–5 OLGB	445.72	Ol gabbro	80.61	0.49	4	64.82	2.01	9	87.45	0.74	7			0
82R-3-2, 0–5 FETI	445.72	Gabbronorite	43.22	1.15	3	30.02	0.79	3	56.93	2.66	9	47.15	2.12	10
83R-2, 3–9	453.86	Troctolite	82.58	0.14	8	66.85	2.60	9	86.58	0.46	6			0
83R-7, 77–81	460.84	Troctolite	84.20	0.74	11	72.44	4.07	10	88.91	1.21	8	86.57	0.16	2
86R-4, 123–130	486.60	Ol feti gabbro	42.90	0.93	6	36.03	1.34	9	64.71	1.33	4	55.43	1.58	4
86R-6, 143–145	489.57	Inst of gabbro	41.40	0.04	2	38.17	7.42	6	61.51	3.18	3	50.74	2.15	4

Note: The standard deviations and number of analyses for each specimen are also shown.

Abbreviations are: SD, standard deviation; Mg#, Mg/(Mg+Fe); cpx or cp, clinopyroxene; XMgc, Mg# of clinopyroxene; XMgo, Mg# of orthopyroxene; opx or op, orthopyroxene; No., number of analyses. Other abbreviations are the same as in Table 1. Contacting olivine gabbro and Fe-Ti oxide gabbro are indicated by "OLGB" and "FETI" in the interval column. Depth in meter below sea floor.

Minor Element Abundance in Constituent Minerals

Clinopyroxene

The TiO_2 content of clinopyroxene in olivine gabbro increases as the An content in plagioclase and Mg# of mafic minerals decrease (Fig. 6A). Clinopyroxene in troctolitic microgabbros exhibit a wide range in TiO_2 from 0.5 to 1.4 wt%, with averages for individual samples as high as 1.1 wt%. Clinopyroxenes in coarse troctolites exhibit a similar range in TiO_2 as those in olivine gabbros but on average individual samples have lower TiO_2 contents (<0.6 wt%). The TiO_2 content of clinopyroxene in the Fe-Ti oxide gabbros tends to decrease as An content in plagioclase and Mg# of mafic minerals decrease (Fig. 6A). TiO_2 contents in clinopyroxene cores reach a maximum in pigeonite gabbros and interstitial olivine-bearing Fe-Ti oxide gabbros, which are rich in Fe-Ti oxides. TiO_2 decreases remarkably as the Mg# decreases in interstitial olivine-bearing Fe-Ti oxide gabbros and olivine Fe-Ti oxide gabbros. Gabbronorite, olivine gabbronorite, and disseminated Fe-Ti oxide olivine gabbro, all of which are relatively poor in Fe-Ti oxide, show a slight increase in TiO_2 content of clinopyroxene as An content in plagioclase decreases.

For olivine gabbro and troctolite, the TiO_2 content of clinopyroxene markedly increases from the core to the rim, whereas in Fe-Ti oxide gabbro, the TiO_2 content is almost constant or decreases slightly. This change in the TiO_2 zoning pattern and the variation in TiO_2 content with Mg# can be explained by the crystallization of Fe-Ti oxides, which began during the crystallization of the gabbronorite and reached a maximum during the crystallization of pigeonite gabbro or interstitial olivine-bearing Fe-Ti oxide gabbro.

The Na_2O content of clinopyroxenes increases as the Mg# decreases from olivine gabbro to pigeonite gabbro (Fig. 6B). A further decrease in Mg# of clinopyroxene leads to a slight decrease in Na_2O content. The Na_2O content of clinopyroxene, consequently, reaches a maximum in the pigeonite gabbro, whose grain size is the largest among the Fe-Ti oxide gabbros. There is a consistent relationship between Na_2O content and the grain size of clinopyroxene; the Na_2O content increases with an increase in grain size. This relationship suggests that the Mg#-Na_2O relationship of clinopyroxene is controlled not only by magma composition but by sub-liquidus processes, such as adcumulus growth or reaction with trapped melt. The Na_2O content tends to be high in troctolite as compared to that for olivine gabbros.

The Al_2O_3 content of clinopyroxene decreases steadily from troctolite to olivine Fe-Ti oxide gabbro as the Mg# of clinopyroxene decreases; the clinopyroxene of the troctolite contains 3 to 4 wt% Al_2O_3, whereas that of the olivine Fe-Ti oxide gabbro contains only 1.0 to 1.6 wt% Al_2O_3 (Fig. 7A). This decrease in Al_2O_3 content is probably due to the fractionation of plagioclase in each batch of magma, which is consistent with the decrease in Al_2O_3 content in MORB glass with the decrease in MgO content (BVSP, 1981). Clinopyroxene in olivine gabbros showing vermicular intergrowth with orthopyroxene tends to be poor in Al_2O_3.

The MnO content in clinopyroxene shows a steady increase from troctolite to olivine Fe-Ti oxide gabbro, as Mg#s decrease; from 0.1 wt% for clinopyroxenes in troctolites to 0.5 wt% for those in olivine Fe-Ti oxide gabbros (Fig. 7B). The

Table 3. Average chemical composition of olivine in gabbros from Hole 735B.

Core, section, interval (cm)	Rock type	Olivine					
		SiO_2	FeO	MnO	MgO	CaO	NiO
118-735B-							
76R-4, 12–19	Gabbronorite	36.16	35.87	0.548	30.16	0.031	
		0.19	0.07	0.105	0.00	0.017	
40R-5, 0–4	Olivine gabbronorite	36.74	35.12	0.585	29.52	0.038	0.013
		0.12	0.44	0.061	0.28	0.022	0.026
43R-3, 95–102	Olivine gabbronorite	36.39	35.37	0.617	28.57	0.043	0.021
		0.42	1.43	0.049	1.16	0.009	0.036
76R-3, 34–41 CT	Olivine gabbronorite	36.40	35.41	0.598	28.07	0.038	0.006
		0.26	1.47	0.049	0.95	0.011	0.012
77R-2, 101–107	Olivine gabbronorite	36.26	37.09	0.651	27.44	0.029	
		0.16	0.76	0.032	0.33	0.016	
36R-4, 5–9	Dissem ox ol gabbro	36.76	35.31	0.691	28.85	0.041	
		0.17	1.46	0.038	1.06	0.015	
37R-3, 71–76 CT	Dissem ox ol gabbro	36.15	39.69	0.645	25.88	0.055	
		0.23	0.52	0.050	0.01	0.022	
40R-5, 4–8	Dissem ox ol gabbro	36.52	35.52	0.626	28.90	0.037	0.011
		0.33	1.46	0.067	1.06	0.023	0.011
43R-4, 64–66	Dissem ox ol gabbro	36.51	36.03	0.591	28.21	0.046	0.033
		0.23	0.39	0.038	0.37	0.015	0.023
46R-3, 121–128	Dissem ox ol gabbro	35.99	39.23	0.673	24.59	0.046	0.016
		0.25	1.10	0.061	0.99	0.023	0.027
77R-2, 5–8	Dissem ox ol gabbro	36.50	36.13	0.619	27.67	0.074	
		0.22	0.64	0.031	0.36	0.019	
20R-1, 111–114	Ol pigeonite gabbro	36.18	39.29	0.680	25.61	0.065	
		0.18	0.54	0.016	0.65	0.042	
37R-3, 76–79	Ol pigeonite gabbro	36.08	36.06	0.692	26.58	0.051	
		0.56	1.17	0.035	0.22	0.019	
38R-4, 24–28	Ol pigeonite gabbro	36.13	39.08	0.646	25.86	0.045	0.050
		0.16	0.68	0.048	0.64	0.007	0.042
45R-1, 5–12	Ol pigeonite gabbro	35.95	39.00	0.724	25.20	0.056	0.025
		0.18	1.27	0.093	0.50	0.023	0.029
47R-2, 117–127	Interst ol ox gabbro I	36.22	37.01	0.699	27.12	0.054	0.010
		0.18	1.79	0.053	0.30	0.017	0.013
47R-3, 143–149 CT	Interst ol ox gabbro I	36.40	36.88	0.579	27.68	0.037	0.024
		0.57	2.87	0.058	2.15	0.020	0.027
48R-3, 112–116	Interst ol ox gabbro I	35.80	40.98	0.688	24.36	0.059	0.030
		0.13	1.64	0.060	0.32	0.010	0.030
48R-4, 82–84	Interst ol ox gabbro I	35.10	42.21	0.628	22.33	0.046	0.008
		0.17	1.06	0.046	1.02	0.023	0.009
49R-1, 42–46	Interst ol ox gabbro I	35.41	41.19	0.666	23.01	0.054	0.013
		0.38	0.45	0.082	0.43	0.006	0.023
50R-2, 43–47	Interst ol ox gabbro I	36.12	39.96	0.670	24.64	0.048	
		0.33	1.06	0.038	1.07	0.011	
50R-3, 62–67	Interst ol ox gabbro I	35.99	38.67	0.634	26.32	0.047	0.009
		0.25	1.85	0.073	1.24	0.032	0.011
51R-1, 94–99	Interst ol ox gabbro I	36.08	39.30	0.705	25.73	0.051	0.001
		0.24	1.12	0.080	0.71	0.015	0.001
52R-3, 121–123	Interst ol ox gabbro I	35.06	44.15	0.713	21.11	0.031	0.016
		0.20	0.75	0.026	0.65	0.027	0.020
53R-1, 47–54	Interst ol ox gabbro I	34.54	48.50	0.879	17.71	0.037	
		0.43	0.89	0.083	1.08	0.026	
53R-1, 123–127	Interst ol ox gabbro I	34.75	45.82	0.877	19.90	0.030	0.008
		0.20	1.08	0.109	0.22	0.026	0.009
54R-5, 117–119	Interst ol ox gabbro I	34.29	46.65	0.827	18.50	0.069	0.002
		0.53	1.33	0.077	1.23	0.019	0.004
55R-2, 101–105	Interst ol ox gabbro I	34.10	46.87	0.883	17.48	0.078	0.007
		0.29	1.94	0.048	1.57	0.014	0.016
34R-4, 8–12	Interst ol ox gabbro II	36.04	38.17	0.681	25.84	0.051	0.019
		0.19	0.86	0.069	0.86	0.010	0.027
47R-3, 56–61	Interst ol ox gabbro II	35.44	41.77	0.796	23.34	0.055	
		0.24	0.66	0.051	0.20	0.022	
49R-2, 94–100	Interst ol ox gabbro II	36.57	37.02	0.635	28.11	0.045	0.033
		0.23	0.89	0.040	0.65	0.014	0.040
52R-1, 91–100	Interst ol ox gabbro II	35.11	43.56	0.696	21.91	0.066	0.034
		0.36	1.32	0.055	1.01	0.026	0.028
54R-1, 131–136	Olivine oxide gabbro	32.95	52.16	1.159	13.19	0.061	0.006
		0.14	0.40	0.044	0.20	0.031	0.011
54R-3, 20–24	Olivine oxide gabbro	33.39	54.03	1.125	12.93	0.093	0.007
		0.33	0.88	0.105	1.22	0.031	0.009
54R-3, 125–127	Olivine oxide gabbro	33.00	51.23	1.058	14.15	0.068	0.023
		0.31	0.49	0.039	0.49	0.021	0.021
55R-2, 110–120	Olivine oxide gabbro	34.07	48.51	0.943	17.43	0.064	0.003
		0.21	0.81	0.047	0.39	0.006	0.006
55R-3, 83–86	Olivine oxide gabbro	34.17	49.77	0.857	16.70	0.071	0.012
		0.29	0.93	0.036	0.95	0.010	0.013

Table 3 (continued).

Core, section, interval (cm)	Rock type	Olivine SiO$_2$	FeO	MnO	MgO	CaO	NiO
56R-2, 49–52	Olivine oxide gabbro	33.87	51.29	0.998	15.12	0.055	0.016
		0.29	1.03	0.034	0.89	0.012	0.017
56R-2, 49–52	Olivine oxide gabbro	33.57	51.94	1.041	14.74	0.047	0.010
		0.11	0.44	0.034	0.20	0.010	0.021
80R-3, 67–71	Olivine oxide gabbro	33.59	50.69	1.147	15.71	0.069	
		0.14	1.47	0.119	0.55	0.023	
80R-6, 130–135	Olivine oxide gabbro	34.00	50.68	1.181	16.09	0.067	
		0.21	1.00	0.041	0.55	0.017	
86R-4, 123–130	Olivine oxide gabbro	34.36	45.79	0.859	19.29	0.055	
		0.30	1.37	0.061	0.29	0.031	
48R-2, 109–113	Ol oxide microgabbro	35.32	43.52	0.705	21.66	0.051	0.036
		0.37	1.47	0.066	1.26	0.013	0.021
80R-7, 10–18	Ol oxide microgabbro	33.66	51.80	0.984	15.10	0.051	
		0.22	1.03	0.070	0.57	0.018	
80R-7, 23–25	Ol oxide microgabbro	33.74	47.71	0.721	17.40	0.052	0.026
		0.37	0.46	0.057	0.28	0.013	0.035
83R-7, 77–81	Troctolite	40.61	15.19	0.238	45.41	0.037	0.206
		0.14	0.68	0.028	0.50	0.011	0.032
83R-2, 3–9	Troctolite	40.18	16.75	0.276	44.56	0.054	
		0.20	0.15	0.051	0.22	0.021	
79R-7, 99–102	Troctolite	39.26	20.30	0.357	40.56	0.057	
		0.27	0.87	0.040	0.99	0.027	
80R-1, 41–45	Ol gabbro-Troctolite	39.79	17.49	0.301	43.13	0.042	0.152
		0.23	0.50	0.029	0.40	0.011	0.042
73R-3, 73–75	Vermic cpx ol gabbro	39.47	20.54	0.302	40.70	0.039	0.089
		0.19	0.52	0.028	0.30	0.015	0.033
81R-5, 1–7	Vermic cpx ol gabbro	39.37	20.58	0.294	40.61	0.039	0.093
		0.16	0.40	0.031	0.43	0.011	0.032
71R-2, 82–84	Vermic cpx ol gabbro	38.82	22.05	0.336	39.06	0.039	0.096
		0.11	0.23	0.028	0.41	0.010	0.039
81R-7, 64–66	Vermic cpx ol gabbro	38.95	21.24	0.295	39.87	0.033	0.060
		0.24	0.61	0.031	0.43	0.019	0.015
62R-4, 21–24	Olivine gabbro	38.74	26.24	0.415	36.50	0.062	
		0.10	0.54	0.047	0.34	0.008	
72R-5, 123–125	Olivine gabbro	39.78	20.81	0.317	41.49	0.058	
		0.19	0.39	0.024	0.35	0.023	
59R-4, 29–35	Olivine gabbro	38.56	26.45	0.414	36.13	0.047	0.082
		0.26	0.96	0.042	0.96	0.016	0.029
21R-2, 49–51	Olivine gabbro	38.44	22.04	0.325	37.90	0.034	0.094
		0.41	0.60	0.047	1.21	0.011	0.045
60R-1, 18–20	Olivine gabbro	38.28	25.65	0.389	35.78	0.039	0.062
		0.26	0.58	0.042	1.04	0.007	0.020
59R-3, 70–72	Olivine gabbro	38.25	27.90	0.411	35.14	0.043	0.070
		0.06	0.61	0.049	0.51	0.014	0.028

Note: Standard deviations are also shown below the average of oxide weight percent.
Abbreviations are: dissem ox ol gabbro, disseminated Fe-Ti oxide olivine gabbro; ol pigeonite gabbro, olivine pigeonite gabbro; interst ol ox gabbro I, interstitial olivine-bearing Fe-Ti oxide gabbro; olivine oxide gabbro, olivine Fe-Ti oxide gabbro; ol oxide microgabbro, olivine Fe-Ti oxide microgabbro; ol gabbro, olivine gabbro; vermic cpx ol gabbro, vermicular clinopyroxene olivine gabbro; CT, near contacts between Fe-Ti oxide gabbro and olivine gabbro.

MnO content in both olivine and orthopyroxene also increases as Mg#s decrease.

The Cr_2O_3 content markedly decreases as the Mg# of clinopyroxene decreases as rock types change from troctolite to olivine gabbro (Fig 7C). The content of Cr_2O_3 is less than 0.1 wt% for all of the Fe-Ti oxide gabbros. This remarkable decrease can be explained by early-stage fractionation of chromian spinel and clinopyroxene, as observed in troctolite and magnesian olivine gabbros (Robinson, Von Herzen, et al., 1989).

Orthopyroxene

As in the case of clinopyroxene, the Al_2O_3 content of orthopyroxene decreases as its Mg# decreases (Fig. 8B). In olivine gabbro, orthopyroxenes contain up to 2.0 wt% Al_2O_3, whereas they contain less than 0.5 wt% Al_2O_3 in the most evolved olivine Fe-Ti oxide gabbro. The MnO content of orthopyroxene increases steadily from 0.2 wt% in troctolites to 1.0 wt% in olivine Fe-Ti oxide gabbros as the Mg# decreases (Fig. 8C). The TiO_2 content of orthopyroxene shows a similar variation to that in clinopyroxene; as the Mg# decreases, it reaches a maximum in pigeonite gabbros and olivine pigeonite gabbros (up to 0.4 wt%) and then decreases in interstitial olivine-bearing Fe-Ti oxide gabbros and olivine Fe-Ti oxide gabbros (Fig. 8A). In the olivine Fe-Ti oxide gabbros the TiO_2 content is less than 0.2 wt%. The Cr_2O_3 contents of orthopyroxenes show the same variation as those in clinopyroxenes; decreasing from 0.25 wt% in troctolites to less than 0.1 wt% in Fe-Ti oxide gabbros.

Plagioclase

Plagioclase in Fe-Ti oxide gabbros commonly appears dusty in thin section in plane light (Pl. ', Fig. 2). The dusty appearance is due to the abundance of tiny exsolution lamellae of opaque iron oxides, suggesting that the plagioclase in Fe-Ti

Table 4. Average chemical composition of plagioclase in gabbros from Hole 735B.

Core, section, interval (cm)	Rock type	Plagioclase (wt%)					
		SiO_2	Al_2O_3	Fe_2O_3	CaO	Na_2O	K_2O
118-735B-							
12R-1, 45–47	Gabbronorite	58.57	26.29	0.190	8.40	6.20	0.116
		0.29	0.27	0.052	0.16	0.23	0.021
19R-5, 47–50	Gabbronorite	58.40	26.16	0.189	8.19	6.67	0.060
		0.81	0.59	0.045	0.72	0.42	0.039
19R-5, 55–60	Gabbronorite	58.32	27.14	0.159	8.96	6.29	0.112
		0.35	0.16	0.056	0.29	0.26	0.024
74R-6, 27–35	Gabbronorite	58.62	26.05	0.301	8.17	6.35	0.138
		0.60	0.32	0.120	0.52	0.40	0.019
76R-4, 12–19	Gabbronorite	56.74	26.36	0.322	8.58	6.49	0.088
		0.50	0.41	0.134	0.38	0.21	0.023
40R-5, 0–4	Olivine gabbronorite	57.41	26.49	0.223	8.72	6.13	0.107
		0.80	0.61	0.066	0.67	0.46	0.012
43R-3, 95–102	Olivine gabbronorite	57.80	26.04	0.171	8.26	6.38	0.098
		0.57	0.17	0.032	0.25	0.20	0.014
76R-3, 34–41 CT	Olivine gabbronorite	58.15	26.02	0.179	8.31	6.34	0.111
		0.48	0.27	0.053	0.16	0.18	0.015
77R-2, 101–107	Olivine gabbronorite	58.29	26.08	0.195	8.19	6.55	0.099
		0.27	0.26	0.043	0.31	0.24	0.018
36R-4, 5–9	Dissem ox ol gabbro	58.10	26.60	1.183	8.41	6.56	0.055
		0.32	0.21	0.122	0.36	0.23	0.032
37R-3, 71–76 CT	Dissem ox ol gabbro	58.95	26.52	0.117	8.29	6.35	0.099
		0.28	0.04	0.097	0.10	0.18	0.042
40R-5, 4–8	Dissem ox ol gabbro	57.59	26.31	0.249	8.52	6.18	0.108
		0.57	0.29	0.214	0.40	0.30	0.018
43R-4, 64–66	Dissem ox ol gabbro	57.62	26.49	0.179	8.84	6.31	0.083
		0.57	0.43	0.045	0.40	0.21	0.014
46R-3, 121–128	Dissem ox ol gabbro	58.74	26.20	0.226	8.29	6.48	0.104
		0.60	0.37	0.105	0.40	0.20	0.036
77R-2, 5–8	Dissem ox ol gabbro	58.46	26.48	0.173	8.59	6.20	0.093
		0.54	0.22	0.072	0.58	0.13	0.020
20R-1, 111–114	Ol pigeonite gabbro	59.30	25.59	0.105	7.47	6.74	0.072
		0.67	0.43	0.051	0.29	0.21	0.035
37R-3, 76–79	Ol pigeonite gabbro	58.49	26.12	0.198	8.01	6.79	0.076
		0.75	0.40	0.144	0.59	0.43	0.034
37R-3, 80–82	Ol pigeonite gabbro	58.23	25.67	0.136	7.76	6.69	0.078
		0.76	0.35	0.042	0.48	0.26	0.050
38R-3, 85–88	Ol pigeonite gabbro	57.45	25.24	0.231	7.69	6.83	0.097
		0.24	0.11	0.059	0.02	0.24	0.028
38R-4, 24–28	Ol pigeonite gabbro	58.71	25.80	0.126	7.70	6.72	0.105
		0.47	0.30	0.050	0.43	0.20	0.040
45R-1, 5–12	Ol pigeonite gabbro	58.89	25.66	0.207	7.78	6.55	0.144
		0.40	0.26	0.064	0.30	0.21	0.013
21R-2, 27–32	Pigeonite gabbro	60.13	25.71	0.208	7.41	7.10	0.155
		0.38	0.08	0.079	0.47	0.23	0.031
23R-3, 34–37	Pigeonite gabbro	58.71	25.54	0.206	7.77	6.89	0.100
		0.48	0.27	0.049	0.27	0.21	0.044
24R-2, 120–126	Pigeonite gabbro	59.55	25.45	0.149	7.42	7.15	0.090
		0.26	0.15	0.069	0.16	0.14	0.027
28R-1, 109–114	Pigeonite gabbro	59.95	25.12	0.176	6.93	7.42	0.137
		0.41	0.35	0.053	0.48	0.29	0.054
28R-3, 72–77	Pigeonite gabbro	59.53	25.52	0.166	7.27	7.24	0.172
		0.61	0.58	0.038	0.46	0.27	0.019
44R-2, 16–24	Pigeonite gabbro	59.24	24.88	0.138	7.37	7.05	0.214
		0.35	0.28	0.049	0.28	0.15	0.076
46R-4, 109–113	Pigeonite gabbro	59.76	25.36	0.239	7.52	6.71	0.134
		0.49	0.24	0.203	0.07	0.22	0.020
14R-1, 93–97	Interst ol ox gabbro I	59.17	25.79	0.149	7.62	6.67	0.129
		1.11	0.69	0.087	0.80	0.38	0.050
21R-1, 82–89 CT	Interst ol ox gabbro I	60.01	25.58	0.132	7.61	6.73	0.073
		0.14	0.16	0.096	0.14	0.36	0.053
47R-2, 117–127	Interst ol ox gabbro I	58.56	26.07	0.149	7.95	6.57	0.135
		0.24	0.14	0.077	0.32	0.35	0.016
47R-3, 143–149 CT	Interst ol ox gabbro I	59.23	25.69	0.205	7.54	7.22	0.099
		0.32	0.19	0.089	0.21	0.24	0.041
48R-2, 56–65	Interst ol ox gabbro I	60.06	25.58	0.211	7.30	7.01	0.135
		0.34	0.23	0.047	0.22	0.11	0.023
48R-3, 112–116	Interst ol ox gabbro I	59.64	25.67	0.141	7.50	6.94	0.155
		0.16	0.06	0.042	0.14	0.06	0.021
48R-4, 82–84	Interst ol ox gabbro I	59.55	25.37	0.167	7.47	6.80	0.094
		0.59	0.32	0.079	0.27	0.26	0.041
49R-1, 42–46	Interst ol ox gabbro I	59.40	25.41	0.231	7.52	6.74	0.122
		0.48	0.44	0.092	0.26	0.15	0.036
50R-2, 43–47	Interst ol ox gabbro I	60.17	25.77	0.210	7.65	6.69	0.097
		0.97	0.43	0.088	0.52	0.30	0.044

Table 4 (continued).

Core, section, interval (cm)	Rock type	Plagioclase (wt%)					
		SiO_2	Al_2O_3	Fe_2O_3	CaO	Na_2O	K_2O
50R-3, 62–67	Interst ol ox gabbro I	59.23	25.16	0.408	7.20	6.78	0.144
		0.65	0.26	0.667	0.12	0.22	0.019
51R-1, 94–99	Interst ol ox gabbro I	59.32	25.28	0.190	7.56	6.63	0.161
		0.68	0.06	0.075	0.14	0.42	0.025
51R-1, 99–103	Interst ol ox gabbro I	60.02	25.50	0.229	7.38	6.80	0.138
		0.32	0.16	0.108	0.17	0.11	0.016
52R-3, 121–123	Interst ol ox gabbro I	59.71	25.60	0.134	7.51	7.15	0.094
		0.41	0.17	0.043	0.10	0.13	0.034
52R-4, 88–94	Interst ol ox gabbro I	60.25	25.16	0.262	7.01	7.03	0.101
		0.43	0.36	0.166	0.39	0.20	0.053
53R-1, 47–54	Interst ol ox gabbro I	61.16	24.98	0.166	6.71	7.06	0.143
		0.38	0.31	0.055	0.39	0.37	0.030
53R-1, 123–127	Interst ol ox gabbro I	60.67	24.96	0.166	6.63	7.13	0.133
		0.44	0.27	0.093	0.34	0.19	0.034
53R-2, 31–39	Interst ol ox gabbro I	59.56	24.89	0.286	6.71	7.29	0.115
		0.69	0.35	0.269	0.25	0.23	0.041
54R-5, 117–119	Interst ol ox gabbro I	59.35	25.37	0.180	7.59	6.82	0.113
		0.45	0.53	0.047	0.39	0.16	0.037
55R-2, 101–105	Interst ol ox gabbro I	59.91	25.12	0.173	7.08	7.14	0.143
		0.60	0.40	0.072	0.43	0.30	0.041
82R-6, 73–78	Interst ol ox gabbro I	59.82	25.31	0.154	7.25	6.89	0.124
		0.59	0.38	0.052	0.35	0.26	0.026
34R-4, 8–12	Interst ol ox gabbro II	58.41	26.16	0.272	8.41	6.19	0.109
		0.67	0.34	0.101	0.33	0.36	0.040
47R-3, 56–61	Interst ol ox gabbro II	59.13	25.74	0.243	7.75	6.66	0.134
		0.35	0.26	0.207	0.24	0.22	0.018
49R-2, 94–100	Interst ol ox gabbro II	59.15	25.70	0.291	7.58	6.74	0.153
		0.66	0.44	0.185	0.45	0.26	0.027
52R-1, 91–100	Interst ol ox gabbro II	58.98	25.79	0.244	7.54	7.17	0.110
		0.46	0.49	0.139	0.39	0.33	0.075
54R-1, 131–136	Olivine oxide gabbro	60.92	24.15	0.281	6.08	7.47	0.191
		0.55	0.29	0.176	0.23	0.15	0.081
54R-3, 20–24	Olivine oxide gabbro	61.67	24.38	0.181	5.94	7.46	0.240
		0.87	0.44	0.094	0.53	0.27	0.043
54R-3, 125–127	Olivine oxide gabbro	59.80	24.65	0.242	6.55	7.36	0.098
		0.64	0.31	0.111	0.38	0.28	0.044
55R-2, 110–120	Olivine oxide gabbro	60.27	24.98	0.162	6.71	7.28	0.169
		0.22	0.07	0.039	0.31	0.25	0.019
55R-3, 83–86	Olivine oxide gabbro	59.94	25.27	0.187	7.07	7.08	0.137
		0.27	0.20	0.064	0.13	0.14	0.045
56R-2, 11–14	Olivine oxide gabbro	62.25	24.48	0.227	6.12	7.68	0.115
		0.44	0.19	0.126	0.16	0.20	0.065
56R-2, 49–52	Olivine oxide gabbro	60.71	24.56	0.225	6.22	7.36	0.141
		0.31	0.28	0.050	0.43	0.27	0.055
80R-3, 67–71	Olivine oxide gabbro	61.07	24.33	0.169	6.36	7.30	0.185
		0.35	0.32	0.041	0.19	0.25	0.038
80R-6, 130–135	Olivine oxide gabbro	61.08	24.31	0.229	5.92	7.69	0.181
		0.36	0.16	0.051	3.27	0.24	0.019
86R-4, 123–130	Olivine oxide gabbro	59.63	25.25	0.261	7.31	7.06	0.171
		0.21	0.23	0.217	0.28	0.23	0.037
48R-2, 109–113	Ol oxide microgabbro	59.86	25.61	0.182	7.58	6.67	0.103
		0.37	0.36	0.054	0.30	0.72	0.037
80R-7, 10–18	Ol oxide microgabbro	59.83	25.15	0.185	7.03	7.43	0.115
		0.25	0.27	0.091	0.25	0.25	0.036
80R-7, 23–25	Ol oxide microgabbro	59.33	25.14	0.140	7.36	6.97	0.083
		0.51	0.15	0.054	0.25	0.29	0.025
83R-7, 77–81	Troctolite	50.77	31.70	0.106	14.66	3.06	0.027
		1.06	0.70	0.044	0.93	0.44	0.009
83R-2, 3–9	Troctolite	52.02	30.74	0.073	13.29	3.68	0.025
		0.86	0.51	0.048	0.54	0.37	0.017
79R-7, 99–102	Troctolite	51.05	30.77	0.131	13.75	3.47	0.027
		0.87	0.46	0.125	0.60	0.42	0.011
80R-1, 41–45	Troctolite-Ol gabbro	51.63	30.58	0.126	13.60	3.50	0.042
		1.20	0.92	0.073	0.91	0.46	0.021
73R-3, 73–75	Vermic cpx ol gabbro	52.14	30.09	0.191	13.36	3.71	0.038
		1.41	1.02	0.052	1.11	0.60	0.016
81R-5, 1–7	Vermic cpx ol gabbro	52.39	30.19	0.173	12.91	3.93	0.042
		1.15	0.61	0.120	0.73	0.56	0.024
71R-2, 82–84	Vermic cpx ol gabbro	53.33	29.03	0.236	11.99	4.59	0.072
		0.73	0.59	0.55	0.58	0.29	0.019
81R-7, 64–66	Vermic cpx ol gabbro	52.77	29.53	0.090	12.22	4.40	0.026
		0.63	0.60	0.035	0.58	0.35	0.007
62R-4, 21–24	Olivine gabbro	53.64	21.90	0.285	12.56	4.15	0.057
		0.98	0.77	0.042	0.87	0.54	0.011

Table 4 (continued).

Core, section, interval (cm)	Rock type	Plagioclase (wt%)					
		SiO_2	Al_2O_3	Fe_2O_3	CaO	Na_2O	K_2O
72R-5, 123–125	Olivine gabbro	52.42	30.06	0.240	12.49	4.16	0.056
		0.23	0.09	0.051	0.22	0.07	0.009
59R-4, 29–35	Olivine gabbro	54.29	29.27	0.306	11.98	4.59	0.074
		1.32	0.80	0.077	0.98	0.52	0.029
8D-1, 45–48	Olivine gabbro	53.27	29.73	0.138	12.38	4.32	0.023
		0.55	0.33	0.081	0.39	0.23	0.024
22R-3, 118–120	Olivine gabbro	53.54	29.02	0.137	11.78	4.47	0.030
		0.62	0.36	0.049	0.47	0.31	0.017
21R-2, 49–51	Olivine gabbro	53.70	28.74	0.123	11.56	4.46	0.029
		0.13	0.18	0.050	0.11	0.32	0.025
60R-1, 18–20	Olivine gabbro	53.64	28.79	0.306	11.72	4.67	0.059
		0.92	0.70	0.087	0.72	0.42	0.020
31R-2, 120–122	Olivine gabbro	54.32	29.02	0.126	11.51	4.63	0.043
		0.39	0.35	0.035	0.50	0.31	0.023
59R-3, 70–72	Olivine gabbro	55.00	28.70	0.281	11.15	4.79	0.064
		0.38	0.32	0.090	0.29	0.21	0.014

Note: Standard deviations are also shown below the average of oxide weight percent. Abbreviations are the same as in Table 3.

oxide gabbros contains abundant iron, which exsolved as iron oxide during cooling. This is reflected in the plagioclase analyses; in spite of erratic FeO content (because the EPMA analyses were made with a focused beam), it increases as the An content decreases. The K_2O content in plagioclase increases from 0.02 wt% to 0.2 wt% as An content decreases (Fig. 9).

Olivine

The MnO content in olivine steadily increases as a linear function of Fo mol% (Fig. 10B), from 0.2 wt% in troctolites to 1.4 wt% in olivine Fe-Ti oxide gabbros. The MnO variation is quite similar to that in pyroxenes. The NiO content decreases exponentially as Fo content decreases (Fig. 10A), from 0.2 wt% in troctolites to less than 0.04 wt% in all the Fe-Ti oxide gabbros. The variation is due to the fractionation of olivine into which Ni is strongly partitioned compared to silicate melt.

Amphibole

Reddish brown to pale brown amphibole is always present as a minor phase occurring in interstitial areas with Fe-Ti oxides or as inclusions in clinopyroxene. It shows the chemical variations consistent with other silicate phases. This fact and the difference in its mode of occurrence from obviously metamorphic amphiboles suggest that amphibole is magmatic.

The TiO_2 contents of amphiboles show the same variation pattern as in pyroxenes; as Mg# of amphibole decreases, it first increases from troctolite (1 wt%) to gabbronorite (2–4 wt%) and reaches a maximum (up to 5 wt%) for pigeonite gabbro or interstitial olivine-bearing Fe-Ti oxide gabbro, followed by a rapid decrease in olivine Fe-Ti oxide gabbro (4–1 wt%). The K_2O content of amphibole tends to increase very slightly as the Mg# decreases. It reaches a maximum in pigeonite gabbros and interstitial olivine bearing gabbros (0.5–1 wt%) and decreases slightly in olivine Fe-Ti oxide gabbros. The Na_2O contents in amphiboles increase as Mg#s decrease, and is highest in pigeonite gabbros. The Cr_2O_3 contents of amphiboles decrease exponentially with decreasing Mg#, from 2 wt% in troctolites to less than 0.1 wt% in Fe-Ti oxide gabbros. MnO contents in amphiboles increase steadily as Mg#s decrease down to 0.4 wt% in olivine Fe-Ti oxide gabbros. Al_2O_3 contents in amphiboles decrease with decreasing Mg#.

Ilmenite

The MgO content of ilmenite in Fe-Ti oxide gabbros tends to decrease from 2–3 wt% in disseminated Fe-Ti oxide olivine gabbros and olivine gabbronorites to less than 1 wt% in olivine Fe-Ti oxide gabbros as the Mg# of mafic minerals and An content of plagioclase decrease.

RELATIONSHIPS BETWEEN FE-TI OXIDE AND OLIVINE GABBROS

In Hole 735B, Fe-Ti oxide gabbros are commonly found adjacent to and cross-cutting olivine gabbros with sharp contacts between the two (Pl. 3, Figs. 1 and 2). These contacts are marked by abrupt changes in modal mineralogy including the appearance of Fe-Ti oxides in the Fe-Ti oxide gabbro, changes in clinopyroxene morphology, and changes in mineral chemistry (Pl. 3).

Fe-Ti oxide gabbros tend to be more deformed more than the olivine gabbros, possibly because of the presence of abundant Fe-Ti oxides which are more easily deformed than the silicates. For example, centimeter-thick bands of Fe-Ti oxide gabbro are porphyroclastic or mylonitic, whereas the host olivine gabbro shows only minor deformation marked by the presence of wavy extinction in plagioclase and kink bands in olivine. In one such sample, element concentration maps indicate a sharp contact that has not been affected by plastic deformation at all, clearly indicating that deformation took place after the two gabbros were juxtaposed by a magmatic process.

The contacts are generally gently inclined or horizontal, but vertical or steeply dipping contacts are also present. (e.g., Sample 118-735B-82R-3, 0–9 cm). About 1-cm to 1-mm thick veins of Fe-Ti oxide gabbro are observed locally to branch out from thicker Fe-Ti oxide gabbros (e.g., Samples 118-735B-82R-3, 0–9 cm and 47R-3, 143–149 cm). Map analyses of these boundaries indicate that Mg#s of mafic minerals and An content in plagioclase show marked variations within the host olivine gabbro, whereas they are fairly homogeneous in the Fe-Ti oxide gabbro. Across the contacts, there are very steep gradients in chemical plagioclase composition which occur within a few mm of the contacts, (Fig. 11) but more gradual gradients in the Mg# of mafic phases which occur over a distance of several centimeters. Similar gradients in mineral compositions have been observed across contacts in other gabbros from the Southwest Indian Ridge by Meyer et al.

Table 5. Average chemical composition of clinopyroxene in gabbros from Hole 735B.

Core, section, interval (cm)	Rock type	Clinopyroxene											
		SiO_2	Al_2O_3	TiO_2	FeO	MnO	MgO	CaO	Na_2O	Cr_2O_3	Wo	En	Fs
118-735B-													
37R-3, 80–82	Ol pigeonite gabbro	51.20	1.922	0.604	10.88	0.352	13.29	20.20	0.428	0.006	0.428	0.392	0.180
		0.41	0.308	0.121	0.74	0.025	0.15	0.66	0.039	0.08	0.014	0.003	0.012
38R-3, 85–88	Ol pigeonite gabbro	50.44	1.900	0.666	11.29	0.317	13.62	20.00	0.443	0.000	0.419	0.397	0.184
		0.37	0.389	0.227	0.88	0.071	0.11	0.70	0.088	0.001	0.013	0.003	0.014
38R-4, 24–28	Ol pigeonite gabbro	52.27	1.717	0.514	10.51	0.304	14.09	20.11	0.393	0.005	0.420	0.409	0.171
		0.32	0.121	0.083	0.99	0.045	0.36	1.37	0.021	0.012	0.027	0.013	0.017
45R-1, 5–12	Ol pigeonite gabbro	51.69	2.127	0.773	12.03	0.426	13.86	18.51	0.384	0.009	0.393	0.409	0.199
		0.45	0.417	0.151	1.15	0.022	0.91	1.48	0.096	0.016	0.037	0.021	0.016
21R-2, 27–32	Pigeonite gabbro	52.75	2.294	0.779	10.08	0.353	13.26	20.72	0.620	0.007	0.441	0.392	0.167
		0.06	0.141	0.121	0.34	0.04	0.31	0.52	0.026	0.012	0.011	0.010	0.005
23R-3, 34–37	Pigeonite gabbro	51.80	2.185	0.721	10.24	0.341	13.43	20.42	0.541	0.007	0.434	0.397	0.170
		0.27	0.151	0.051	0.39	0.058	0.25	0.78	0.054	0.007	0.014	0.009	0.007
24R-2, 120–126	Pigeonite gabbro	51.75	2.236	0.886	10.31	0.33	13.16	20.55	0.551	0.033	0.438	0.390	0.172
		0.21	0.254	0.057	0.54	0.005	0.16	0.24	0.060	0.039	0.009	0.002	0.008
28R-1, 109–114	Pigeonite gabbro	51.87	1.838	0.752	11.14	0.418	12.91	20.42	0.520	0.030	0.434	0.382	0.185
		0.13	0.063	0.115	0.33	0.012	0.15	0.07	0.058	0.008	0.003	0.000	0.003
28R-3, 72–77	Pigeonite gabbro	52.35	1.717	0.659	10.56	0.339	13.16	20.33	0.531	0.030	0.434	0.391	0.176
		0.00	0.000	0.000	0.00	0	0.00	0.00	0.000	0.000	0.000	0.000	0.000
44R-2, 16–24	Pigeonite gabbro	51.19	2.068	0.846	10.90	0.361	12.78	20.27	0.556	0.001	0.435	0.382	0.183
		0.18	0.112	0.128	0.33	0.011	0.23	0.43	0.052	0.002	0.005	0.001	0.006
46R-4, 109–113	Pigeonite gabbro	51.94	2.335	0.794	10.32	0.35	13.23	19.94	0.571	0.015	0.430	0.397	0.174
		0.27	0.023	0.141	0.97	0.031	0.07	0.13	0.016	0.021	0.008	0.007	0.014
14R-1, 93–97	Interst ol ox gabbro I	51.75	2.272	0.677	10.36	0.317	13.24	21.01	0.423	0.017	0.442	0.388	0.170
		0.38	0.159	0.082	0.59	0.031	0.22	0.51	0.052	0.020	0.007	0.004	0.010
21R-1, 82–89 CT	Interst ol ox gabbro I	51.90	2.172	0.705	10.32	0.334	13.45	20.39	0.534	0.011	0.432	0.397	0.171
		0.11	0.046	0.045	0.56	0.044	0.06	0.096	0.053	0.009	0.014	0.007	0.010
47R-2, 117–127	Interst ol ox gabbro I	51.40	2.400	0.902	9.80	0.318	13.51	19.95	0.559	0.004	0.430	0.405	0.165
		0.23	0.111	0.057	0.86	0.023	0.37	0.40	0.051	0.009	0.012	0.011	0.013
47R-3, 143–149 CT	Interst ol ox gabbro I	51.85	2.185	0.708	10.92	0.305	13.45	19.98	0.509	0.004	0.423	0.396	0.181
		0.13	0.228	0.109	0.53	0.029	0.31	0.57	0.077	0.006	0.013	0.008	0.009
48R-2, 56–65	Interst ol ox gabbro I	52.08	2.112	0.746	11.73	0.354	13.30	20.07	0.444	0.013	0.420	0.388	0.192
		0.02	0.009	0.011	0.63	0.011	0.18	0.88	0.017	0.018	0.017	0.006	0.011
48R-3, 112–116	Interst ol ox gabbro I	51.78	2.011	0.669	11.18	0.337	13.16	20.06	0.457	0.030	0.426	0.389	0.185
		0.06	0.263	0.117	0.54	0.05	0.06	0.36	0.065	0.043	0.008	0.003	0.008
48R-4, 82–84	Interst ol ox gabbro I	51.25	1.955	0.633	11.00	0.33	12.77	20.01	0.421	0.014	0.432	0.383	0.185
		0.25	0.184	0.069	0.74	0.056	0.71	0.75	0.068	0.015	0.023	0.016	0.009
12R-1, 45–47	Gabbronorite	52.29	1.682	0.457	10.70	0.314	13.32	21.04	0.350	0.010	0.439	0.387	0.174
		0.24	0.274	0.084	0.54	0.039	0.21	0.29	0.061	0.012	0.007	0.005	0.008
19R-5, 47–50	Gabbronorite	52.43	1.699	0.500	8.97	0.258	14.05	21.57	0.382	0.031	0.448	0.406	0.146
		0.43	0.189	0.118	0.34	0.03	0.20	0.42	0.039	0.035	0.005	0.002	0.007
19R-5, 47–50	Gabbronorite	51.95	1.820	0.492	11.14	0.358	13.23	20.07	0.412	0.018	0.425	0.390	0.184
		0.38	0.249	0.119	0.92	0.058	0.59	1.38	0.039	0.016	0.027	0.016	0.017
19R-5, 55–60	Gabbronorite	52.85	2.124	0.667	9.02	0.245	14.02	21.05	0.417	0.032	0.442	0.410	0.148
		0.54	0.603	0.173	1.05	0.108	0.21	0.78	0.067	0.040	0.014	0.005	0.018
74R-6, 27–35	Gabbronorite	52.04	1.965	0.726	10.48	0.37	13.49	20.74	0.435	0.011	0.435	0.394	0.172
		0.36	0.207	0.088	0.26	0.052	0.33	0.21	0.059	0.016	0.004	0.006	0.005
76R-4, 12–19	Gabbronorite	51.02	2.281	0.693	10.06	0.326	14.12	20.21	0.476	0.020	0.424	0.412	0.165
		0.25	0.147	0.068	0.61	0.029	0.33	0.66	0.036	0.030	0.015	0.008	0.009
40R-5, 0–4	Olivine gabbronorite	51.65	2.304	0.758	9.18	0.281	14.34	20.27	0.401	0.026	0.428	0.421	0.151
		0.12	0.240	0.101	0.85	0.014	0.28	0.43	0.087	0.026	0.009	0.009	0.014
43R-3, 95–102	Olivine gabbronorite	51.54	2.119	0.726	10.25	0.308	14.25	19.48	0.391	0.023	0.412	0.419	0.169
		0.39	0.208	0.065	0.71	0.039	0.42	1.16	0.044	0.025	0.023	0.012	0.012
76R-3, 34–41 CT	Olivine gabbronorite	51.90	1.969	0.581	10.86	0.358	13.98	18.83	0.402	0.000	0.403	0.416	0.181
		0.38	0.214	0.068	1.20	0.032	0.43	1.07	0.043	0.000	0.026	0.011	0.018
77R-2, 101–107	Olivine gabbronorite	51.84	1.975	0.611	9.93	0.328	13.92	20.78	0.413	0.013	0.434	0.404	0.162
		0.39	0.338	0.128	0.48	0.05	0.44	0.82	0.054	0.020	0.017	0.013	0.008
36R-4, 5–9	Dissem ox ol gabbro	51.70	2.372	0.791	9.15	0.32	14.01	20.52	0.497	0.028	0.435	0.413	0.151
		0.14	0.238	0.060	0.43	0.079	0.26	0.30	0.038	0.038	0.007	0.007	0.007
37R-3, 71–76 CT	Dissem ox ol gabbro	52.64	1.957	0.647	10.48	0.371	14.23	19.98	0.396	0.000	0.417	0.413	0.170
		0.35	0.296	0.158	1.44	0.041	0.23	1.07	0.028	0.000	0.023	0.010	0.021
40R-5, 4–8	Dissem ox ol gabbro	51.67	2.212	0.752	10.17	0.307	14.49	19.28	0.376	0.003	0.407	0.426	0.168
		0.16	0.098	0.052	0.94	0.057	0.44	1.38	0.105	0.003	0.028	0.014	0.015
43R-4, 64–66	Dissem ox ol gabbro	51.67	2.300	0.714	9.72	0.323	14.12	20.50	0.440	0.016	0.430	0.412	0.159
		0.44	0.209	0.067	0.85	0.043	0.23	0.66	0.054	0.018	0.015	0.007	0.012
46R-3, 121–128	Dissem ox ol gabbro	51.80	2.347	0.836	10.69	0.341	13.46	19.66	0.521	0.006	0.421	0.401	0.179
		0.18	0.115	0.046	0.85	0.025	0.55	1.31	0.046	0.006	0.028	0.016	0.014
77R-2, 5–8	Dissem ox ol gabbro	52.03	2.238	0.707	9.49	0.286	14.38	20.10	0.397	0.032	0.423	0.421	0.156
		0.46	0.325	0.200	0.67	0.02	0.25	1.00	0.020	0.049	0.019	0.009	0.012
20R-1, 111–114	Ol pigeonite gabbro	52.27	1.897	0.625	10.96	0.372	13.70	19.75	0.424	0.031	0.417	0.402	0.181
		0.31	0.190	0.118	2.02	0.023	0.47	1.84	0.022	0.037	0.040	0.013	0.033
37R-3, 76–79	Ol pigeonite gabbro	52.07	2.071	0.672	10.04	0.334	13.81	20.15	0.458	0.005	0.427	0.407	0.166
		0.56	0.301	0.208	0.88	0.032	0.57	0.40	0.019	0.005	0.010	0.011	0.015

Table 5 (continued).

Core, section, interval (cm)	Rock type	Clinopyroxene SiO_2	Al_2O_3	TiO_2	FeO	MnO	MgO	CaO	Na_2O	Cr_2O_3	Wo	En	Fs
49R-1, 42–46	Interst ol ox gabbro I	51.46	2.024	0.716	10.96	0.369	13.03	20.32	0.477	0.014	0.432	0.386	0.182
		0.30	0.194	0.087	0.59	0.008	0.19	0.32	0.052	0.021	0.008	0.004	0.009
50R-2, 43–47	Interst ol ox gabbro I	52.17	2.073	0.672	10.83	0.363	13.12	20.44	0.469	0.005	0.434	0.387	0.179
		0.52	0.120	0.127	0.57	0.028	0.15	0.46	0.042	0.010	0.010	0.004	0.009
50R-3, 62–67	Interst ol ox gabbro I	51.44	2.187	0.755	10.77	0.358	12.93	20.09	0.513	0.006	0.432	0.387	0.181
		0.16	0.223	0.019	0.70	0.054	0.37	0.69	0.034	0.011	0.018	0.008	0.010
51R-1, 94–99	Interst ol ox gabbro I	51.59	2.209	0.755	11.31	0.36	13.01	20.12	0.541	0.007	0.428	0.385	0.188
		0.33	0.189	0.111	0.57	0.036	0.17	1.00	0.039	0.010	0.018	0.008	0.011
51R-1, 99–103	Interst ol ox gabbro I	51.69	2.265	0.838	11.17	0.34	13.07	20.28	0.502	0.009	0.430	0.385	0.185
		0.16	0.100	0.074	0.56	0.045	0.13	0.47	0.055	0.016	0.010	0.003	0.009
52R-3, 121–123	Interst ol ox gabbro I	51.73	2.061	0.723	11.20	0.337	12.95	20.63	0.436	0.007	0.435	0.380	0.185
		0.35	0.313	0.164	0.44	0.031	0.31	0.40	0.056	0.015	0.009	0.007	0.007
52R-4, 88–94	Interst ol ox gabbro I	51.39	1.826	0.667	12.60	0.412	12.25	19.95	0.437	0.003	0.426	0.364	0.210
		0.24	0.173	0.111	0.57	0.027	0.32	0.56	0.052	0.005	0.014	0.009	0.008
53R-1, 47–54	Interst ol ox gabbro I	51.98	1.831	0.686	12.70	0.42	12.28	20.51	0.452	0.018	0.432	0.360	0.209
		0.27	0.206	0.084	0.56	0.068	0.19	0.61	0.047	0.021	0.011	0.007	0.008
53R-1, 123–127	Interst ol ox gabbro I	51.58	1.766	0.697	12.63	0.424	12.16	20.00	0.415	0.017	0.428	0.362	0.211
		0.55	0.134	0.119	0.46	0.044	0.08	0.80	0.032	0.033	0.012	0.003	0.010
53R-2, 31–39	Interst ol ox gabbro I	51.15	1.796	0.704	12.41	0.433	12.26	19.80	0.470	0.026	0.425	0.366	0.208
		0.33	0.226	0.155	0.34	0.038	0.18	0.53	0.039	0.024	0.009	0.005	0.007
54R-5, 117–119	Interst ol ox gabbro I	52.04	1.801	0.617	12.10	0.371	12.83	19.55	0.421	0.006	0.417	0.381	0.202
		0.17	0.238	0.145	1.16	0.059	0.25	0.53	0.029	0.008	0.012	0.007	0.019
55R-2, 101–105	Interst ol ox gabbro I	51.47	1.424	0.454	13.93	0.44	11.84	19.24	0.440	0.012	0.413	0.354	0.233
		0.77	0.266	0.109	0.81	0.038	0.21	0.29	0.061	0.014	0.009	0.007	0.011
82R-6, 73–78	Interst ol ox gabbro I	52.00	2.040	0.683	10.62	0.404	13.28	20.71	0.441	0.017	0.436	0.389	0.175
		0.46	0.206	0.082	1.00	0.032	0.056	0.42	0.052	0.035	0.012	0.012	0.016
34R-4, 8–12	Interst ol ox gabbro II	51.56	2.245	0.778	10.60	0.327	13.11	20.19	0.500	0.022	0.432	0.390	0.177
		0.27	0.201	0.091	0.67	0.046	0.25	0.59	0.056	0.018	0.014	0.007	0.010
47R-3, 56–61	Interst ol ox gabbro II	51.72	2.317	0.835	10.43	0.355	13.19	20.65	0.531	0.006	0.438	0.389	0.173
		0.29	0.188	0.079	0.42	0.029	0.09	0.51	0.033	0.008	0.010	0.004	0.007
49R-2, 94–100	Interst ol ox gabbro II	52.35	1.772	0.540	10.68	0.352	13.84	19.92	0.420	0.010	0.419	0.405	0.176
		0.29	0.336	0.108	1.13	0.045	0.40	1.19	0.084	0.010	0.025	0.010	0.019
52R-1, 91–100	Interst ol ox gabbro II	51.34	2.169	0.781	11.22	0.358	12.94	20.23	0.535	0.025	0.431	0.383	0.186
		0.35	0.280	0.138	0.74	0.046	0.28	0.74	0.062	0.032	0.17	0.006	0.012
54R-1, 131–136	Olivine oxide gabbro	50.80	1.464	0.640	14.09	0.446	10.78	19.45	0.536	0.008	0.428	0.330	0.242
		0.19	0.043	0.049	0.45	0.011	0.20	0.99	0.047	0.009	0.018	0.009	0.010
54R-3, 20–24	Olivine oxide gabbro	51.49	1.167	0.413	15.88	0.498	10.88	19.22	0.398	0.002	0.411	0.324	0.265
		0.11	0.189	0.093	1.50	0.051	0.52	0.72	0.027	0.005	0.016	0.015	0.025
54R-3, 125–127	Olivine oxide gabbro	50.80	1.305	0.478	14.81	0.493	10.86	19.56	0.389	0.008	0.423	0.327	0.250
		0.19	0.048	0.069	0.30	0.033	0.08	0.42	0.027	0.009	0.008	0.003	0.005
55R-2, 110–120	Olivine oxide gabbro	51.69	1.769	0.518	12.34	0.404	12.33	19.70	0.463	0.009	0.424	0.369	0.207
		0.14	0.466	0.121	1.58	0.067	0.75	0.39	0.030	0.013	0.005	0.022	0.026
55R-3, 83–86	Olivine oxide gabbro	51.77	1.585	0.570	14.10	0.41	12.16	19.06	0.436	0.007	0.406	0.360	0.234
		0.29	0.091	0.077	1.08	0.042	0.43	1.07	0.053	0.013	0.024	0.013	0.016
56R-2, 11–14	Olivine oxide gabbro	51.66	1.447	0.504	14.49	0.455	11.46	19.02	0.484	0.011	0.411	0.344	0.244
		0.18	0.180	0.137	0.15	0.011	0.75	1.26	0.089	0.016	0.026	0.023	0.003
56R-2, 49–52	Olivine oxide gabbro	51.53	1.445	0.493	14.49	0.503	11.47	19.24	0.489	0.003	0.414	0.343	0.243
		0.25	0.029	0.069	0.59	0.058	0.29	0.64	0.018	0.006	0.014	0.007	0.010
80R-3, 67–71	Olivine oxide gabbro	51.35	1.469	0.490	13.52	0.528	11.92	20.13	0.423	0.013	0.426	0.351	0.223
		0.24	0.180	0.076	0.94	0.049	0.46	0.29	0.049	0.014	0.005	0.013	0.016
80R-6, 130–135	Olivine oxide gabbro	51.46	1.330	0.519	14.60	0.573	11.47	19.52	0.470	0.006	0.416	0.340	0.243
		0.27	0.094	0.108	1.10	0.045	0.21	0.98	0.035	0.013	0.019	0.006	0.019
86R-4, 123–130	Olivine oxide gabbro	52.09	1.743	0.413	12.40	0.397	12.49	20.20	0.485	0.000	0.427	0.368	0.205
		0.20	0.093	0.129	0.54	0.065	0.08	0.30	0.061	0.000	0.006	0.002	0.009
48R-2, 109–113	Ol oxide microgabbro	51.91	1.898	0.674	12.54	0.344	13.56	18.72	0.402	0.016	0.395	0.398	0.206
		0.20	0.199	0.100	1.17	0.044	0.64	0.87	0.062	0.015	0.022	0.017	0.016
80R-7, 10–18	Ol oxide microgabbro	51.41	1.546	0.502	13.46	0.441	12.00	19.87	0.458	0.024	0.422	0.355	0.223
		0.44	0.200	0.113	0.63	0.064	0.17	0.63	0.050	0.021	0.011	0.007	0.011
80R-7, 23–25	Ol oxide microgabbro	50.99	1.843	0.569	12.98	0.385	12.20	19.13	0.440	0.011	0.414	0.367	0.219
		0.53	0.139	0.100	0.47	0.012	0.43	0.98	0.071	0.006	0.021	0.013	0.008
83R-7, 77–81	Troctolite	52.33	3.608	0.576	3.90	0.125	16.32	21.83	0.490	1.237	0.459	0.477	0.064
		0.09	0.194	0.054	0.54	0.038	0.46	0.71	0.049	0.022	0.017	0.010	0.009
83R-2, 3–9	Troctolite	52.60	3.355	0.512	4.69	0.143	16.97	20.70	0.376	0.833	0.432	0.492	0.076
		0.33	0.261	0.033	0.41	0.042	1.02	1.19	0.068	0.374	0.029	0.024	0.006
79R-7, 99–102	Troctolite	51.93	3.191	1.086	4.39	0.175	15.87	22.36	0.442	0.539	0.467	0.461	0.072
		0.47	0.531	0.223	0.09	0.04	0.20	0.51	0.075	0.090	0.005	0.005	0.001
73R-3, 73–75	Vermic cpx ol gabbro	52.89	2.734	0.505	5.50	0.153	16.46	21.02	0.332	0.180	0.436	0.475	0.089
		0.43	0.254	0.102	0.63	0.03	0.93	1.49	0.042	0.035	0.033	0.024	0.010
81R-5, 1–7	Vermic cpx ol gabbro	52.74	2.673	0.520	5.24	0.164	16.22	21.39	0.351	0.215	0.445	0.470	0.085
		0.45	0.279	0.121	0.50	0.027	0.53	1.09	0.052	0.037	0.022	0.015	0.008
71R-2, 82–84	Vermic cpx ol gabbro	52.51	2.571	0.593	6.80	0.143	16.50	19.52	0.330	0.186	0.409	0.480	0.111
		0.41	0.255	0.255	1.14	0.037	1.95	2.66	0.055	0.050	0.064	0.047	0.016
81R-7, 64–66	Vermic cpx ol gabbro	52.46	2.768	0.558	6.57	0.211	17.57	18.53	0.465	0.097	0.385	0.508	0.106
		1.20	0.837	0.129	0.52	0.015	0.62	0.39	0.162	0.041	0.015	0.009	0.006

Table 5 (continued).

Core, section, interval (cm)	Rock type	Clinopyroxene											
		SiO_2	Al_2O_3	TiO_2	FeO	MnO	MgO	CaO	Na_2O	Cr_2O_3	Wo	En	Fs
62R-4, 21–24	Olivine gabbro	52.60	2.867	0.892	6.71	0.23	16.04	20.36	0.421	0.135	0.425	0.466	0.109
		0.34	0.349	0.151	0.60	0.073	1.04	1.37	0.056	0.080	0.030	0.025	0.011
72R-5, 123–125	Olivine gabbro	53.03	2.716	0.558	5.75	0.174	16.66	20.80	0.355	0.156	0.429	0.478	0.093
		0.33	0.146	0.058	0.36	0.025	0.44	1.05	0.037	0.037	0.020	0.014	0.006
59R-4, 29–35	Olivine gabbro	52.50	3.300	0.636	6.42	0.18	16.31	20.33	0.400	0.231	0.424	0.472	0.104
		0.77	0.476	0.194	0.80	0.026	1.52	1.73	0.064	0.081	0.041	0.039	0.013
8D-1, 45–48	Olivine gabbro	52.45	2.964	0.542	5.17	0.174	15.63	22.36	0.359	0.253	0.465	0.452	0.084
		0.49	0.274	0.114	0.04	0.036	0.27	0.27	0.008	0.177	0.001	0.001	0.001
22R-3, 118–120	Olivine gabbro	52.21	2.425	0.645	5.77	0.191	14.86	21.20	0.292	0.164	0.457	0.446	0.097
		0.35	0.528	0.041	0.51	0.039	0.22	1.23	0.002	0.019	0.021	0.012	0.010
21R-2, 49–51	Olivine gabbro	51.71	2.727	0.649	5.73	0.184	15.48	21.20	0.319	0.070	0.449	0.456	0.095
		0.37	0.088	0.102	0.48	0.017	0.82	0.49	0.039	0.022	0.019	0.014	0.006
60R-1, 18–20	Olivine gabbro	50.72	3.054	0.931	6.60	0.213	14.78	21.34	0.416	0.120	0.454	0.437	0.110
		0.41	0.203	0.312	0.37	0.008	1.00	0.26	0.001	0.035	0.015	0.021	0.008
31R-2, 120–122	Olivine gabbro	52.72	2.665	0.605	6.02	0.162	16.19	20.94	0.360	0.121	0.435	0.468	0.098
		0.44	0.145	0.169	1.00	0.023	0.51	1.04	0.038	0.038	0.021	0.016	0.016
59R-3, 70–72	Olivine gabbro	51.79	2.962	0.830	7.46	0.225	15.00	21.04	0.451	0.108	0.441	0.437	0.122
		0.16	0.248	0.064	0.56	0.044	0.32	0.66	0.070	0.055	0.014	0.010	0.009

Note: Standard deviations are also shown below the average of oxide weight percent. Abbreviations are the same as in Table 3.

(1989) who attributed the steeper plagioclase gradients to very slow diffusion rates in plagioclase. In gabbros from Hole 735B, different diffusion rates in plagioclase and mafic phases have produced disequilibrium phase assemblages near contacts between gabbro types, e.g., co-existing calcic plagioclase and iron-rich olivine (Fig. 12). Because of this, only analyses of minerals at least 2 cm from contacts have been used in the downhole mineral plots (Figs. 2, 3) and in mineral co-variation plots (Figs. 4, 5).

Seventeen contacts between Fe-Ti oxide gabbro and olivine gabbro have been examined (Pl. 3, Figs. 4–6). At the sharpest contact (Sample 118-735B-79R-7, 2–9 cm), an oscillatory zoned calcic plagioclase in an olivine gabbro is sharply cut by a relatively homogeneous sodic plagioclase within an Fe-Ti oxide gabbro having an irregularly serrated boundary (Pl. 3, Figs. 3 and 4; Figs. 11A and 11B). Under the optical microscope, twin boundaries in the plagioclase can be traced continuously over the boundary, with a slight kinking at the contact because of the compositional difference (Pl. 3, Figs. 1–3). These observations suggest that sodic plagioclase grew on the disrupted calcic plagioclase of the olivine gabbro. An overgrowth of iron-rich clinopyroxene on olivine in olivine gabbro was also observed in this sample (Pl. 3, Fig. 4). Consequently, we infer that the melt from which the Fe-Ti oxide gabbro crystallized intruded into either solid or almost solidified olivine gabbro and that the boundaries are intrusive contacts.

In general, minerals in Fe-Ti oxide gabbro veins exhibit a wide range in compositions compared to their host olivine gabbros (Fig. 13). Furthermore, there is an inverse relationship between mineral compositions in Fe-Ti oxide gabbro veins and mineral compositions in host olivine gabbros (Fig. 13). Thus, the most evolved mineral compositions are found in Fe-Ti oxide gabbro veins that intrude the most primitive olivine gabbros. In addition to this complementary relationship, variable chemical exchange between Fe-Ti oxide gabbro veins and host olivine gabbro is indicated by an inverse relationships between delta An content (difference in plagioclase composition in the vein and in the unreacted gabbro host) and the thickness of the reaction zone. The thickness of the reaction zone is determined either by measuring the distance within a single crystal that is zoned away from the contact (diffusion distance in Fig. 14) or by measuring the distance over which multiple plagioclase grains exhibit chemical zoning away from the contact (penetration distance in Fig. 14).

The variation in the diffusion and penetration distance may have been caused by difference in thermal history (temperature or heating duration), chemical contrast between intruded melt and its host, and amounts of trapped melt in the host olivine gabbro. The negative correlation of the diffusion and penetration distance with the difference in the mineral compositions, however, can only be explained by decreases in temperature (or heating duration) and in the abundance of trapped melt as the host olivine gabbro becomes more primitive. There may be some trapped melt in the host olivine gabbro showing large penetration distance at the contact with Fe-Ti oxide gabbro, because in such samples plagioclase composition changes along grain boundaries deeply into the olivine gabbro (Pl. 3, Fig. 5; Fig. 11C), which cannot be explained by grain boundary diffusion.

The evolved magma might have intruded into the cumulus pile of olivine gabbro whose lower, more primitive portion was almost solidified, while the relatively evolved upper portion still contained trapped melt. The common occurrence of dikes or sills of evolved Fe-Ti oxide gabbro and fairly primitive troctolitic microgabbro from Hole 735B (Robinson, Von Herzen, et al., 1989) suggest that the disruption of solidified or partially solidified lower oceanic crust commonly took place even near mid-oceanic ridge, at least in the region near the fracture zones. The steady downcore increase of the diffusion distance in plagioclase at the contact between olivine and Fe-Ti oxide gabbros suggests that cooling from the base or wall of a magma chamber, which was modeled by Morton and Sleep (1985) assuming a deep hydrothermal cell. The deep hydrothermal activity is substantiated by abundant hydrothermal alteration even at the base of Hole 735B. The close association of the hydrothermal alteration and Fe-Ti oxide gabbros suggest that the fracture system filled by evolved melts was resumed during the subsequent hydrothermal circulation.

ORIGIN OF THE DOWNHOLE MINERALOGICAL VARIATIONS IN THE FE-TI OXIDE GABBROS

As described above, the Fe-Ti oxide gabbros are characterized by several downhole mineralogical cycles that are marked by decreases in the An content of plagioclase and the Mg# of mafic minerals (Figs. 2 and 3). These trends are opposite from those observed among the olivine gabbros and troctolites. Reverse fractionation trends have been reported from the marginal series of the Jimberlana Intrusion (Camp-

Table 6. Average chemical composition of orthopyroxene in gabbros from Hole 735B.

Core, section, interval (cm)	Rock type	Orthopyroxene										
		SiO_2	Al_2O_3	TiO_2	FeO	MnO	MgO	CaO	Cr_2O_3	Wo	En	Fs
118-735B-												
12R-1, 45–47	Gabbronorite	52.96	0.803	0.247	24.33	0.611	20.50	1.180	0.023	0.0242	0.5857	0.3900
		0.18	0.080	0.097	1.02	0.070	0.55	0.267	0.028	0.0055	0.0135	0.0174
19R-5, 47–50	Gabbronorite	52.69	0.987	0.278	22.66	0.562	21.51	1.374	0.015	0.0280	0.6105	0.3615
		0.60	0.198	0.068	2.13	0.117	1.39	0.390	0.015	0.0078	0.0340	0.0376
19R-5, 55–60	Gabbronorite	54.26	1.126	0.336	20.37	0.490	23.32	1.297	0.010	0.0261	0.6536	0.3203
		0.25	0.110	0.050	0.09	0.023	0.03	0.162	0.018	0.0032	0.0026	0.0013
74R-6, 27–35	Gabbronorite	53.13	0.802	0.454	22.15	0.655	21.56	1.414	0.005	0.0290	0.6159	0.3550
		0.15	0.072	0.034	0.46	0.046	0.24	0.140	0.005	0.0028	0.0059	0.0051
76R-4, 12–19	Gabbronorite	52.51	0.996	0.346	21.64	0.588	22.98	1.504	0.013	0.0299	0.6348	0.3353
		0.29	0.121	0.064	1.05	0.041	0.32	0.439	0.017	0.0090	0.0077	0.0134
40R-5, 0–4	Olivine gabbronorite	53.25	1.020	0.362	20.86	0.556	23.09	1.437	0.007	0.0288	0.6445	0.3267
		0.21	0.061	0.030	0.45	0.031	0.19	0.402	0.009	0.0079	0.0048	0.0068
43R-3, 95–102	Olivine gabbronorite	52.94	1.039	0.346	20.18	0.532	22.55	1.161	0.011	0.0240	0.6500	0.3260
		0.49	0.228	0.050	1.73	0.045	0.66	0.144	0.015	0.0027	0.0234	0.0238
76R-3, 34–41 CT	Olivine gabbronorite	52.61	1.146	0.281	21.56	0.558	21.65	1.077	0.020	0.0224	0.6271	0.3505
		0.17	0.083	0.033	0.23	0.009	0.02	0.225	0.011	0.0047	0.0004	0.0043
77R-2, 101–107	Olivine gabbronorite	52.83	1.017	0.306	21.84	0.590	22.15	1.125	0.010	0.0230	0.6290	0.3480
		0.24	0.064	0.028	0.59	0.045	0.55	0.188	0.012	0.0039	0.0092	0.0107
36R-4, 5–9	Dissem ox ol gabbro	53.13	1.010	0.379	21.35	0.617	22.48	1.145	0.000	0.0233	0.6371	0.3395
		0.34	0.283	0.110	0.07	0.007	0.18	0.287	0.000	0.0059	0.0050	0.0009
37R-3, 71–76 CT	Dissem ox ol gabbro	53.54	0.851	0.238	23.09	0.623	22.25	1.037	0.003	0.0207	0.6189	0.3604
		0.13	0.082	0.075	0.13	0.029	0.09	0.037	0.004	0.0007	0.0027	0.0020
40R-5, 4–8	Dissem ox ol gabbro	52.65	1.088	0.314	22.82	0.603	21.48	1.088	0.054	0.0223	0.6125	0.3652
43R-4, 64–66	Dissem ox ol gabbro	53.47	1.017	0.323	20.75	0.524	23.12	1.424	0.006	0.0286	0.6461	0.3253
		0.16	0.031	0.018	0.56	0.015	0.24	0.161	0.005	0.0032	0.0068	0.0088
20R-1, 111–114	Ol pigenoite gabbro	52.90	0.795	0.342	22.27	0.593	21.46	1.562	0.005	0.0321	0.6118	0.3561
		0.07	0.051	0.046	0.77	0.047	0.50	0.423	0.005	0.0090	0.0095	0.0083
37R-3, 76–79	Ol pigenoite gabbro	53.38	0.743	0.175	21.50	0.593	21.87	0.868	0.021	0.0181	0.6327	0.3493
		0.36	0.059	0.091	0.64	0.049	1.16	0.070	0.030	0.0018	0.0199	0.0180
37R-3, 80–82	Ol pigenoite gabbro	51.98	0.776	0.244	23.88	0.660	20.63	0.997	0.016	0.0206	0.5938	0.3856
		0.21	0.104	0.063	0.44	0.056	0.40	0.106	0.032	0.0021	0.0081	0.0084
38R-3, 85–88	Ol pigenoite gabbro	51.42	0.797	0.287	25.01	0.688	20.44	1.130	0.012	0.0230	0.5793	0.3976
		0.17	0.097	0.073	0.52	0.072	0.19	0.029	0.021	0.0005	0.0071	0.0066
38R-4, 24–28	Ol pigenoite gabbro	53.00	0.784	0.355	22.30	0.584	21.71	1.414	0.002	0.0288	0.6160	0.3551
		0.23	0.077	0.140	0.77	0.041	0.45	0.427	0.003	0.0086	0.0064	0.0133
45R-1, 5–12	Ol pigenoite gabbro	52.65	0.855	0.314	23.30	0.657	21.07	1.615	0.024	0.0329	0.5969	0.3702
21R-2, 27–32	Pigeonite gabbro	53.57	0.773	0.226	24.06	0.742	20.70	1.267	0.014	0.0259	0.5895	0.3846
		0.15	0.226	0.055	0.44	0.092	0.14	0.102	0.017	0.0021	0.0052	0.0052
23R-3, 34–37	Pigeonite gabbro	53.28	0.857	0.283	21.48	0.590	22.51	1.359	0.010	0.0275	0.6333	0.3392
		0.35	0.041	0.045	0.60	0.043	0.50	0.252	0.013	0.0052	0.0095	0.0105
24R-2, 120–126	Pigeonite gabbro	52.86	0.655	0.289	23.84	0.682	20.64	1.359	0.011	0.0279	0.5899	0.3822
		0.32	0.113	0.079	1.03	0.054	0.40	0.366	0.018	0.0077	0.0117	0.0100
28R-1, 109–114	Pigeonite gabbro	52.61	0.818	0.274	25.03	0.751	20.06	1.130	0.030	0.0233	0.5745	0.4023
		0.26	0.060	0.021	0.04	0.002	0.06	0.158	0.038	0.0032	0.0030	0.0002
28R-3, 72–77	Pigeonite gabbro	52.73	0.712	0.247	25.04	0.740	19.75	1.283	0.018	0.0266	0.5688	0.4046
		0.31	0.063	0.026	0.78	0.031	0.36	0.275	0.041	0.0057	0.0067	0.0111
44R-2, 16–24	Pigeonite gabbro	52.21	0.695	0.302	25.19	0.739	19.47	1.279	0.010	0.0266	0.5640	0.4094
		0.22	0.123	0.048	1.09	0.099	0.89	0.312	0.017	0.0065	0.0249	0.0185
46R-4, 109–113	Pigeonite gabbro	52.45	0.974	0.321	23.22	0.635	20.49	1.167	0.013	0.0244	0.5963	0.3793
		0.37	0.121	0.015	0.64	0.061	0.51	0.130	0.011	0.0027	0.0118	0.0124
14R-1, 93–97	Interst ol ox gabbro I	52.50	0.824	0.318	24.35	0.642	20.00	1.182	0.013	0.0246	0.5795	0.3959
		0.44	0.226	0.085	0.36	0.053	0.56	0.108	0.025	0.0021	0.0096	0.0084
21R-1, 82–89 CT	Interst ol ox gabbro I	53.19	0.892	0.313	23.42	0.678	21.26	1.072	0.030	0.0219	0.6045	0.3736
		0.14	0.210	0.083	0.07	0.040	0.33	0.250	0.025	0.0052	0.0071	0.0030
47R-2, 117–127	Interst ol ox gabbro I	52.78	1.121	0.365	22.13	0.531	21.66	1.201	0.012	0.0247	0.6200	0.3553
47R-3, 143–149 CT	Interst ol ox gabbro I	52.94	0.697	0.246	25.41	0.645	19.53	1.889	0.033	0.0386	0.5557	0.4056
48R-2, 56–65	Interst ol ox gabbro I	53.39	0.762	0.263	23.96	0.622	20.62	1.112	0.004	0.0229	0.5914	0.3857
		0.11	0.077	0.053	0.95	0.039	0.71	0.118	0.009	0.0025	0.0156	0.0170
48R-3, 112–116	Interst ol ox gabbro I	53.08	0.770	0.312	25.24	0.749	20.44	1.269	0.000	0.0257	0.5756	0.3987
48R-4, 82–84	Interst ol ox gabbro I	52.36	0.719	0.290	24.76	0.659	20.03	1.122	0.001	0.0232	0.5766	0.4001
		0.99	0.089	0.040	0.35	0.025	0.66	0.028	0.002	0.0009	0.0115	0.0107
49R-1, 42–46	Interst ol ox gabbro I	52.02	1.054	0.270	24.53	0.681	19.84	0.956	0.033	0.0200	0.5787	0.4013
		0.18	0.080	0.033	0.54	0.067	0.15	0.122	0.013	0.0025	0.0079	0.0060
50R-2, 43–47	Interst ol ox gabbro I	53.12	0.750	0.282	23.93	0.669	20.34	1.425	0.010	0.0294	0.5847	0.3859
		0.52	0.081	0.039	0.32	0.036	0.20	0.136	0.017	0.0028	0.0054	0.0030
50R-3, 62–67	Interst ol ox gabbro I	52.38	0.807	0.285	24.26	0.671	20.03	1.105	0.003	0.0230	0.5816	0.3954
		0.46	0.130	0.030	0.66	0.060	0.51	0.197	0.007	0.0038	0.0095	0.0122
51R-1, 94–99	Interst ol ox gabbro I	52.28	0.711	0.273	26.07	0.657	19.79	1.003	0.027	0.0205	0.5630	0.4165
		0.11	0.179	0.038	1.13	0.078	0.78	0.245	0.033	0.0049	0.0175	0.0208
51R-1, 99–103	Interst ol ox gabbro I	52.98	0.846	0.295	24.37	0.670	20.75	1.436	0.026	0.0291	0.5852	0.3857
		0.01	0.100	0.033	0.15	0.000	0.10	0.363	0.018	0.0073	0.0041	0.0032
52R-3, 121–123	Interst ol ox gabbro I	52.62	0.851	0.210	25.87	0.682	19.40	0.993	0.000	0.0206	0.5603	0.4191
		0.27	0.511	0.031	0.83	0.027	0.02	0.060	0.000	0.0015	0.0071	0.0086

Table 6 (continued).

Core, section, interval (cm)	Rock type	Orthopyroxene										
		SiO_2	Al_2O_3	TiO_2	FeO	MnO	MgO	CaO	Cr_2O_3	Wo	En	Fs
52R-4, 88–94	Interst ol ox gabbro I	51.70	0.694	0.265	26.89	0.800	17.59	1.223	0.005	0.0262	0.5242	0.4496
		0.35	0.019	0.047	0.67	0.001	0.34	0.010	0.007	0.0002	0.0106	0.0108
53R-1, 123–127	Interst ol ox gabbro I	51.97	0.420	0.174	28.56	0.838	17.31	1.238	0.019	0.0260	0.5058	0.4683
		0.30	0.016	0.013	0.54	0.068	0.26	0.448	0.027	0.0092	0.0034	0.0126
53R-2, 31–39	Interst ol ox gabbro I	51.42	0.696	0.290	26.91	0.658	17.12	2.198	0.006	0.0468	0.5065	0.4467
54R-5, 117–119	Interst ol ox gabbro I	52.38	0.871	0.254	25.89	0.673	19.18	1.136	0.001	0.0237	0.5556	0.4208
		0.18	0.145	0.050	0.77	0.047	0.65	0.089	0.003	0.0020	0.0164	0.0144
55R-2, 101–105	Interst ol ox gabbro I	51.41	0.448	0.179	28.31	0.851	16.59	1.446	0.006	0.0310	0.4949	0.4740
		0.35	0.099	0.046	0.96	0.060	1.03	0.5463	0.010	0.0122	0.0293	0.0178
82R-6, 73–78	Interst ol ox gabbro I	52.04	0.746	0.243	26.75	0.763	18.62	1.218	0.030	0.0254	0.5396	0.4350
		0.35	0.170	0.031	0.67	0.120	0.029	0.208	0.033	0.0043	0.0077	0.0115
34R-4, 8–12	Interst ol ox gabbro II	52.61	0.986	0.303	23.65	0.617	20.35	1.277	0.011	0.0266	0.5892	0.3842
		0.18	0.151	0.052	0.42	0.059	0.25	0.438	0.016	0.0091	0.0073	0.0061
47R-3, 56–61	Interst ol ox gabbro II	52.82	0.785	0.268	23.67	0.618	20.89	1.091	0.020	0.0224	0.5976	0.3800
		0.25	0.166	0.042	1.12	0.034	0.63	0.175	0.029	0.0035	0.0167	0.0189
49R-2, 94–100	Interst ol ox gabbro II	53.17	0.790	0.222	23.34	0.610	21.31	1.092	0.010	0.0223	0.6055	0.3722
		0.30	0.073	0.042	1.35	0.058	1.03	0.199	0.008	0.0043	0.0252	0.0217
52R-1, 91–100	Interst ol ox gabbro II	52.20	0.989	0.225	25.45	0.637	19.60	1.087	0.010	0.0226	0.5654	0.4120
		0.37	0.291	0.026	0.52	0.048	0.51	0.130	0.011	0.0028	0.0107	0.0102
54R-1, 131–136	Olivine oxide gabbro	51.16	0.425	0.079	30.62	0.974	15.56	0.833	0.002	0.0180	0.4667	0.5153
		0.14	0.062	0.041	0.12	0.021	0.26	0.029	0.003	0.0007	0.0045	0.0043
54R-3, 20–24	Olivine oxide gabbro	51.26	0.410	0.169	33.07	0.960	13.78	1.465	0.011	0.0315	0.4127	0.5558
		0.05	0.046	0.021	0.13	0.085	0.18	0.285	0.018	0.0057	0.0010	0.0054
54R-3, 125–127	Olivine oxide gabbro	50.73	0.365	0.115	29.29	0.894	14.93	2.984	0.022	0.0640	0.4456	0.4904
		0.06	0.006	0.019	0.01	0.042	0.08	0.071	0.030	0.0013	0.0007	0.0020
55R-2, 110–120	Olivine oxide gabbro	52.57	0.804	0.296	25.56	0.714	19.77	1.210	0.010	0.0249	0.5651	0.4100
55R-3, 83–86	Olivine oxide gabbro	52.61	0.435	0.203	28.56	0.762	17.35	2.148	0.000	0.0442	0.4969	0.4589
56R-2, 11–14	Olivine oxide gabbro	51.51	0.467	0.198	31.40	0.959	14.89	1.106	0.003	0.0239	0.4472	0.5290
		0.02	0.021	0.035	0.14	0.004	0.01	0.057	0.004	0.0012	0.0018	0.0006
56R-2, 49–52	Olivine oxide gabbro	51.15	0.527	0.239	29.82	0.892	15.68	1.193	0.025	0.0258	0.4713	0.5029
		0.20	0.063	0.008	0.17	0.086	0.27	0.083	0.019	0.0020	0.0037	0.0017
80R-3, 67–71	Olivine oxide gabbro	51.57	0.507	0.196	28.11	0.888	17.87	1.223	0.004	0.0255	0.5178	0.4568
		0.28	0.118	0.035	1.19	0.081	0.55	0.055	0.005	0.0010	0.0183	0.0173
80R-6, 130–135	Olivine oxide gabbro	51.65	0.538	0.180	30.59	0.984	16.13	1.311	0.009	0.0276	0.4712	0.5013
		0.24	0.082	0.051	0.78	0.037	0.32	0.226	0.013	0.0049	0.0079	0.0104
86R-4, 123–130	Olivine oxide gabbro	52.15	0.638	0.198	26.51	0.780	18.50	1.325	0.002	0.0277	0.5389	0.4333
		0.20	0.067	0.051	1.06	0.045	0.50	0.266	0.005	0.0056	0.0132	0.0173
80R-7, 10–18	Olivine oxide gabbro	51.19	0.760	0.229	29.12	0.857	16.92	1.239	0.000	0.0261	0.4955	0.4784
80R-7, 23–25	Olivine oxide gabbro	51.58	0.792	0.209	27.32	0.716	17.61	1.095	0.000	0.0233	0.5222	0.4545
83R-7, 77–81	Troctolite	57.50	0.739	0.092	9.01	0.232	32.58	0.556	0.078	0.0105	0.8566	0.1329
		0.12	0.208	0.037	0.06	0.036	0.64	0.148	0.108	0.0030	0.0041	0.0011
73R-3, 73–75	Vermic cpx ol gabbro	55.40	1.753	0.237	12.94	0.262	28.81	0.880	0.093	0.0172	0.7849	0.1979
		0.35	0.526	0.056	0.32	0.044	0.53	0.134	0.039	0.0025	0.0054	0.0062
81R-5, 1–7	Vermic cpx ol gabbro	55.25	1.932	0.165	12.90	0.277	28.59	0.753	0.123	0.0149	0.7861	0.1990
71R-2, 82–84	Vermic cpx ol gabbro	54.62	1.228	0.378	14.63	0.366	27.24	0.964	0.095	0.0192	0.7536	0.2272
		0.31	0.138	0.161	0.98	0.013	1.00	0.184	0.030	0.0038	0.0210	0.0172
62R-4, 21–24	Olivine gabbro	54.99	1.448	0.348	16.11	0.384	26.94	0.989	0.020	0.0194	0.7343	0.2463
		0.09	0.070	0.077	0.09	0.040	0.38	0.264	0.014	0.0053	0.0056	0.0003
59R-4, 29–35	Olivine gabbro	54.98	1.252	0.234	16.51	0.393	26.56	0.741	0.044	0.0146	0.7305	0.2549
		0.36	0.113	0.043	0.83	0.022	0.67	0.097	0.016	0.0019	0.0149	0.0141
60R-1, 18–20	Olivine gabbro	53.71	1.412	0.351	16.21	0.359	26.09	0.930	0.039	0.0186	0.7278	0.2536
		0.35	0.009	0.081	0.84	0.001	0.30	0.129	0.039	0.0025	0.0138	0.0113
31R-2, 120–122	Olivine gabbro	53.52	2.055	0.361	16.52	0.290	26.05	1.159	0.017	0.0230	0.7205	0.2565
59R-3, 70–72	Olivine gabbro	54.31	1.366	0.297	17.81	0.406	25.77	0.872	0.026	0.0172	0.7079	0.2748
		0.43	0.242	0.100	0.99	0.051	0.99	0.171	0.018	0.0035	0.0207	0.0177

Note: Standard deviations are also shown below the average of oxide weight percent. Abbreviations are the same as in Table 3.

bell, 1977) and from the marginal zone in the Muskox Intrusion (Bahattacharji and Smith, 1964). These marginal cumulates occupy the lower portions of the intrusions filling connecting pipes. In the upper border group of the Skaergaard Intrusion, a downward trend to more evolved compositions has been interpreted as crystallization from the roof downward in the intrusion (Wager and Brown, 1967; Naslund, 1984).

The unimodal distribution of the mineral chemistry among the Fe-Ti oxide gabbros (Fig. 1) indicates that they might have been derived from a common, moderately fractionated magma, which may have existed either at the top or on the side of the cumulus pile of olivine gabbro. In the former case, the evolved magma may have intruded downward into the pile with progressive fractional crystallization. In the latter case, the chamber may have been reversely stratified and lateral intrusion occurred. The lateral intrusion model seems unrealistic because it is difficult to maintain a reversely stratified magma chamber (Sparks and Huppert, 1984); the melt in equilibrium with the most evolved gabbros, the olivine Fe-Ti oxide gabbros, deep in the section likely was higher in silica and lower in iron so had a lower density than the melt in equilibrium with the less evolved gabbronorites and pigeonite gabbros higher in the section so would have risen through the cumulus pile.

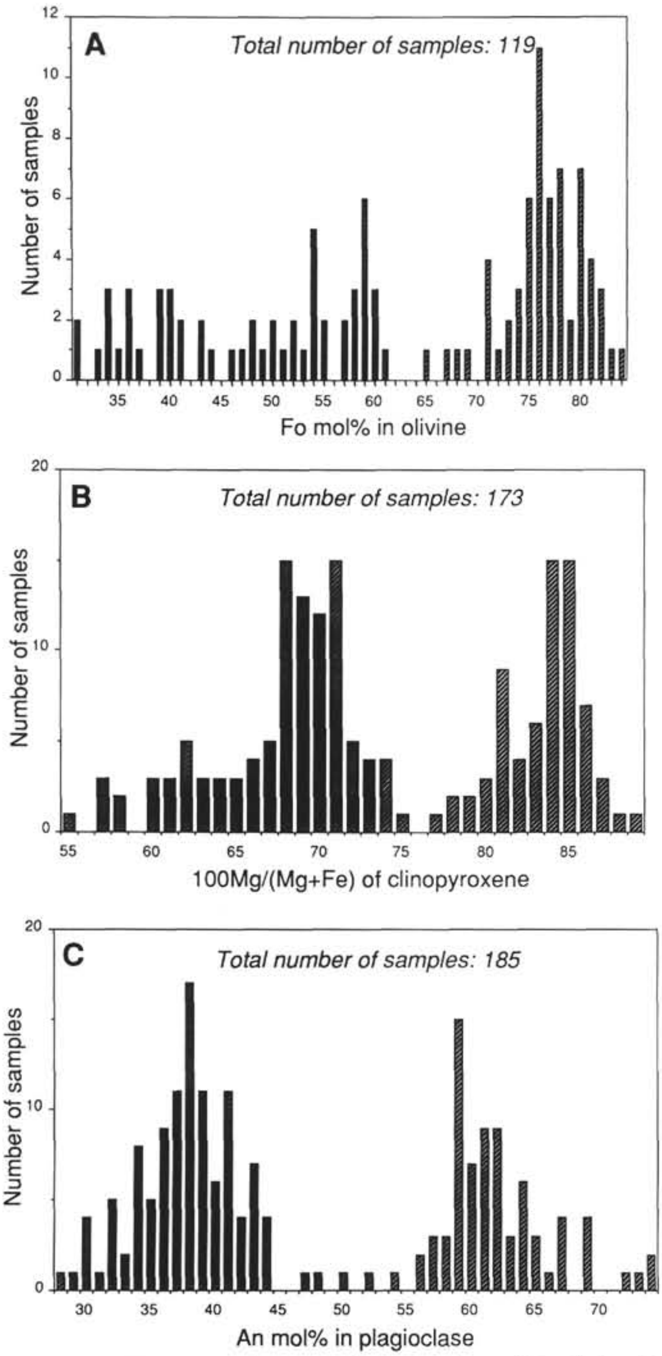

Figure 4. **A.** Frequency histograms of average Fo mol% in olivine. **B.** Average 100 Mg/(Mg+Fe) of clinopyroxene. **C.** Average An mol% in plagioclase in gabbros from Hole 735B. Note that histograms show bimodal distribution pattern, specifically for An mol% and Mg/(Mg+Fe) ratio of clinopyroxene. Each peak corresponds to olivine gabbro-troctolite and iron-titanium oxide gabbros.

The downward intrusion of fractionated magma into a solidifying cumulus pile is plausible if magma chambers beneath mid-ocean ridges are chemically zoned, as proposed by Pallister and Hopson (1981) and Casey and Karson (1981). In their models, magma situated at the margin of the chamber, and away from the spreading center, is more evolved than that at the center of the chamber. A similar zonation may be attained in a small ephemeral magma chamber with limited supply of primitive magmas. In such a case, evolved melt may overly a completely- or almost-solidified cumulus pile of primitive gabbros. Disrupting the cumulus pile may have caused the overlying evolved magma to fill the fractures and crystallize as a dike- and sill-complex. Progressive downward intrusion may have caused continued evolution; thus, the deeper intrusives show more evolved characteristics. The contact relationship between olivine gabbro and Fe-Ti oxide gabbro suggests that the magma body should have been cooled from the base. In a steady state magma chamber model, this situation may only be achieved if the intrusion took place away from the ridge center, assuming a deep hydrothermal cell (Morton and Sleep, 1985). This indicates that the evolved melt may have existed away from the accretion center, which is consistent with the zoned magma chamber model mentioned above. The downward evolution of Fe-Ti oxide gabbros in Unit IV can be explained by downward crystallization from the roof of a thick dike. Accordingly, the base of Unit IV may correspond to the proximity of the center of the dike, the lower half of which was displaced by faulting and is missing from the section of Hole 735B.

SUMMARY

The major petrological characteristics of gabbros from Hole 735B are (1) the intimate association of evolved (Fe-Ti oxide gabbro) and primitive (olivine gabbro and troctolite) gabbros, with rare gabbros having intermediate mineral chemistry, (2) the likely co-genetic relationship between evolved and primary gabbros suggested by systematic mineralogical variations among all the gabbros from Hole 735B, and (3) the sharp contacts between evolved and primitive and evolved gabbros, suggesting that these contacts were formed by the intrusion of evolved magma into solid or almost solidified olivine gabbro host.

We suggest that a body of fairly homogeneous olivine gabbro cumulates formed on the floor and walls of a magma chamber. This isotropic (unlayered) unit of gabbro cumulates was overlain by a body of isolated melt which fractionated to produce gabbronorites and dense iron-rich melts that migrated back into the cumulate pile along cooling and deformation fractures. Downward penetration of melt led to further fractionation and the production of evolved gabbros rich in Fe-Ti oxides. This model requires an unreplenished ephemeral magma chamber (Meyer et al., 1989) which is consistent with low magma supply rates along the Southwest Indian Ridge (Dick et al., 1984). High cooling rates and extensive fractional crystallization may have been enhanced by the proximity to the Atlantis II Fracture Zone.

ACKNOWLEDGMENTS

We wish to thank the scientists, technicians, officers, and crew aboard the *JOIDES Resolution*, and the shore-based ODP staff for their support and cooperation during and after Leg 118. We are grateful to Toshitsugu Fujii, Hiroko Nagahara, and Natsuko Takahashi for fruitful discussions and encouragements. This paper benefitted considerably from the many comments by Peter Thy.

REFERENCES

Ambler, E. P., and Ashley, P. M., 1977. Vermicular orthopyroxene-magnetite symplectites from the Wateranga layered mafic intrusion, Queensland, Australia. *Lithos*, 10:163–172.

Batiza, R., and Vanko, D. A., 1985. Petrologic evolution of large failed rifts in the eastern Pacific: petrology of volcanic and plutonic rocks from the Mathematician Ridge area and the Guadalupe Trough. *J. Petrol.*, 26:564–602.

Bhattacharji, S., and Smith, C. H., 1964: Flowage differentiation. *Science*, 145:150–153.

Bowen, N. L., and Schairer, J. F., 1935. The system MgO-FeO-SiO_2. *Am. J. Sci.*, 26:151–217.

BVSP, 1981. *Basaltic Volcanism on the Terrestrial Planets*: (Lunar and Planetary Institution), New York (Pergamon Press).

Casey, J. F., and Karson J. A., 1981. Magma chamber profiles from the Bay of Islands ophiolite complex. *Nature*, 292:295–301.

Campbell, I. H., 1977. A study of macro-rhythmic layering and cumulus processes in the Jimberiana Intrusion, Western Australia. Part I: The upper layered series. *J. Petrol.*, 189:183–215.

Davidson, P. M., and Lindsley, D. H., 1989. Thermodynamic analysis of pyroxene-olivine-quartz equilibria in the system CaO-MgO-FeO-SiO_2. *Am. Mineral.*, 74:18–30.

Elthon D., 1987. Petrology of Gabbroic rocks from the Mid-Cayman Rise spreading center. *J. Geophys. Res.*, 92:658–682.

Hébert, R., Bideau, D., and Hekinian, R., 1983. Ultramafic and mafic rocks from the Garret Transform Fault near 13°N30'S on the East Pacific Rise: igneous petrology. *Earth Planet. Sci. Lett.*, 65:107–125.

Hodges, F. N., and Papike, J. J., 1976. DSDP site 334: Magmatic cumulates from oceanic layer 3. *J. Geophys. Res.*, 81:4135–4151.

Hoover, J. D., 1978. Petrologic features of the Skaergaard marginal border group. *Year Book, Carnegie Instn. Wash.*, 77:732–739.

Meyer, P. S., Dick, J. B., and Thompson, G., 1989. Cumulate gabbros from the Southwest Indian Ridge, 54°S-7°16'E: implications for magmatic processes at a slow spreading ridge. *Contrib. Mineral. Petrol.*, 103:44–63.

Miyashiro, A., and Shido, F., 1980. Differentiation of gabbros in the Mid-Atlantic Ridge near 24°N. *Geochem. J.* 14:145–154.

Morton, J. L., and Sleep, N. H., 1985. A mid-ocean ridge thermal model: constraints on the volume of axial hydrothermal heat flux. *J. Geophys. Res.*, 90:11345–11353.

Nakamura, Y., and Kushiro, I., 1970. Compositional relationships of coexisting orthopyroxene, pigeonite and augite in a tholeiitic andesite from Hakone volcano. *Contrib. Mineral. Petrol.*, 26:265–275.

Naslund, H. R., 1984. Petrology of the Upper Border Series of the Skaergaard intrusion. *J. Petrol.*, 25:185–212.

———, 1976. Mineralogical variations in the upper part of the Skaergaard intrusion, East Greenland. *Year Book, Carnegie Instn. Wash.*, 75:640–644.

Pallister, J. S., and Hopson, C. A., 1981. Samail ophiolite plutonic suite: field relations, phase variation, cryptic variation and layering, and a model of a spreading ridge magma chamber. *J. Geophys. Res.*, 86:2593–2644.

Robinson, P. T., Von Herzen, R., et al., 1989: *Proc. ODP, Init. Repts.*, 118: College Station, TX (Ocean Drilling Program).

Sinton, J. M., Wilson, D. S., Christie, D. M., Hey, R. N., and Delaney, J. R., 1983. Petrologic consequences of rift propagation on oceanic spreading rides. *Earth Planet. Sci. Lett.*, 62:193–207.

Sparks, R. S., and Huppert, H. E., 1984. Density changes during the fractional crystallization of basaltic magmas: fluid dynamic implications. *Contrib. Mingral. Petrol.*, 85:300–309.

Tiezzi. L. J., and Scott, R. B., 1980. Crystal fractionation in a cumulate gabbro, Mid-Atlantic Ridge, 26°N. *J. Geophys. Res.*, 85:5438–5454.

Wager, L. R., and Brown, G. M., 1967. *Layered Igneous Rocks*: San Francisco (Freeman).

Walker, D., and Delong, S. E., 1984. A small Soret effect in spreading center gabbros. *Contrib. Mineral. Petrol.*, 85:203–208.

Date of initial receipt: 19 October 1989
Date of acceptance: 26 June 1990
Ms 118B-125

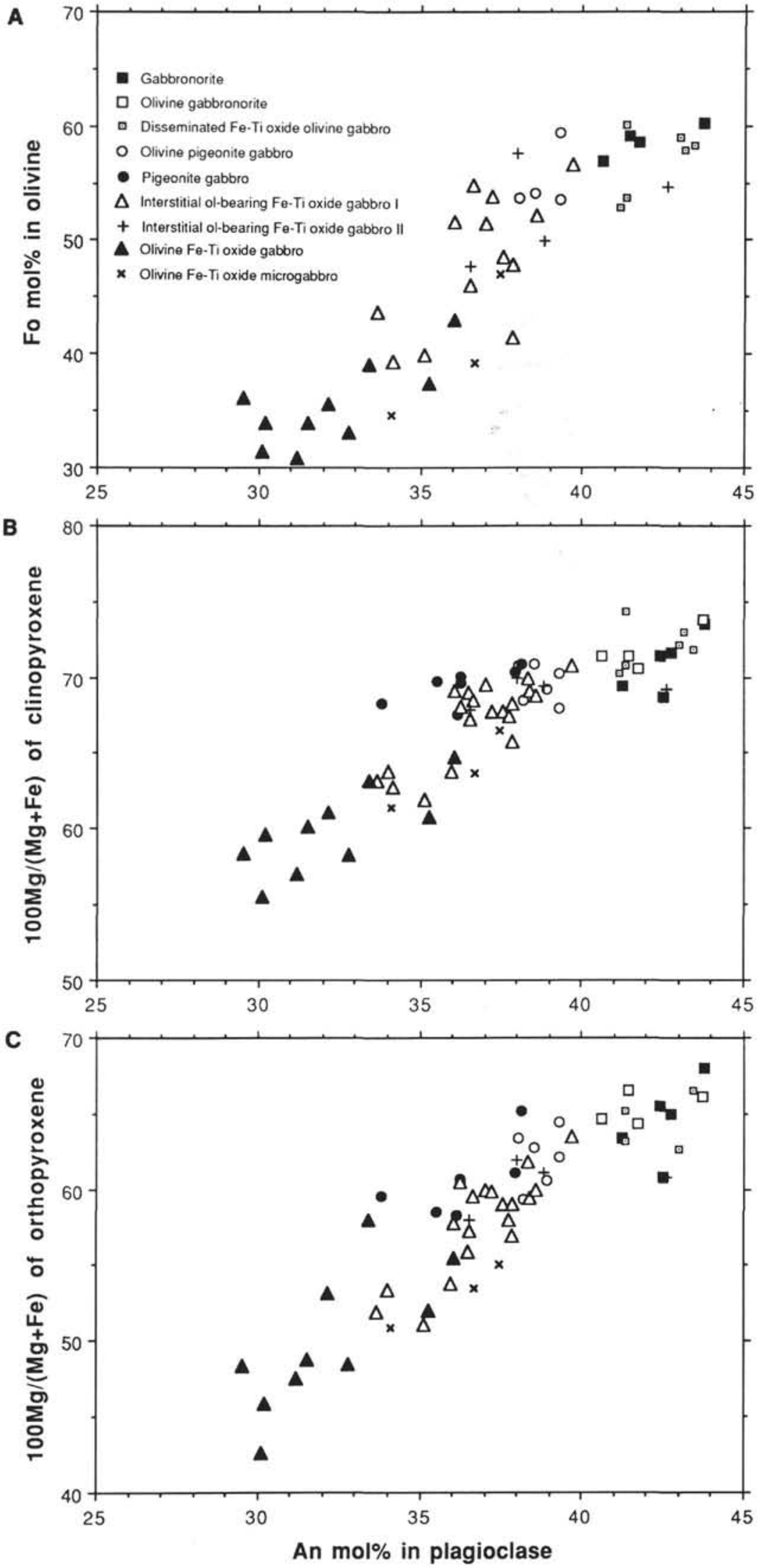

Figure 5. Average An content in plagioclase vs. average Mg/(Mg+Fe) ratios of mafic minerals (**A**, Olivine. **B**, Clinopyroxene (augite-diopside), **C**, Orthopyroxene) in Fe-Ti oxide gabbros from Hole 735B. Symbols are the same as in Figure 3.

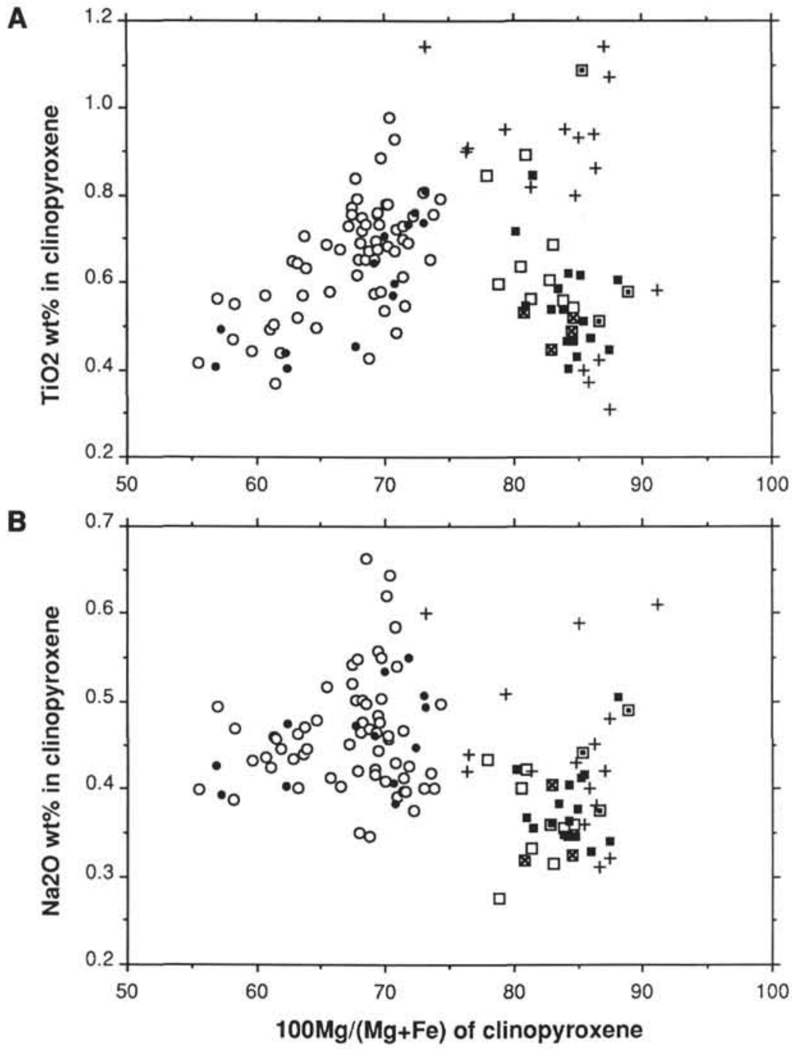

Figure 6. TiO_2 content (**A**) and Na_2O content (**B**) vs. Mg/(Mg+Fe) ratio of clinopyroxene (augite-diopside). Data are based on average of clinopyroxene cores. Symbols are the same as in Figure 4.

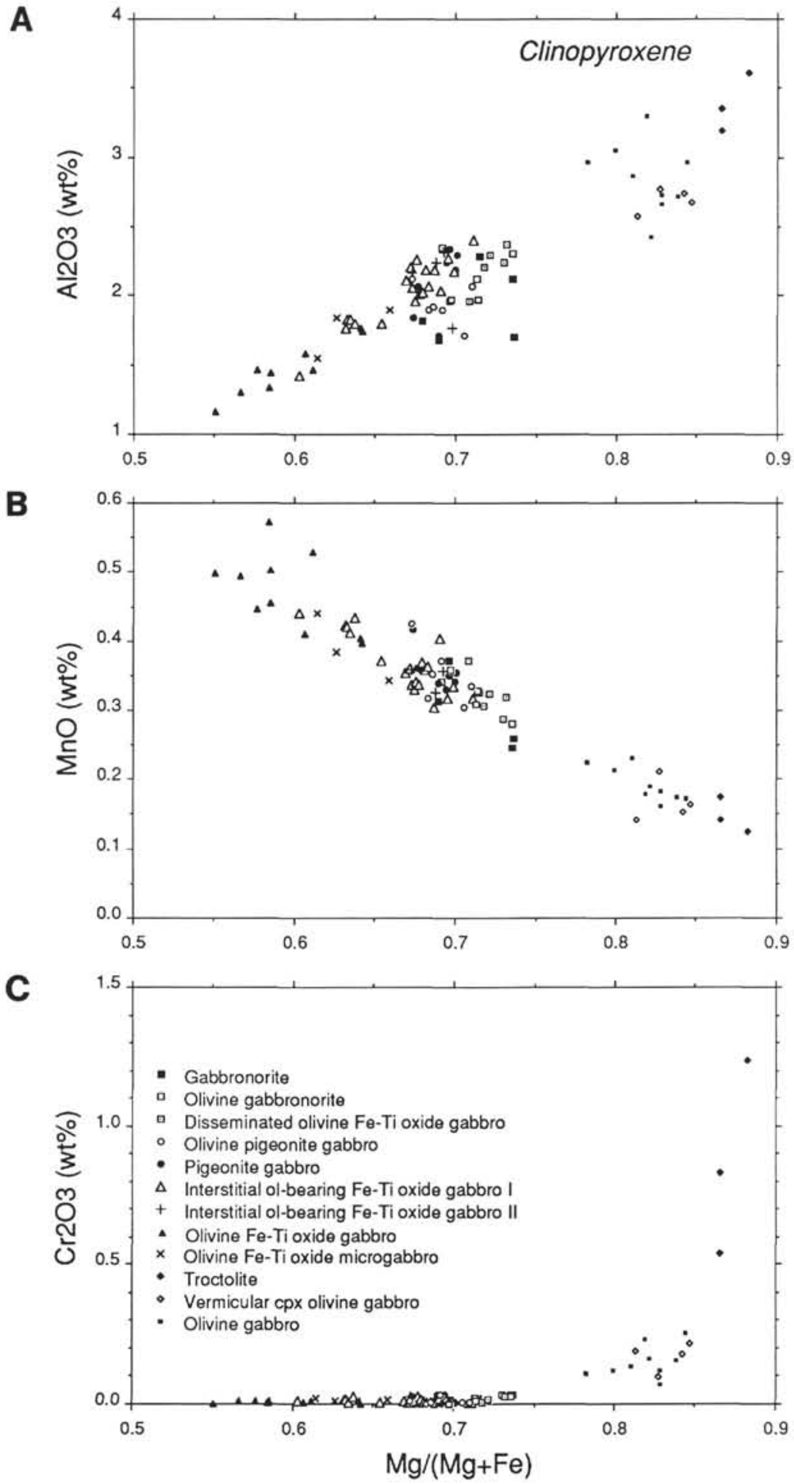

Figure 7. Mg/(Mg+Fe) ratio vs. Al_2O_3 (**A**), MnO (**B**), and Cr_2O_3 (**C**) contents of clinopyroxene. Symbols are the same as in Figure 3, except for troctolite (solid diamond), vermicular clinopyroxene olivine gabbro (open diamond), and olivine gabbro (small solid square).

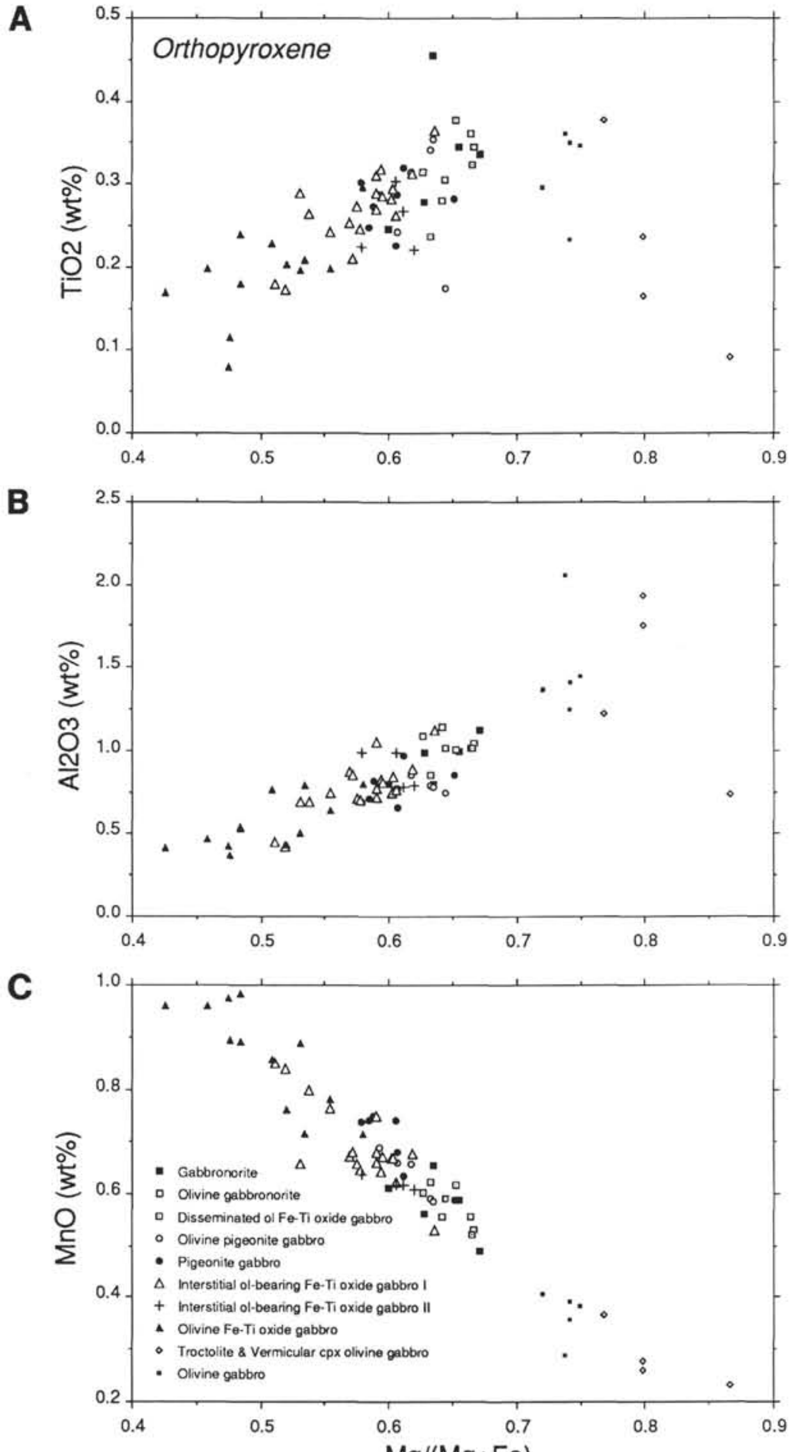

Figure 8. Mg/(Mg+Fe) ratio vs. TiO_2 (**A**), Al_2O_3 (**B**), and MnO (**C**) contents of orthopyroxene. Symbols are the same as in Figure 7.

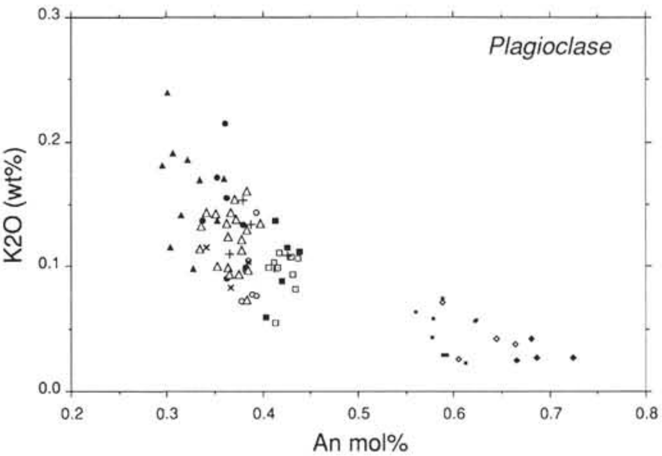

Figure 9. Anorthite mol% vs. Orthoclase mol% in plagioclase. Symbols are the same as in Figure 7.

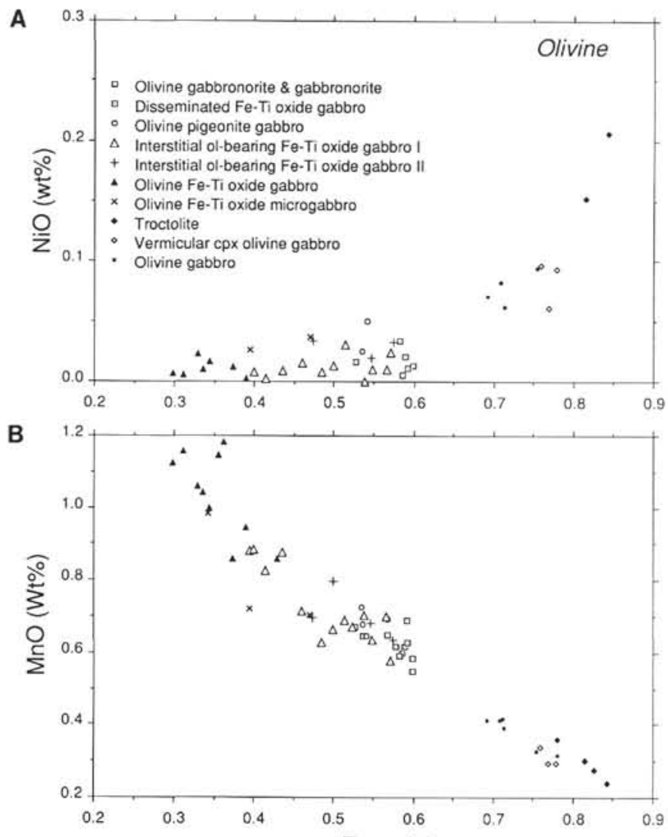

Figure 10. Fo mol% vs. NiO (A) and MnO (B) contents of olivine. Symbols are the same as in Figure 7.

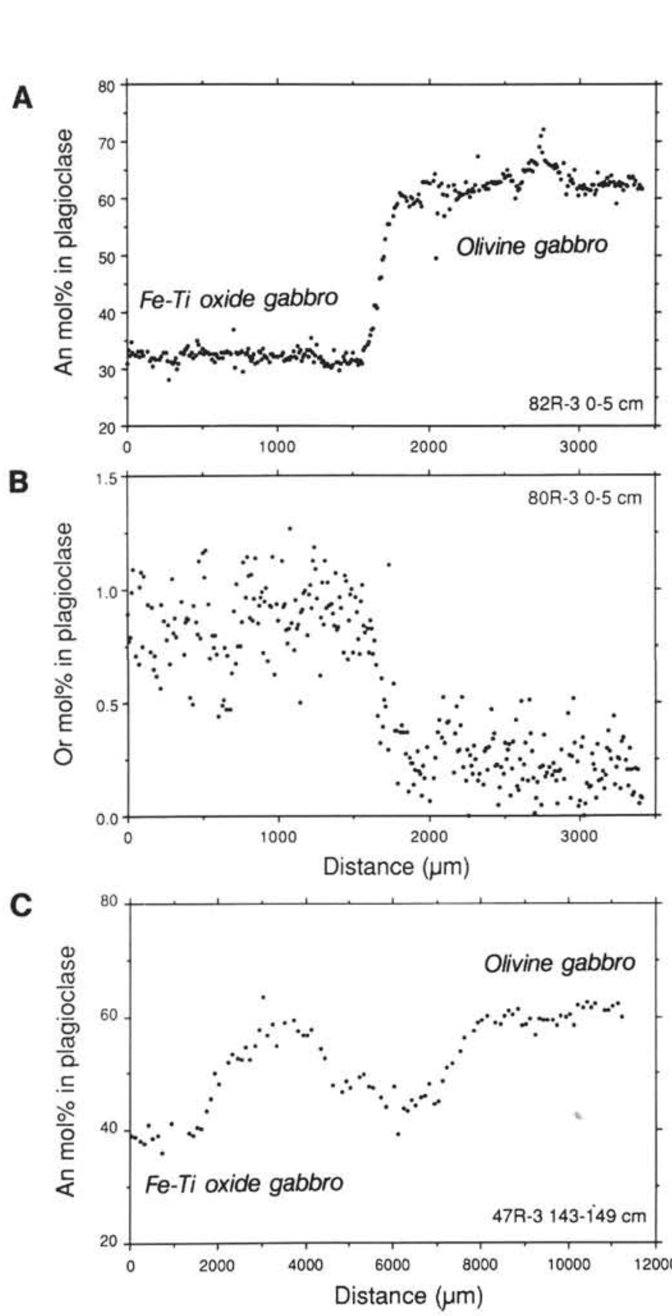

Figure 11. Step scanning profiles of plagioclase composition at the contact between troctolitic olivine gabbro and extremely evolved Fe-Ti oxide gabbro **(A)–(B)** (Sample 118-735B-82R-3, 0–5 cm) and olivine gabbro and Fe-Ti oxide gabbro **(C)** (Sample 118-735B-47R-3, 143–149). Note the difference of scales in **(A)–(B)** and **(C)**. A calcium-rich peak at the contact of Sample 118-735B-47R-3, 143–149 cm **(C)** corresponds to a zoned calcic plagioclase of the olivine gabbro.

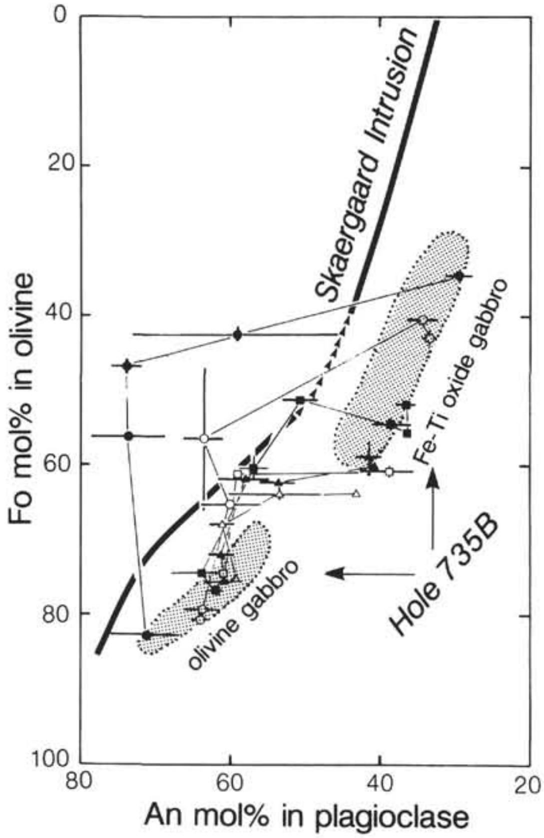

Figure 12. Anorthite content of plagioclase vs. Forsterite mol% of olivine at contacts between olivine gabbro and Fe-Ti oxide gabbro. Data for each contact are connected by a line. Olivine and plagioclase occurring nearby are paired. Bars indicate compositional ranges. Samples are; solid circle: 118-735B-79R-7, 2–9 cm, open circle: 118-735B-82R-3, 0–5 cm, solid square: 118-735B-47R-3, 143–149 cm, solid triangle: 118-735B-76R-3, 35–41 cm, open square: 118-735B-10D-2, 20–24 cm, open triangle: 118-735B-76R-1, 63–70 cm. Arrows on the Skaergaard trend indicate the temporal cessation of olivine crystallization. Bars indicate ranges of the chemical compositions. At each contact, upon crossing the boundary from olivine gabbro to Fe-Ti oxide gabbro, first Fo mol% changes markedly keeping plagioclase composition constant, but at the contact An mol% changes dramatically.

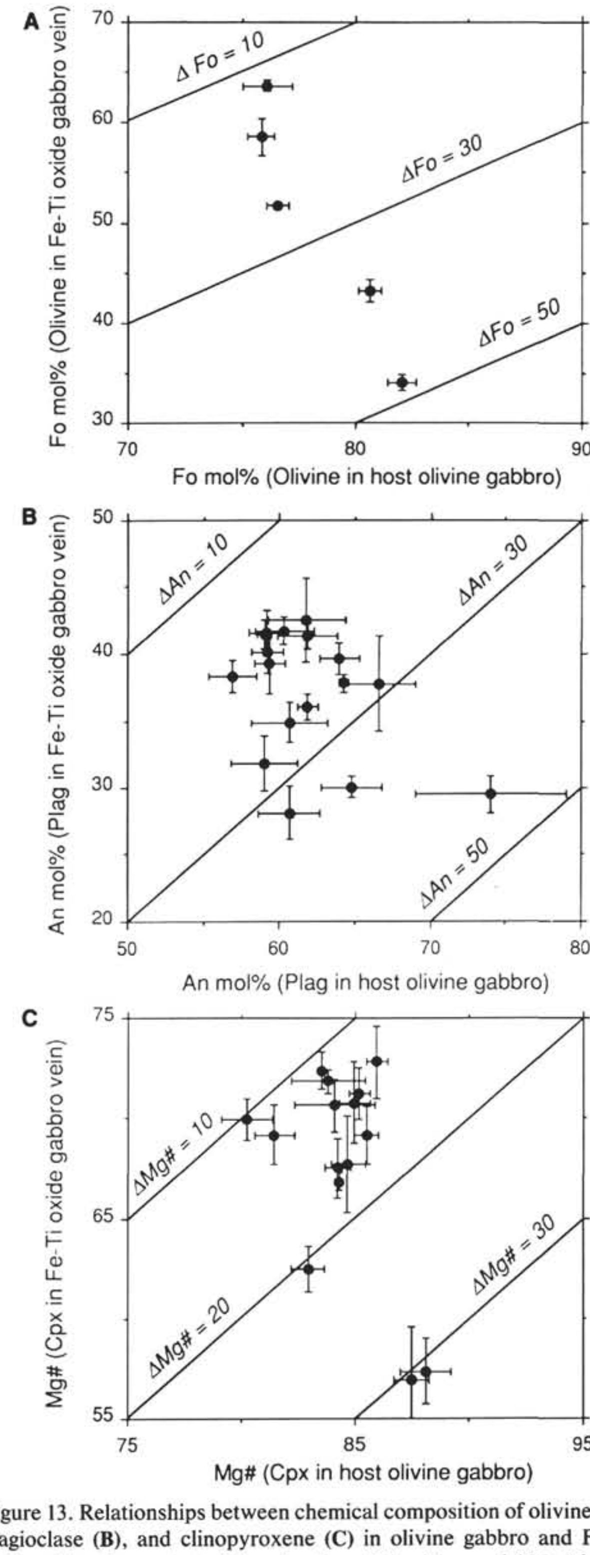

Figure 13. Relationships between chemical composition of olivine (**A**), plagioclase (**B**), and clinopyroxene (**C**) in olivine gabbro and Fe-Ti oxide gabbro in contact with each other. ΔFo, ΔAn, and ΔMg# imply Fo of olivine, An of plagioclase, and Mg# of clinopyroxene in host olivine gabbro minus Fo of olivine, An of plagioclase, and Mg# of clinopyroxene in Fe-Ti oxide gabbro vein, respectively. Bars indicate standard deviations. The data for olivine gabbro and troctolite were obtained 1–3 cm away from the contact and exhibit pristine composition without chemical effect of intruded evolved melts.

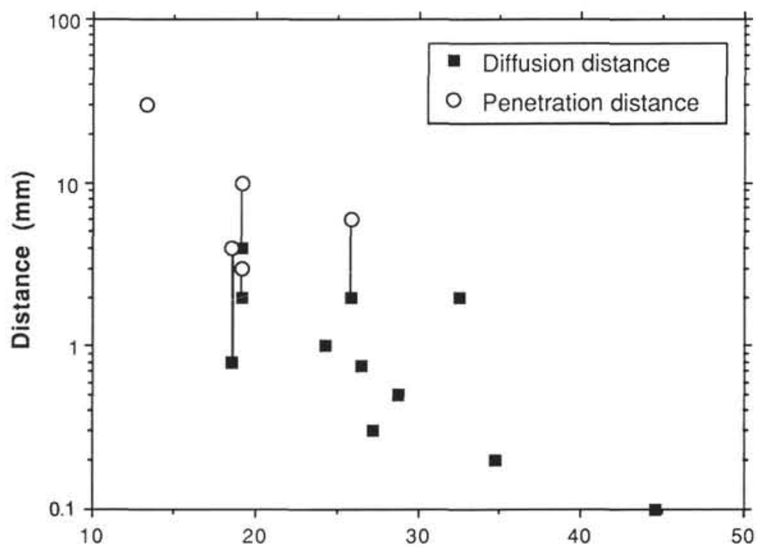

Figure 14. Relationships between compositional difference of plagioclase in contacting olivine and Fe-Ti oxide gabbros, and diffusion or penetration distance observed in plagioclase. Diffusion distance implies the zoned width in single plagioclase at the contact. Penetration distance implies the width within which plagioclase in olivine gabbro shows chemical heterogeneity commonly from the grain boundaries toward inside the grains. Vertical lines connect data for the same sample.

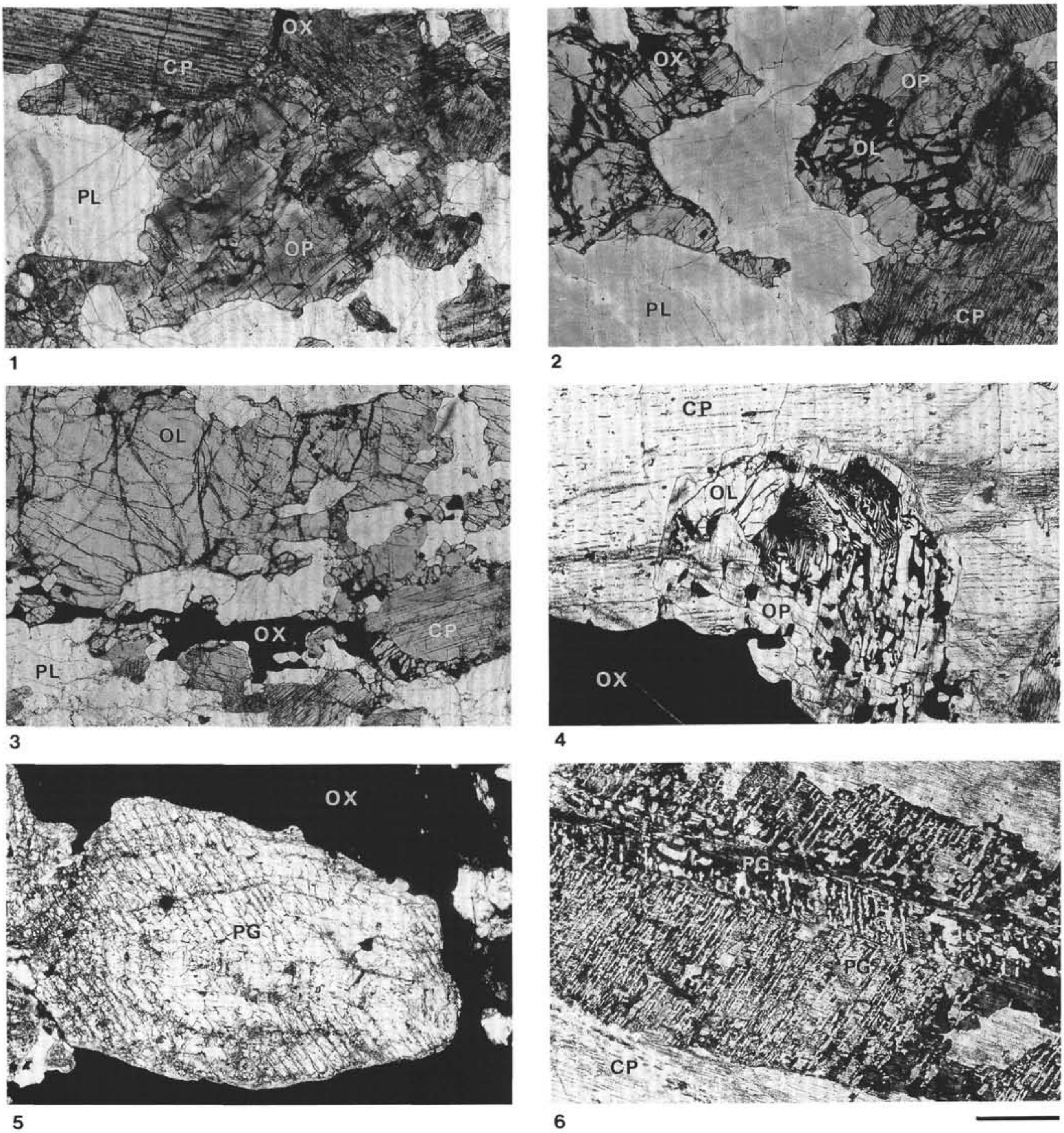

Plate 1. Thin section photomicrograph of Fe-Ti oxide gabbros. Scale bar is 1 mm long for all the photos. **1.** Sample 118-735B-76R-4, 12–19 cm. Gabbronorite containing plagioclase, orthopyroxene and clinopyroxene with small amount of Fe-Ti oxides. **2.** Sample 118-735B-40R-5, 0–4 cm. Olivine gabbronorite containing plagioclase, olivine, orthopyroxene, and clinopyroxene with small amount of Fe-Ti oxides. **3.** Sample 118-735B-46R-3, 121–128 cm. Disseminated Fe-Ti oxide olivine gabbro containing plagioclase, large olivine, clinopyroxene, and Fe-Ti oxides. **4.** Sample 118-735B-76R-1, 63–70 cm. Gabbronorite in contact with olivine gabbro. The photomicrograph shows orthopyroxene and Fe-Ti oxides symplectite surrounding olivine. The corona structure is observed only very close to the contact. **5.** Sample 118-735B-38R-3, 80–85 cm. Inverted pigeonite surrounded by Fe-Ti oxides in olivine pigeonite gabbro. **6.** Sample 118-735B-38R-3, 85–88 cm. Inverted pigeonite in the core of clinopyroxene in pigeonite gabbro. Inverted pigeonite is also present as an isolated grain. Abbreviations in the photos are; OL: olivine, PL: plagioclase, OP: orthopyroxene, CP: clinopyroxene, PG: inverted pigeonite, OX: Fe-Ti oxides.

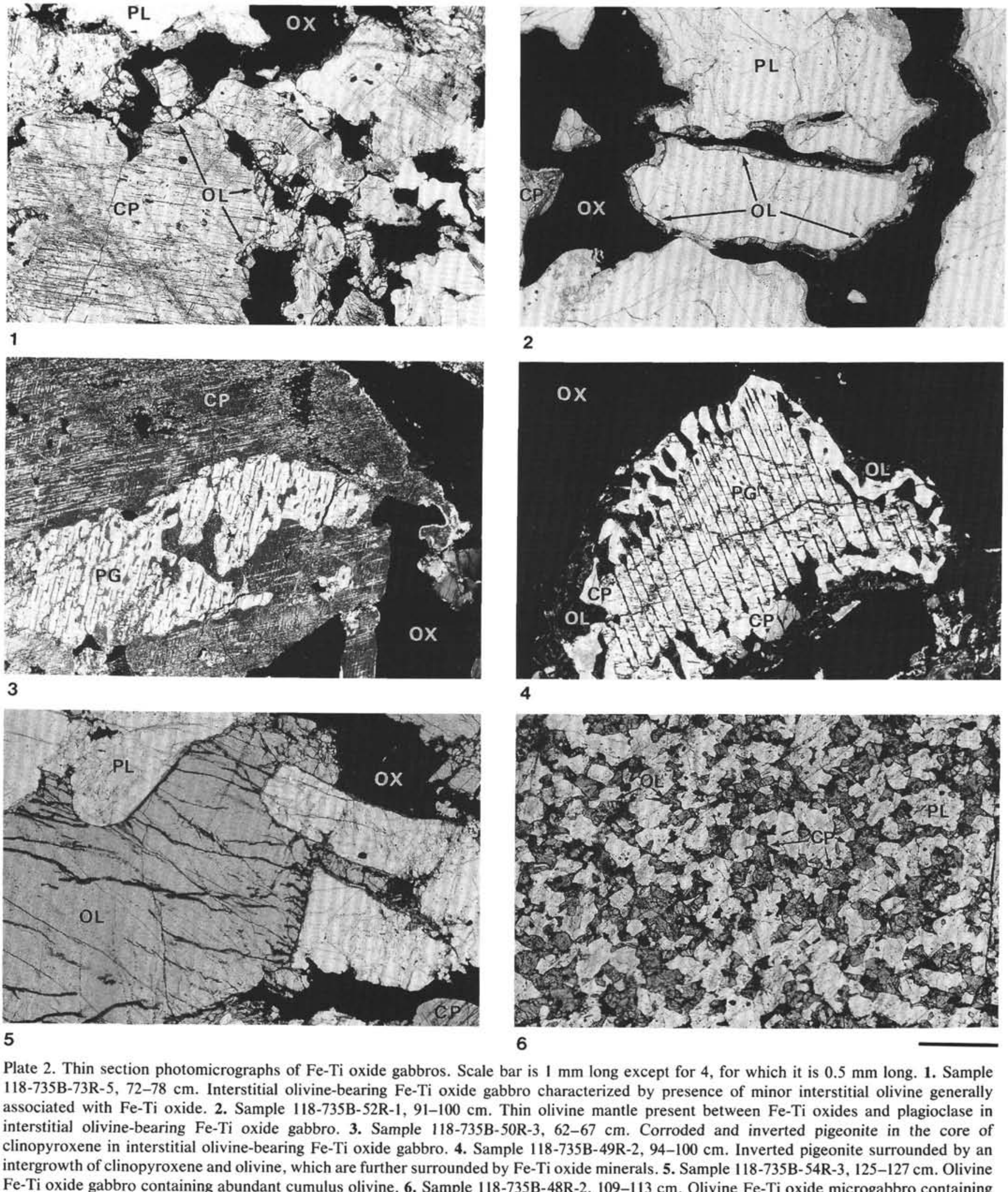

Plate 2. Thin section photomicrographs of Fe-Ti oxide gabbros. Scale bar is 1 mm long except for 4, for which it is 0.5 mm long. **1.** Sample 118-735B-73R-5, 72–78 cm. Interstitial olivine-bearing Fe-Ti oxide gabbro characterized by presence of minor interstitial olivine generally associated with Fe-Ti oxide. **2.** Sample 118-735B-52R-1, 91–100 cm. Thin olivine mantle present between Fe-Ti oxides and plagioclase in interstitial olivine-bearing Fe-Ti oxide gabbro. **3.** Sample 118-735B-50R-3, 62–67 cm. Corroded and inverted pigeonite in the core of clinopyroxene in interstitial olivine-bearing Fe-Ti oxide gabbro. **4.** Sample 118-735B-49R-2, 94–100 cm. Inverted pigeonite surrounded by an intergrowth of clinopyroxene and olivine, which are further surrounded by Fe-Ti oxide minerals. **5.** Sample 118-735B-54R-3, 125–127 cm. Olivine Fe-Ti oxide gabbro containing abundant cumulus olivine. **6.** Sample 118-735B-48R-2, 109–113 cm. Olivine Fe-Ti oxide microgabbro containing plagioclase, olivine, clinopyroxene, and Fe-Ti oxides. Abbreviations are the same as in Plate 1.

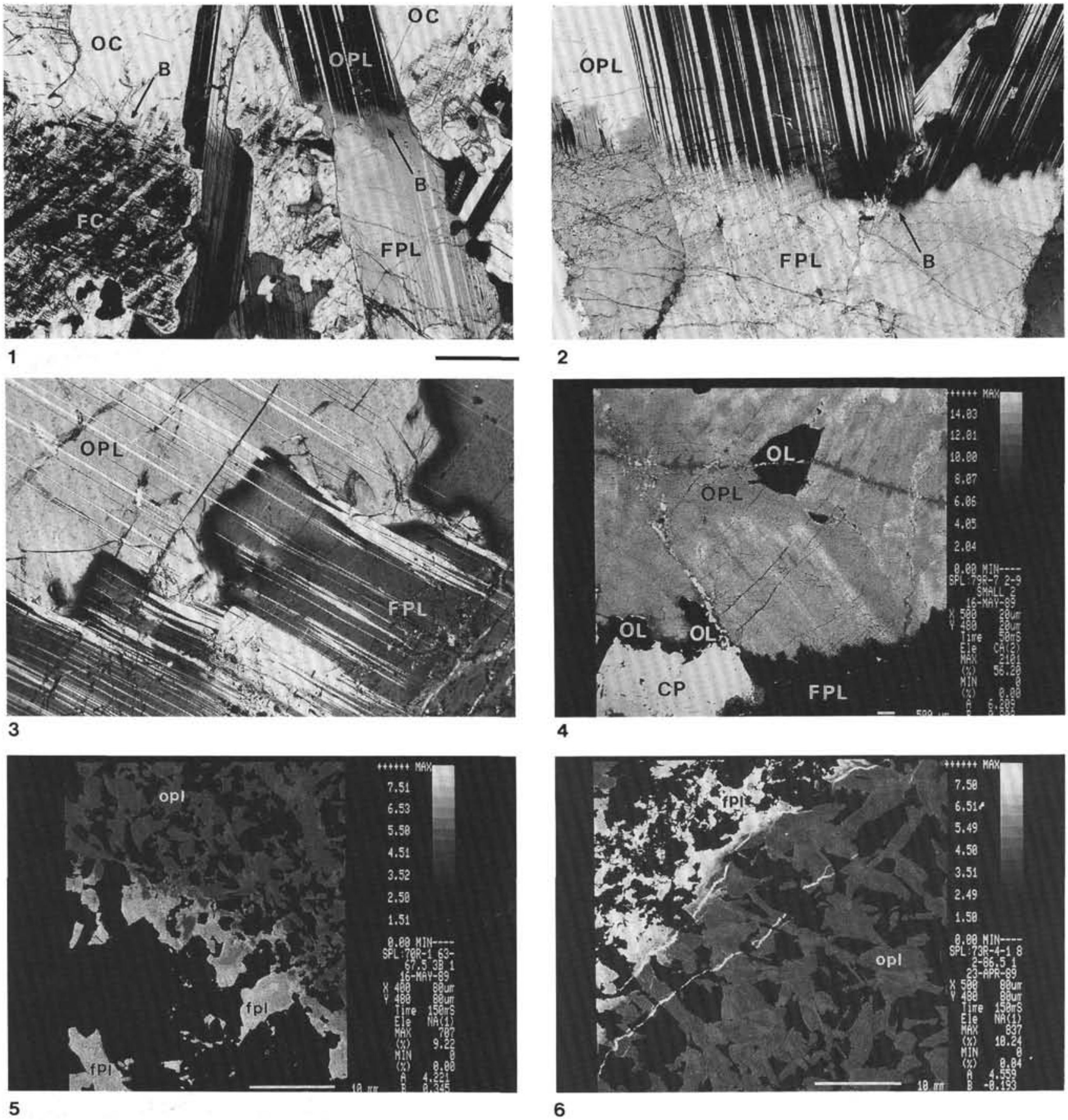

Plate 3. Thin section photomicrographs and element distribution map of contact zones between olivine and Fe-Ti oxide gabbros. Scale bar is 1 mm for Figs. 1. and 2., and 0.2 mm for Fig. 3. **1.** Sample 118-735B-73R-5, 72–78 cm. Slightly diffuse contact between olivine gabbro (above) and Fe-Ti oxide gabbro (below). Note that clinopyroxene in Fe-Ti oxide gabbro contains many exsolution lamellae of opaque minerals, whereas no lamellae is present in clinopyroxene of olivine gabbro. **2.** Sample, 118-735B-79R-7, 2–9 cm. Sharp contact between olivine gabbro (above) and Fe-Ti oxide gabbro (below). Polysynthetic twins are continuous in plagioclase of both gabbros, though extinction position is different because of the difference in An content. This photomicrograph indicates that sodic plagioclase of Fe-Ti oxide gabbro overgrew the fractured calcic plagioclase of olivine gabbro. **3.** Enlarged view of the left side of Fig. 2., showing that chemical composition of plagioclase changes within hundred microns from the olivine gabbro to the Fe-Ti oxide gabbro. Note the continuous twin boundaries. **4.** Calcium distribution map at the contact of olivine gabbro and Fe-Ti oxide gabbro (the same sample as in Fig. 2). Black area is mostly plagioclase with an An content of 30. Note that the zoning pattern is sharply cut by plagioclase in Fe-Ti oxide gabbro. **5.** Sample 118-735B-70R-1, 63–68 cm. Sodium distribution map of the boundary between olivine gabbro and Fe-Ti oxide gabbro. The zoning in plagioclase indicates that the boundary is more irregular and diffused than those in Figs. 1 and 2. **6.** Sample 118-735B-73R-4, 82–87 cm. Fe-Ti oxide dike (1.5 cm thick) in olivine gabbro. The boundary is more diffused than the case in Figs. 1 and 2, but is less diffused than that in Fig. 5. White veins are late stage albite. OC: clinopyroxene in olivine gabbro, FC: clinopyroxene in Fe-Ti oxide gabbro, OPL: plagioclase in olivine gabbro, FPL: plagioclase in Fe-Ti oxide gabbro, B: boundary of olivine and Fe-Ti oxide gabbros. Other abbreviations are the same as in Plate 1. Numbers besides the brightness bar in the element distribution maps are CaO wt% for Fig. 4 or Na_2O wt% for Figs. 5 and 6.